ACTIVATION OF CYCLIC PHENOL PHOSPHATE ANALOGUES AS POTENTIAL INHIBITORS OF AUTOTAXIN

A Thesis Submitted to the College of

Graduate Studies and Research

in Partial fulfillment of the requirements

for the Degree of

Master of Science

In the College of Pharmacy and Nutrition

University of Saskatchewan

Saskatoon, Saskatchewan

Canada

By

Kholud A. Algabbass

PERMISSION TO USE

In presenting this thesis/dissertation in partial fulfillment of the requirements for a Postgraduate degree from the University of Saskatchewan, I agree that the Libraries of this University may make it freely available for inspection. I further agree that permission for copying of this thesis/dissertation in any manner, in whole or in part, for the scholarly purposes may be granted by the professor(s) who supervised my thesis/dissertation work or, in their absence, by the Dean of the College in which my thesis work was done. It is understood that any copying or publication or use of this thesis/dissertation or parts thereof for financial gain shall not be allowed without my written permission. It is also understood that due recognition shall be given to me and to the University of Saskatchewan in any scholarly use made of any material in my thesis/dissertation.

Request for permission to copy or make other use of material in this thesis, in whole or in parts, should be addressed to:

Head of the College of Pharmacy and Nutrition

107 Wiggins Rd

University of Saskatchewan

Saskatoon, Saskatchewan S7N 5E5

Canada

ABSTRACT

Autotaxin (ATX) is a member of the nucleotide pyrophosphatase/phosphodiesterase family of ectoenzymes (NPP/ENPP). ATX is mostly present in blood, but it is also expressed at high levels in the brain, kidney, lymphoid organs, ovary, lung, and intestine. ATX has lysophospholipase D activity that catalyzes the hydrolysis of lysophosphatidylcholine (LPC) into lysophosphatidic acid (LPA) and choline. LPA is a bioactive lipid mediator that facilitates many physiological and pathological processes including cell survival, proliferation, and migration. ATX/LPA signalling has been associated with in a number of human diseases including obesity, diabetes, rheumatoid arthritis, multiple sclerosis, neuropathic pain, Alzheimer's disease, and cancer. Elevated ATX expression is found in various tumours and has been associated with tumour growth. Because most LPA is produced by ATX activity, an inhibitor of ATX would block subsequent LPA signalling, which is a target for anticancer drug development. Therefore, ATX has become an attractive drug target for developing new anticancer therapies. Our objective for this project is to prepare and assess a series of novel cyclic phenol phosphate analogues for their ability to function as irreversible ATX inhibitors *in vitro*.

In order to investigate the ability of the cyclic phenol phosphate analogues to inhibit ATX, the following aims were outlined: (i) the development of synthetic methodologies for the preparation of a series of cyclic phenol phosphate analogues as potential inhibitors of ATX; (ii) an assessment of the aqueous stability of these analogues over 6 h in 50 mM TRIS buffer at 37 °C and pH 8.0 using high performance liquid chromatography (HPLC) for analysis; (iii) the determination of the ability of these compounds to inactivate ATX *in vitro*.

In order to investigate the ability of the cyclic phenol phosphate analogues to inhibit ATX, we proposed and designed strategies to synthesize a series of acyl and alkyl ether

derivatives of cyclic phenol phosphate analogues. Our initial strategy to synthesize acyl derivatives utilized the dealkylation of **1** (4-methoxy-1,3-bezenedimethanol); however, this approach was unsuccessful despite attempts to optimize reaction conditions and introduction of alcohol protecting groups. These unsuccessful reactions were likely the result of multiple competing reactions. A second strategy to synthesize alkyl ether derivatives analogues was developed, and we successfully synthesized two model analogues; **A1** (unsubstituted cyclic phenol phosphate) and **A2** (methoxy-substituted cyclic phenol phosphate). We accomplished this through a multi-step synthetic procedure using the salicylaldehyde and its derivatives as our starting materials. We also synthesized an alcohol starting material with a saturated fourteen-carbon ether linkage by modified literature procedures, but incorporation of the cyclic phosphate moiety was unsuccessful. We also evaluated the stability of the synthesized analogues under specific conditions. Analogues **A1** and **A2** were incubated in 50 mM TRIS buffer at 37 °C and pH 8.0 over six hours and determined to be stable under these conditions, suggesting any ATX inhibitory activity would be the result of the parent compound rather than any decomposition products. Finally, these compounds have been submitted to our colleagues at the University of Memphis for assessment of their *in vitro* ATX inhibitory ability; however, they have not been able to carry out the ATX inhibition assay yet. Also, we carried out the preliminary in silico docking studies. Our proposed and synthesized analogues of both acyl and alkyl ether derivatives of cyclic phosphate analogues were docked to the active site of the ATX (PDB ID: 3NKM) to assess their binding affinity. The results of the docking experiment revealed no major differences. However, both **A1** and **A2** show the highest values (i.e. lowest affinity), which indicate that the long side chains of the other ligands play a role in binding to ATX.

Thus, the proposed cyclic phenol phosphates have not been previously prepared and can

therefore represent a new orientation for the study of ATX inhibitor compounds and may lead to the development of new treatments for ATX-related human diseases in the future, including cancer.

ACKNOWLEDGMENTS

In the name of Allah, the Most Gracious and the Most Merciful

Alhamdulillah, all praises to ALLAH, the Almighty, the greatest of all, on whom ultimately we depend for sustenance and guidance. Thanks to ALLAH for giving me this opportunity, determination, strength, and patience to complete my thesis finally, after all the challenges and difficulties. His continuous grace and mercy were with me throughout my life and ever more during the tenure of my research. Also, I cannot forget the ideal man of the world and most respectable personality, Prophet Mohammed (Peace Be Upon Him).

I would like to express my sincere gratitude to my supervisor Dr. Ed S. Krol for the continuous support of my Master study, for his patience, guidance, motivation, compassion, immense knowledge, and optimistic encouragement during the course of my studies. The door to Dr. Krol's office was always open whenever I ran into a trouble spot or had a question about my research or writing. He consistently allowed this research to be my own work but steered me in the right direction whenever he thought I needed it. Without his assistance and dedicated involvement in every step throughout the process, this thesis would have never been accomplished. I would like to thank you very much for your support and understanding over these past years, and I could not have imagined having a better advisor and mentor for my Master study. I know I cannot thank you enough, but I hope to be a reflection of your curious personality in my own academic career.

Also, I would like to express my deep heartfelt appreciation to the Chair of my research committee Dr. Jean Alcorn for her continued encouragement, advice and help, and the other members of the advisory committee Dr. Jian Yang and Dr. Meena Sakharkar for their insightful comments and encouragement. I am also thankful to Dr. Bryan M. Hill, the Chair of the department chemistry at Brandon University, for serving as my external examiner, and for his valuable comments and suggestion that enrich my thesis.

I appreciate and thank all my lab mates for their friendship and support: Isaac Asiamah, Kevin Allen, Leah McGurn, Ahmed Almousa, and Yunyun Di for all of their help, support, both scientifically and socially. A special thank and acknowledgment go to Isaac Asiamah and Kevin Allen for teaching me how to do synthesis in the Laboratory, and Leah McGurn for helping me in the stability study and Mass spectrometer. I would like to send a special thank to Sarah Petriew, a summer student who worked in our group and successfully synthesized one of the precursor compounds for this project. Also, Dr. Keith Brown for NMR training, Ms. Deboral Michel for her help in particular with the mass spectrometer, and all my friends and colleagues for their help and support.

Sincere thanks to the Scholarship and financial support from College of Pharmacy, Umm Al-Qura University (UQU, Saudi Arabia), Saudi Arabian Cultural Bureau in Canada (SACB), University of Saskatchewan (U of S), and the Natural Sciences and Engineering Research Council (NSERC).

Lastly, but most importantly, I am grateful to my great family, relatives, and friends back home and here in Canada for their unconditional love and prayers. I would like specially thank the source of my strength and motivation, my mom (Najat) who had never failed me and always believed in me. I love you mom and I really appreciate all that you did and still doing for me. To my siblings: Khayrieah, Alla (who was accompanying me during all the time of my journey), Ebtisam, Eman, Alya, Omar, Sumaya (who joined us for the last year) for being always by my side. Finally my nieces (Judy and July) and my nephews (AbdullElah and AbdullMalek) who have unique abilities to melt my frustrations with smiles. Thanks to everyone for providing me with unfailing support and continuous encouragement throughout my years of study and through the process of researching and writing this thesis. This accomplishment would not have been possible without you. Thank you.

Kholud Algabbass

DEDICATION

This thesis is dedicated to...

…My great mother (Najat)
Without your love, prayers, and support
This study would not have been possible

…My Beloved father (Ali)
Your memories will always be
my personal source of motivation
You are truly missed and
You will always be an inspiration

…My lovely brothers (Alaa and Omar)
and sisters (Khayrieah, Ebtisam, Eman,
Alya, and Sumaya)
Your truly love, care, and patience
has been a great support for me
during my study

TABLE OF CONTENTS

LIST OF FIGURES

LIST OF SCHEMES

LIST OF TABLES

LIST OF ABBREVIATIONS

Ac_2O	Acetic anhydride
Asn	Asparagine
Asp	Aspartate
ATX	Autotaxin
BBr_3	Boron tribromide
BrP-LPA	Bromophosphonate analogue of LPA
Ca^{2+}	Calcium ion
COPD	Chronic Obstructive Pulmonary Disease
cPA	Cyclic Phosphatidic Acid
DAG	Diacylglycerol
DCM	Dichloromethane
DGK	Diacylglycerol kinase
DMAP	4-dimethylaminopyridine
DMSO	Dimethyl sulfoxide
EDG	Endothelial differentiation gene
ENPPs	Ecto-Nucleotide Pyrophosphatase/Phosphodiesterase
ENPP 2	Ecto-Nucleotide Pyrophosphatase/Phosphodiesterase 2
EtOAc	Ethyl acetate
EtOH	Ethanol
GSH	Glutathione
Hex	Hexane
His	Histidine

IPF	Idiopathic pulmonary fibrosis
K^+	Potassium ion
KOH	Potassium hydroxide
LCAT	Lecithincholesterol acyltransferase
LC-MS	Liquid Chromatography-Mass Spectrometry
LPA	Lysophosphatidic Acid
LPC	Lysophosphatidylcholine
LPE	Lysophosphatidylethanolamine
LPLs	Lysophospholipids
LPS	Lysophosphatidylserine
MeOH	Methanol
MOE	Molecular Operating Environment
MS	Mass Spectroscopy
Na^+	Sodium ion
$NaBH_4$	Sodium borohydride
$NaHCO_3$	Sodium bicarbonate
NMR	Nuclear Magnetic Resonance
NPP 2	Nucleotide Pyrophosphatase/Phosphodiesterase 2
NPP/s	Nucleotide Pyrophosphatase/Phosphodiesterase
NucA	Anabaena nuclease A
OH	Hydroxyl group
$_O$-QM	*ortho*-quinone methides
P2Y	Purinergic receptor

PAI-1	Plasminogen activator inhibitor-1
PA	Phosphatidic acid
PC	Phosphatidylcholine
PDB	Protein data bank
PDE	Phosphodiester
PD-Iα	Ecto-phosphodiesterase I/nucleotide pyrophosphatase
PE	Petroleum Ether
$PLA_{1/2}$	Phospholipase A_1 or A_2
PLD	Phospholipase D
PLs	Phospholipids
$PS\text{-}PLA_1$	Phosphatidylserine-specific phospholipase A_1
*p*TsOH	*p*-Toluenesulfonic acid
ROS	Reactive Oxygen Species
RT	Room Temperature
RP-HPLC	Reversed-phase High Performance Liquid Chromatography
S1P	Sphingosine-1-phosphate
SMB	Somatomedin B-like
SPC	Sphingosylphosphorylcholine
$SPLA_2\text{-IIA}$	Secretory phospholipase A_2 group IIA
TBDMSCl	tert-Butyldimethylsilyl chloride
TBDMS	tert-Butyldimethylsilyl
TEA	Triethylamine
THF	Tetrahydrofuran

Thr	Threonine
Tyr	Tyrosine
UPAR	Urokinase-type plasminogen activator
XaNPP	Xanthomonas axonapodis

CHAPTER 1: INTRODUCTION

Despite developments in drug discovery of chemotherapeutic agents, cancer still remains one of the primary causes of death due to the development of resistance to chemotherapy and the recurrence of cancer cells.[1] Available cancer treatments have shown many disadvantages, such as severe side effects and little selectivity to target cancer cells. Therefore, great effort has been directed toward the development of improved anti-tumour therapies.

Autotaxin (ATX) is an extracellular enzyme, and is a member of the nucleotide pyrophosphatase/phosphodiesterase family of ectoenzymes (NPP/ENPP) that catalyze hydrolysis of phosphodiester bonds of different compounds.[2-4] The mammalian ENPP family contains seven members (ENPP 1–7) and ATX is known as ENPP 2/NPP 2. ATX is a glycoprotein that was first isolated from A2058 melanoma cells and classified as an autocrine motility factor in 1992. It was later found to be responsible for cell proliferation, survival, migration, and invasion.[5]

Following the initial disclosure, further investigation by Umezu-Goto et al.[6] and Tokumura et al.[7] showed that ATX possesses lysophospholipase D (lysoPLD) activity, which is responsible for the hydrolysis of lysophosphatidycholine (LPC) to lysophosphatidic acid (LPA) and choline.[6, 7] LPA is a bioactive phospholipid with different functions in many cell types, and it can promote a variety of physiological events. It exhibits its action by binding to specific G protein-coupled receptors (GPCRs) and stimulating a wide variety of cellular functions, including cell proliferation, migration, and survival.[6, 8, 9]

ATX-mediated formation of LPA is associated with a number of disease states, including obesity,[10] diabetes,[11] rheumatoid arthritis,[12] neuropathic pain,[13, 14] and cancers.[8, 15, 16] One particular area of interest is the relationship between the ATX enzyme and cancer progression.

Many studies have investigated the function of ATX-LPA signalling in tumour formation and metastasis since the discovery of ATX as the autocrine motility factor for melanoma cells.[3, 4, 17] Subsequent experiments have identified the role of ATX in tumorigenesis, cancer progression, tumour cell motility, tumour cell invasion, metastatic processes, and angiogenesis.[8, 15, 18-21] Overexpression of ATX has been frequently demonstrated in different human tumours,[8, 15, 20, 22] including neuroblastoma,[23] glioblastoma,[24, 25] hepatocellular carcinoma,[26] B-cell lymphoma,[27] melanoma,[5] breast cancer,[28] renal cell carcinoma,[29] thyroid carcinoma,[30] and lung cancer.[31]

As a consequence, intervention in the ATX−LPA signalling cascade has increasingly drawn the attention of researchers in an attempt to understand its functions in physiology and pathophysiology.[3, 4] Also, this knowledge is essential in developing new chemical entities that could lead to the discovery of novel medicines to treat several pathological conditions. Accordingly, a variety of synthetic chemical inhibitors have been designed and synthesized by both academic research groups and pharmaceutical industries. Different chemical categories of ATX inhibitors have been summarized in recent review articles.[3, 4, 32] Many of the initial inhibitors were lipid-like structures in order to mimic the shape and properties of the natural substrate (LPC) or the product (LPA) phospholipids of the enzymatic reaction. Although a number of these analogues show potent inhibitory activity, such derivatives usually suffer from poor solubility and bioavailability due to the presence of a long lipophilic chain, limiting their use for *in vivo* applications.[4, 32] More recently, small-molecule inhibitors have been discovered through approaches utilizing screening of chemical libraries or have been designed taking the crystal structure of ATX into consideration.[4, 32, 33]

In 2011, a crystal structure of mouse ATX was solved by Nishimasu et al.,[34] whereas the crystal structure of rat ATX was solved by Hausmann et al.[35] Both crystal structures share 93 %

sequence identity with human ATX. This progress has been an important step in understanding the ATX binding site and critical interactions required for enzymatic activity, hence helping to develop new potent inhibitors for this promising therapeutic target.[3, 32] Subsequent investigations into ATX structure[36-39] have led to the development of small-molecule compounds that demonstrated high inhibitory activities and afforded helpful tools for research; however, additional applications in animal model studies have yet to be demonstrated.[4, 32]

At present, most ATX inhibitors developed are reversible inhibitors. Indeed, only a limited number of irreversible inhibitors have been reported. Since the reduction of side-effects and low toxicity are major goals of cancer chemotherapy, a potential advantage of irreversible, mechanism-based ATX inhibitors is their target specificity. Thus, there is still a need to design and synthesize novel, potent, and selective compounds that would provide effective inhibition to ATX activity to reduce conversion of LPC to LPA. This inhibition would decrease the unwanted cell proliferation, survival, and migration to prevent, or at least reduce, the advance of certain cancers. Therefore, our overall goal in this study is to synthesize and assess a series of cyclic phenol phosphate analogues and investigate their ability to function as irreversible ATX inhibitors. We expect to provide insight into the structure of the enzyme and to understand the critical structural features to inhibit ATX activity, which is likely to lead to the development of new treatments for human diseases in the future, including cancer.

CHAPTER 2: LITERATURE REVIEW

2.1 History of Autotaxin

Autotaxin is a glycoprotein enzyme with a molecular mass of 125 kDa.[5] In 1992, ATX was identified as a potent autocrine motility stimulating factor found in the media derived from A2058 human melanoma cells. The name ATX is derived from its first property as an autocrine motility factor because the A2058 melanoma cells that secrete ATX also respond to ATX itself. At that time, the enzymatic activity of ATX was unknown. Two years later, it was found that ATX has a significant homology to the nucleotide pyrophosphatase/phosphodiesterase (NPP/ENPP) family[40] found extracellularly as secreted ectoenzymes that catalyze hydrolysis of pyrophosphate or phosphodiester bonds in different extracellular compounds such as nucleotides, lysophospholipids, and choline phosphate esters.[2] The mammalian ENPP family contains seven members (ENPP 1–7) that are divided into two subclasses (ENPP 1–3 and ENPP 4–7) depending on their primary structure; ATX is known as ectonucleotide pyrophosphatase/phosphodiesterase 2 (ENPP 2 or NPP 2). The mystery remained until 2002, when plasma lysophospholipase D (lysoPLD) was purified and found to be identical to ATX.[6, 7, 41] ATX is unique among NPP/ENPP enzymes because of its lysoPLD activity, which hydrolyzes lysophosphatidylcholine (LPC) to generate the lipid mediator lysophosphatidic acid (LPA).[6] ATX has a higher affinity for LPC than nucleotides, suggesting that LPC is the preferred physiological substrate for ATX. LPA is a bioactive phospholipid with different functions in many cell types, and it exhibits its action by binding to specific G protein-coupled receptors (GPCRs) and stimulating a wide variety of cellular functions, including migration, proliferation, and survival.[4, 42]

Furthermore, ATX is expressed in different biological fluids such as plasma, serum, seminal plasma, cerebrospinal fluid, urine, and saliva, in both human and animals.[8] Although

ATX is ubiquitous, it is expressed at a high level in the brain, kidney, lymphoid organs, ovary, lung, and intestine.[43]

2.2 ENPP Family

ATX/NPP 2/ENPP 2 is one of the seven known members of the NPP/ENPP family, which are numbered according to their order of discovery.[2] The ENPP family members can be divided into two major subgroups ENPP 1–3 and ENPP 4–7.[36] ATX/ENPP 2 shares a common structure with NPP 1 and NPP 3; therefore, they have a domain structure composed of two N-terminal somatomedin B-like (SMB) domains, a central catalytic phosphodiester (PDE) domain containing a series of determinants that are important for catalysis, and a C-terminal nuclease-like (NUC) domain.[2, 19, 36, 43] Even though it has been asserted that the NUC domain is important for the lysoPLD activity, the function of the NUC and SMB domains are generally unknown.[34] The second subgroup, ENPP 4–7, has only the PDE domain and lacks the SMB and NUC domains.[2, 36] Although these enzymes share the same catalytic domain, which belongs to the alkaline phosphatase superfamily, the mammalian ENPP family members have various physiological roles according to their particular substrate.

ATX/ENPP 2 is a secreted protein and the only member that exhibits lysoPLD activity and participates in LPA signalling. The other ENPP family members are transmembrane proteins, and they can be either type-I (ENPP 4–7) or type-II (ENPP 1–3). Of these members, ATX is the best described so far. ENPP 1 is an ectoenzyme that catalyzes hydrolysis of extracellular nucleotides to release inorganic pyrophosphate (Ppi), which plays an important role in calcification. ENPP 6 and ENPP 7 are choline-specific ecto-phospholipases C, probably serving catabolic functions. However, the functions of ENPP 4 and ENPP 5 have not yet been identified.[2]

2.3 Overview of the Crystal Structures of Autotaxin

2.3.1 Overall Architecture

In 2011, two different research groups presented the crystal structures of mouse[34] and rat[35] ATX both alone and in complex with different molecules.[4, 39] The overall structures of mouse ATX (Figure 2-1) and rat ATX in various crystal structure forms are virtually identical[39] and 93 % identical to human ATX.[34, 35] Briefly, the ATX structure encompasses four domains: two N-terminal somatomedin B-like domains 1 and 2 (SMB1 and SMB2), a central catalytic phosphodiesterase (PDE) domain, and a C-terminal nuclease-like domain (NUC) (Figure 2-2).[4, 39] The structure of the individual domains of ATX consists of known folds. Also, two linker regions are present: the L1 linker region links both the SMB-like domain 2 and the catalytic domain, whereas the L2 linker (or lasso loop) region links both the catalytic PDE domain and the NUC domain (Figure 2-2).

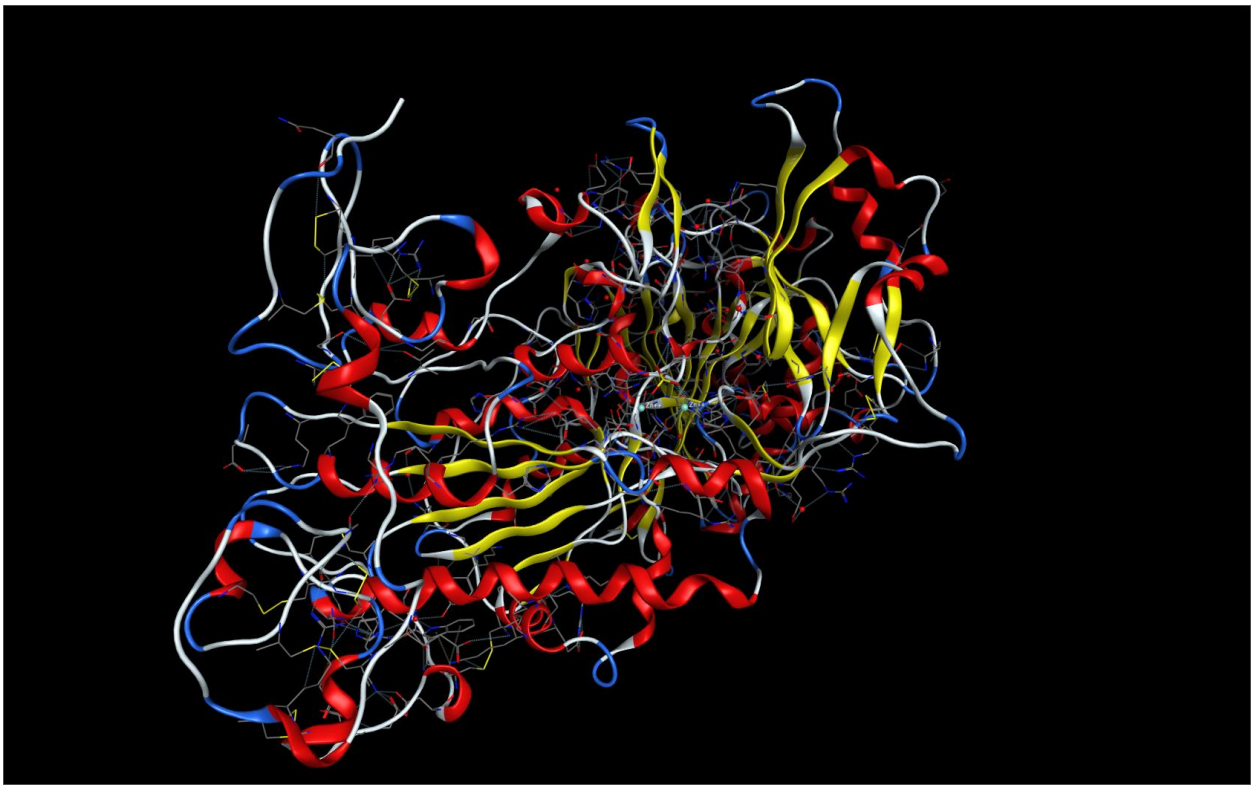

Figure 2-1: Crystal structure of mouse Autotaxin[44] (PDB ID Code: 3NKM at 2.0 Å Resolution).

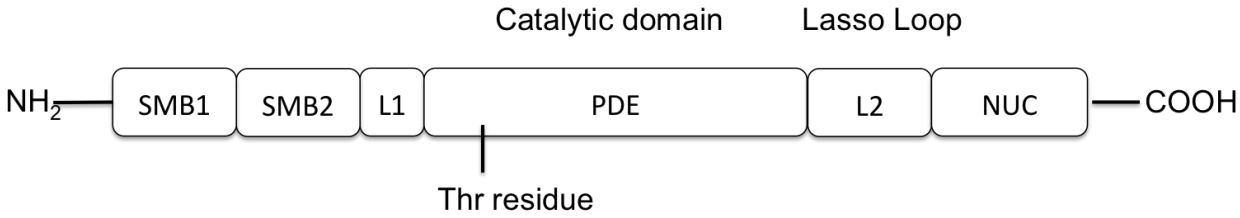

Figure 2-2: Overall architecture of ATX and domain organization. (Adapted from4)

2.3.2 Somatomedin B-like Domains of ATX

The SMB1 and SMB2 are found in all ATX isoforms; they form a disulfide-bonded knot fold in which eight cysteine residues are stabilized by four intermolecular disulfide linkages.[34, 39] Although there is low sequence identity (15 %) between both SMB-like domains, they are highly similar. The structure of SMB-like domains of ATX is similar to the SMB domain of vitronectin (PDB ID 1OC0), an extracellular matrix protein that regulates tumour cell adhesion and migration by the interaction of its SMB domain with urokinase-type plasminogen activator (uPAR) receptor and plasminogen activator inhibitor-1 (PAI-1).[45] The disulfide bond pattern is preserved as well among the three domains; however, the amino acid residues of the vitronectin SMB domain, which interacts with PAI-1 and uPAR, are not preserved in the ATX SMB-like domains, indicating that the function of the ATX SMB domain is not interacting with PAI-1 and is different from other SMB domains.

2.3.3 Catalytic Phosphodiesterase Domain and the Active Site

The central catalytic phosphodiesterase (PDE) domain interacts with both SMD and NUC domains, and it contains the active site for hydrolysis of nucleotides and lysophospholipids (Figure 2-2).[4] The ATX active site contains threonine (Thr) as a nucleophile, and two zinc ions (Zn^{2+}). The key residue in the active site of mouse and rat ATX is Thr209,[4, 34, 35] whereas the active residue in human ATX is Thr210.[4, 46] The Thr209 and the two Zn^{2+} ions are coordinated by conserved aspartate (Asp) and histidine (His) residues.[4, 34, 39] Significantly, the first Zn^{2+} ion is coordinated by Asp311, His315, and His474, whereas the second Zn^{2+} ion is coordinated by Asp171, Thr209, and His359. These Zn^{2+} ions are vastly conserved among the ENPP family members and are important for lysoPLD activity of ATX and ENPP 1.[34] The catalytic domain of ATX and ENPP 1 has a similar structure to a bacterial NPP enzyme from *Xanthomonas*

axonapodis (XaNPP; PDB ID 2GSU).[47] Both the catalytic residues and the two Zn^{2+} ions are found at the same location in ATX and XaNPP, indicating that they have a similar catalytic mechanism. In addition to the coordinating residues and the two Zn^{2+} ions, the preserved Asparagine (Asn) Asn230 and Tyrosine (Tyr) Tyr306 of ATX superimpose with Asn111 and Tyr206 of XaNPP, respectively.[34] These investigations support the hypothesis that ATX catalyzes LPC by the same catalytic mechanism as XaNPP.

2.3.4 A Shallow Groove and a Deep Hydrophobic Pocket

The catalytic sites are nearly identical in ATX, ENPP 1, and XaNPP.[38] All of them encompass the Thr nucleophile with two Zn^{2+} ions, coordinated by Asp and His residues. These Zn^{2+} ions participate in bond-breaking steps.[37] Additionally, all three enzymes possess a shallow groove that is capable of binding nucleotide substrates.

Moreover, the PDE domain encompasses a hydrophobic lipid-binding pocket, which is unique for ATX among the ENPP family and any other phospholipase enzyme.[38, 48] The pocket, which is about 15 Å deep, is located inside the hydrophobic core of the catalytic domain down from the shallow groove.[37, 38] Formation of this pocket in ATX is due to the absence of 18 amino acid residues in ATX that are found in all other ENPPs and the bacterial NPP enzyme. Therefore, the absence of these sequences leads to the formation of the pocket in ATX, which allows ATX to function as a lysoPLD. Furthermore, this pocket can accommodate various LPA and LPC species with different chain lengths and saturations in particular conformations.[4, 38] Specifically, the short chain saturated molecules, 14:0 and 16:0 LPA, can be accommodated in the hydrophobic pocket, whereas 18:0 does not seem to fit.[38] Conversely, the unsaturated LPA species such as 18:1 and 18:3 can bend at the unsaturated bonds, whereas 22:6 adopts a U-

shaped conformation inside the pocket.

2.3.5 Tunnel of Autotaxin

ATX appears to have a hydrophobic tunnel or channel that forms a T-junction with the substrate-binding pocket.[4, 37, 38] This tunnel is located between the SMB1 and catalytic PDE domain. The absence of the 18 amino acids in ATX is also responsible for formation of this tunnel, which makes it a unique characteristic of ATX that is not present in other NPPs. The tunnel can accommodate the hydrophobic tail of lysophospholipids; therefore, it is possible that the hydrophobic tunnel can serve as an entrance for the LPC to the catalytic site and as an exit for the LPA, allowing the delivery of LPA to its adjacent GPCRs.

2.3.6 Nuclease-Like Domain

The C-terminal nuclease-like domain (NUC) is catalytically inactive.[37] The NUC domain is strongly bound to the PDE domain by a 50-residue lasso loop, which starts at the end of the PDE domain and binds tightly with the NUC domain (Figure 2-2).[35] This binding is reinforced through seven hydrogen bonds, nine salt bridges, and an intramolecular cysteine bridge; together, these maintain the structural rigidity of ATX. These observations demonstrate the important role of the interaction between both the catalytic PDE and the NUC domain for lysoPLD activity of ATX.

In summary, the crystal structures of mouse ATX and rat ATX are virtually identical and are 93 % identical to human ATX. The ATX structure encompasses four domains: the two N-terminal SMB1 and SMB2 domains, the central catalytic PDE domain that contains the catalytic active site, and the C-terminal NUC domain. The active catalytic site of ATX contains the Thr nucleophile and two Zn^{2+} ions. Also, the PDE domain encompasses a hydrophobic lipid-binding

pocket, which is unique to ATX among the ENPP family. This pocket can accommodate various LPA and LPC species with different chain lengths and saturations in particular conformations. Also, ATX has a hydrophobic tunnel that can accommodate the hydrophobic tail of lysophospholipids.

2.4 Domain Arrangement

The modular domain arrangement of the ATX enzyme has been identified. The catalytic PDE domain extensively binds to both the SMB-like domains from one side and to the NUC domain from the other side, with the L1 and L2 linkers reinforcing the whole molecule (Figure 2-2).[34] The domain arrangement is stabilized by a number of hydrophobic and hydrophilic interactions. Similarly, the arrangement of water molecules in a specific order between the catalytic PDE and NUC domains develops a huge network of hydrogen bonds.[34] The L1 linker connects to the catalytic PDE domain, whereas the L2 linker connects with both catalytic PDE and NUC domains. These interactions are combined by the four disulfide bonds. Many of the residues that participate in the interdomain interactions are preserved among the ATX enzymes from various organisms, indicating the biological importance of the observed domain arrangement. In fact, these residues are also extensively preserved between ENPP 1–3, suggesting that the domain arrangement is similar among them.

2.5 Human Autotaxin

Rat, mouse, and human ATX proteins have about 93 % sequence identity.[4, 34, 35] Residue numbers in the human enzyme are n+1 in comparison to the mouse/rat enzyme because of the insertion of an additional amino acid after residue number 37. However, the important functional amino acids residues and their domains are extensively conserved among them. Furthermore, the

ATX enzymes exhibit similar activities toward LPC substrates. These findings suggest that they have almost the exact same structures. Therefore, the crystal structure of rat/mouse ATX can be used as a starting point to design and develop new inhibitors of the human ATX enzyme.

2.6 Substrate Specificity

The substrate specificity of the ENPP family is quite varied. Specifically, ENPP 1–3 can identify nucleotides and their derivatives.[2] In the case of ATX, it recognizes lysophospholipids in addition to nucleotides. ENPP 6 and ENPP 7 identify phosphate ester substrates like LPC, but they hydrolyze LPC to monoacylglycerol and choline phosphate. The substrates of ENPP 4 and ENPP 5 are still unknown.

In particular, a number of substrates of ATX/ENPP 2 have been recognized including phosphodiester, phosphonate esters, sulfo–phosphates, and phospholipids. However, the biological effect of ATX action depends on several factors.[43, 49] These factors include ATX concentration, substrate availability, presence of regulatory cofactors, and the spectrum of LPA expressed on adjacent target cells. Specifically, regulation of ATX expression can be controlled by different factors such as cytokines, oncogenes, and growth factors. Nevertheless, these factors appear to depend on the cell type.[50] ATX produces LPA from extracellular LPC and other non-choline lysophospholipids such as lysophosphatidylserine (LPS) and lysophosphatidylethanolamine (LPE).[38, 51] Although several compounds have been reported to be substrates of ATX, LPC is the major physiological substrate for ATX.[8, 19, 43] LPC is the most abundant phospholipid in blood plasma where its concentration in human reaches about 200 μM.[52, 53] However, the abundant LPC in the circulation is relatively inactive unless it is transformed to LPA by ATX.[15]

In addition to LPC, ATX can also hydrolyze sphingosylphosphorylcholine (SPC) to produce sphingosine-1-phosphate (S1P), a bioactive lipid mediator, *in vitro*[49] (Scheme 2-1). However, the catalytic ability of ATX to hydrolyze SPC to S1P is 4.5 times less than the catalytic efficiency for hydrolysis of LPC to LPA. Thus, it does not seem that ATX contributes in the major pathway to formation of S1P *in vivo*.[54] Furthermore, Tanaka et al.[55] confirmed that ATX is the main enzyme for producing LPA in blood, but not for production of S1P. It has been reported that S1P can also be produced intracellularly by the action of sphingosine kinase.[49, 55] Indeed, it is probable that other lipid-like molecules and possibly lysophospholipids are substrates of ATX.

Furthermore, ATX can also hydrolyze nucleotides and their derivatives *in vitro* such as adenosine-5′-triphosphate (ATP), diadenosine polyphosphates (Ap_nA), uridine diphosphate glucose (UDP-glucose), nicotinamide adenine dinucleotide (NAD^+), and p-nitrophenyl thymidine-5′-monophosphate (pNTM).[4, 56] Although ATX is able to hydrolyze nucleotides *in vitro*, the affinity of ATX for LPC is about 10-fold higher than for nucleotides.[38] Therefore, ATX may not hydrolyze nucleotides *in vivo*.

Obviously, the ENPP family recognizes a wide variety of substrates. Particularly, several compounds have been identified as substrates for ATX. However, the major physiological substrate for ATX is LPC, which is the most abundant phospholipid in blood plasma.

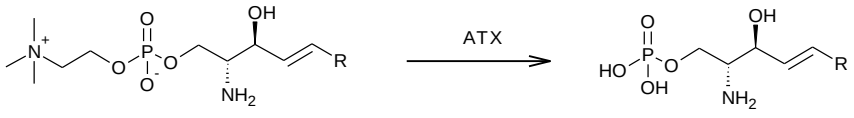

SPC S1P

Scheme 2-1: Hydrolysis of SPC to S1P by ATX.

2.7 Autotaxin Isoforms

In 2008, three isoforms of ATX (α, β, and γ) and their tissue distribution were described in human and mouse[4, 32, 57] and an additional two (δ and ε) in 2012 (Figure 2-3).[4, 58] ATXα was the first identified isoform; it was originally isolated from human melanoma cells as the autocrine motility factor.[5] ATXα consists of 915 amino acids, the longest isoform, and it is characterized by a 52-amino acid insertion in the central catalytic domain.[4, 57] ATXα exhibits the lowest expression levels of all isoforms, both in the central nervous system and the peripheral tissues. ATXβ was originally cloned from a teratocarcinoma cell line, and it is the best studied isoform that is identical to plasma lysoPLD.[4, 7] ATXβ consists of 863 amino acids and is the most abundant isoform that is highly expressed in the peripheral tissues. Virtually all studies on ATX use this isoform.[38] A third isoform, ATXγ, was identified as an ecto-phosphodiesterase I/nucleotide pyrophosphatase (PD-Iα).[4, 23] ATXγ contains 888 amino acids and is mostly expressed in the central nervous system with low expression in the peripheral tissues.[57] ATXγ lacks the same 52-residue insertion found in ATXα although contains an additional 25 amino acids in the NUC domain of the protein. ATXδ is made up of 859 amino acids and has a four-amino acid deletion in the L2 linker region of ATXβ. ATXδ was found to be the second major isoform following ATXβ, and it has very similar biochemical characteristics to ATXβ. Finally, ATXε consists of 911 amino acids and is a less abundant isoform such as ATXα.[4] ATXε is characterized by insertion of 52 amino acids in the catalytic domain, similar to ATXα, along with the four-amino acid deletion in the L2 linker region (Figure 2-3). Overall, all ATX isoforms exhibit similar activities of lysoPLD and substrate preferences.[38] Currently, it is unclear whether any of the ATX isoforms have unique physiological or pathophysiological functions.

In fact, five ATX isoforms and their tissue distribution have been determined in human

and mouse. ATXβ is the most abundant isoform, and it is identical to plasma lysoPLD. All current understanding of ATX is derived from studies of ATXβ; however, all ATX isoforms reveal the same lysoPLD activities and substrate preferences.

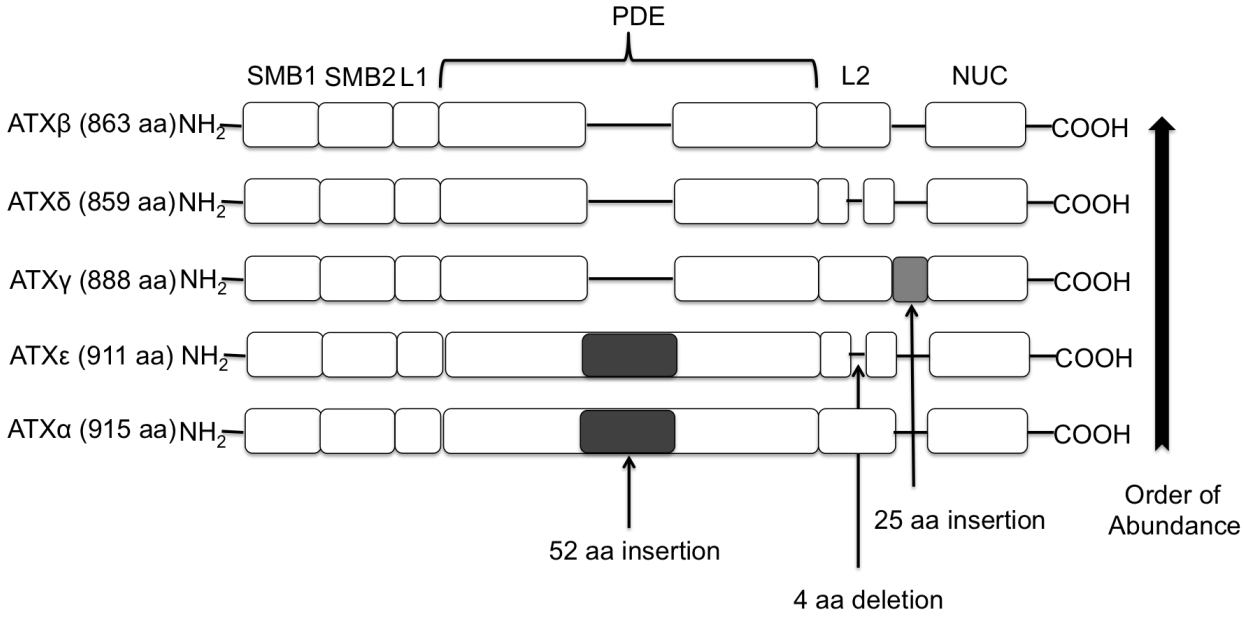

Figure 2-3: Schematic representation of ATX isoforms: α, β, γ, δ, and ε. (Adapted from[4])

2.8 The Catalytic Mechanism of ENPPs

As mentioned previously, the ATX enzyme is one of the members of the widely distributed ENPPs family.[6, 8] These enzymes are known to hydrolyze both pyrophosphate bonds and phosphodiester bonds to produce monophosphate.[59] It has been suggested that the catalytic domain of ENPPs has a similar structure to the superfamily of phosphor- or sulfo-related metalloenzymes, including alkaline phosphatases.[2, 43, 60] The comparison of sequence with alkaline phosphatase indicates that the catalytic mechanism of ENPPs is similar and occurs in two stages. In the first stage of catalysis, an active hydroxyl group (OH) in the catalytic site

residue (Thr210 nucleophile in the case of ATX/ENPP 2) attacks the phosphate group of the LPC substrate, leading to the formation of a covalent phosphate ester linkage intermediate (Scheme 2-2). In the second stage of catalysis, the enzyme intermediate undergoes attack by water and loss of the choline, leading to the release of the phosphorylated compound LPA.

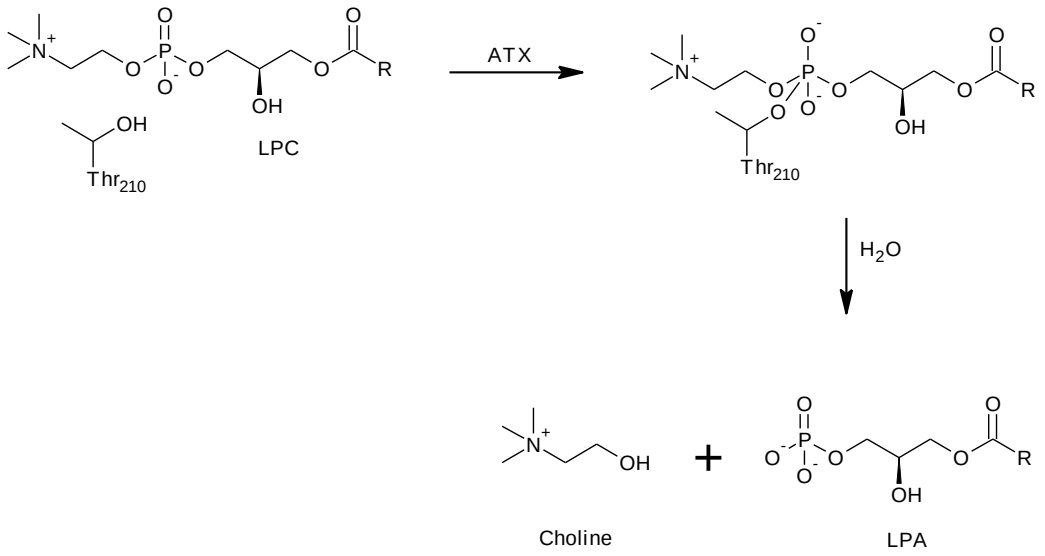

Scheme 2-2: Hydrolysis of LPC by ATX.

2.8.1 Production of LPA by Autotaxin

Generally, ATX is responsible for production of most of the LPA in the blood.[55] It has been found that ATX acts as an extracellular lysoPLD that transforms LPC, the main substrate of ATX, into LPA and choline.[6] LPA is a bioactive form of lysophospholipid that activates cell proliferation, cell survival, migration, and angiogenesis of various cells through activation of GPCRs (Figure 2-4).

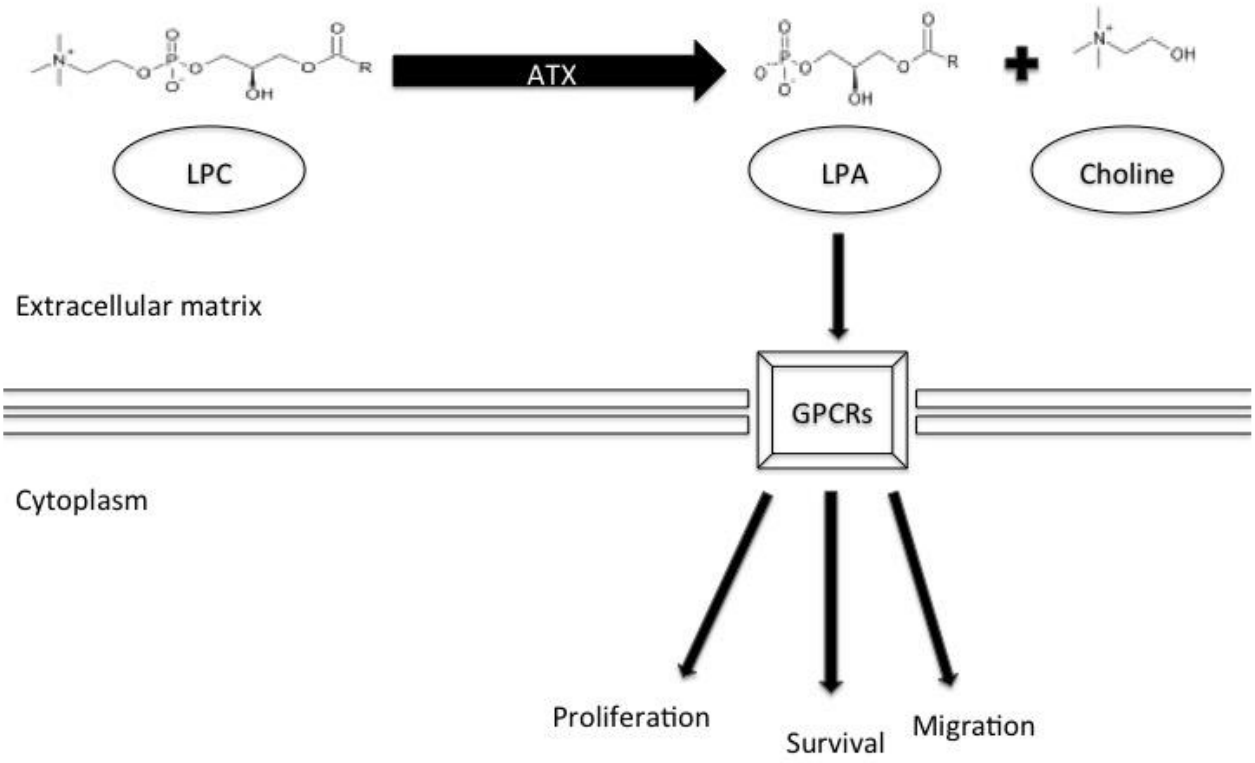

Figure 2-4: ATX is Responsible for Hydrolyzing LPC into LPA and Choline in an Extracellular Environment. (Adapted from[17, 36])

2.9 Lysophosphatidic Acid

Lysophosphatidic acid (1-acyl-glycerol 3-phosphate; LPA) is a simple, natural phospholipid that is composed of a phosphate, a glycerol, and a fatty acid[8, 9] (Figure 2-5). Originally, LPA was known as an intermediate for de novo lipid membrane biosynthesis. Later, it was recognized as an intracellular lipid mediator that stimulates different cellular functions in several cell types. LPA is involved in numerous biological actions, including smooth muscle contraction, platelet aggregation, stimulation of cell proliferation, migration, survival,

angiogenesis, and chemotaxis.[8, 9] It has also been shown to prevent apoptosis. In addition, LPA can be found in different biological fluids, such as plasma, serum, seminal fluid, cerebrospinal fluid, saliva, and urine, both in humans and animals.[8] LPA is present in human plasma at a concentration of about 0.1 μM.[61, 62]

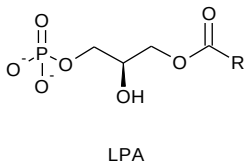

LPA

Figure 2-5: Chemical structure of lysophosphatidic acid, LPA.

2.9.1 LPA Production

At least two pathways are hypothesized for LPA production.[51, 61, 63] In the first pathway, lysophospholipids (LPLs) such as lysophosphatidylcholine (LPC), lysophosphatidylethanolamine (LPE), and lysophosphatidylserine (LPS) are formed by secretory phospholipase A_2 group IIA ($sPLA_2$-IIA) and phosphatidylserine-specific phospholipase A_1 (PS-PLA_1) in the platelets, whereas LPC is generated from phosphatidylcholine (PC) in lipoprotein by lecithincholesterol acyltransferase (LCAT) and phospholipase A_1 (PLA_1)-like enzymes in the plasma. LPLs thus produced are subsequently converted to LPA by ATX by its lysoPLD activity. This pathway produces the major amount of the serum LPA. In the second pathway, phosphatidic acid (PA) is first produced from phospholipids (PLs) or diacylglycerol (DAG) by phospholipase D (PLD) or diacylglycerol kinase (DGK), respectively, and then subsequently converted to LPA by PLA_1 or PLA_2 enzymes. However, this pathway produces only a small amount of LPA that contributes to its serum production.[61] Therefore, ATX is significantly associated with formation of LPA in serum in the first pathway, and it is the enzyme that

displays lysoPLD activity in blood; thus, it can be concluded that ATX is the major enzyme of LPA production in serum.

2.9.2 LPA Receptor Diversity and signalling

LPA exerts its various actions through GPCRs that are specific for LPA.[8, 51] At least six GPCRs for LPA receptors (LPA_{1-6}) have been recognized and can be classified into two subgroups, depending on their primary structure. The first group is the classical LPA receptors (LPA_{1-3}) that are related to an endothelial differentiation gene (EDG) family such as LPA_1/EDG2, LPA_2/EDG4, and LPA_3/EDG7, and they share about 50 % sequence homology with each other. The second subgroup (LPA_{4-6}) consists of LPA_4/P2Y9/GPR23, LPA_5/GPR92, and LPA_6/P2Y5. These receptors belong to a purinergic receptor (P2Y) family whose members target nucleotides rather than LPLs, and they share about 35 % amino acid identity. Recently, GPR87 and P2Y10 were reported to respond to LPA, although further study is required to validate these observations.

All LPA receptors are coupled with different GPCRs (G_i, G_q, G_s, and $G_{12/13}$) that vary in their tissue distribution and signalling pathways.[8, 64] Specifically, LPA_1 is the first receptor recognized for LPA.[42, 64] LPA_1 is widely distributed in the brain, uterus, testis, lung, small intestine, heart, stomach, kidney, spleen, thymus, placenta, and skeletal muscle in both mice and humans. LPA_1 is known to interact with and activate G_i, G_q, and $G_{12/13}$. Activation of the LPA_1 receptor leads to stimulation of a range of cellular responses such as cell proliferation and survival, cell migration, cytoskeletal changes, Ca^{2+} mobilization, and adenylyl cyclase inhibition. The expression of LPA_2 is more restricted compared to LPA_1. LPA_2 is highly expressed in the kidney, uterus, testis, and leukocytes. Similar to LPA_1, LPA_2 interacts with G_i, G_q, and $G_{12/13}$, and

activation of LPA_2 signalling is associated with cell survival and cell migration. Moreover, LPA_3 is highly distributed in the human heart, testis, prostate, and pancreas as well as mouse lung, kidney, uterus, and testis. LPA_3 can interact with G_i and G_q to stimulate Ca^{2+} mobilization and adenylyl cyclase inhibition. Furthermore, LPA_4 is expressed at a relatively high level in the ovary. LPA_4 couples to G_i, G_q, G_s, and $G_{12/13}$, and mediates an increase in intracellular cAMP levels and Ca^{2+} mobilization. Additionally, LPA_5 is highly distributed in the spleen and small intestine. LPA_5 interacts with G_q and $G_{12/13}$ and mediates stress fiber formation and increased intracellular Ca^{2+} levels and cAMP. In contrast, LPA_6 couples to $G_{12/13}$ and is expressed in hair follicles.[8] LPA_6 was recognized as an important mediator for human hair growth and is a causative gene for human hair loss.[64]

2.10 Pathological Role of Autotaxin with Disease States

The ENPP family can hydrolyze an extensive range of substrates, and they influence multiple physiological processes.[65] It has been observed that dysfunction of ENPP members is involved in the pathophysiology of numerous disease states. Specifically, ATX has been involved in a number of human diseases including obesity, diabetes, rheumatoid arthritis, multiple sclerosis, neuropathic pain, Alzheimer's disease, and cancer.[16] Because ATX and LPA are expressed in various biological fluids, they can be used as potential biomarkers to make predictions about certain diseases.[8] From a clinical point of view, the level of ATX seems to reflect the pathophysiological status in different disorders. In particular, the serum concentration and the activity of ATX are elevated in patients with chronic liver diseases; however, ATX declined in patients with postoperative prostate cancer. Also, Tokumura et al.[66] found that lysoPLD activity elevated gradually in women throughout pregnancy. Further, ATX/lysoPLD activity relatively increased in the peritoneal fluid of patients with ovarian cancer, compared to

the serum lysoPLD activity among healthy individuals.[67] Although ATX can be detected in the urine of nephrosis patients, the serum ATX level is not affected in these patients.[68]

2.10.1 Pathological Role of LPA/ATX in Cancer

One particular area of interest is the relationship between the ATX enzyme and cancer progression. Many studies have investigated the function of ATX-LPA signalling in tumour formation and metastasis since the discovery of ATX as the autocrine motility factor for melanoma cells.[17] Subsequent experiments have identified the potential functions of overexpression of ATX in cancer progression, tumour cell invasion, and metastatic process, which involves the promotion of tumour angiogenesis in several malignant tumour tissues.[8, 19] High expression of ATX has been reported in different forms of tumours, including neuroblastoma, hepatocellular carcinoma, breast cancer, renal cell carcinoma, glioblastoma, lung cancer, B-cell lymphomas, and thyroid carcinoma.[17, 20] Mechanisms regulating ATX expression are complicated and not fully understood. However, increasing evidence points to a critical function of ATX and LPA receptor signalling in cancer.[17] Briefly, high expression levels of ATX and LPA receptors are found in a number of human malignancies. It has been reported in mouse models that overexpression of either ATX or LPA receptors stimulates metastasis and tumour formation, while knockdown has the reverse effect.

Moreover, ATX mediates its effects via production of LPA; overexpression of ATX in cancers leads to elevated local levels of LPA.[4] High LPA levels have been reported in the plasma and/or ascitic fluids of patients who have ovarian and pancreatic cancer, multiple myeloma, follicular lymphoma, and hepatocellular carcinoma. In particular, the serum levels of LPA are elevated by 90 % in patients with ovarian cancers when compared with normal physiological

levels.[20, 69] Also, the ascitic fluids of patients with ovarian cancer have 10 times higher concentrations of LPA than healthy individuals. Furthermore, Yang et al.[28] compared the expression of ATX level between both breast cancer and normal tissues, and they found a correlation between ATX expression and the invasiveness of breast cancer cells. Moreover, Baumforth et al.[70] established that up-regulation of ATX elevated the formation of LPA, which led to improved viability and growth of Hodgkin lymphoma cells, whereas particular down-regulation of ATX led to a decline in LPA levels, and thus, decreased cell survival and growth.

In addition, overexpression of LPA receptors represents a significant function in carcinogenesis, invasiveness, potential of metastasis, and resistance of treatment in many kinds of tumours.[71] Hama et al.[72] demonstrated that LPA and ATX activate cell motility and migration in different cancer cell lines via the LPA_1 receptor. Also, ATX expression facilitates bone metastasis via activation of LPA_1 receptors in cancer cells and silencing of ATX expression decreases bone metastasis in these cells.[73] Another study showed the effect of LPA on human colon cancer cells. Shida and collaborators also demonstrated that colon carcinoma cells highly expressed LPA_1 but exhibited only low expression of LPA_2 and no significant expression of LPA_3.[74] Also, it has found that LPA markedly increased the proliferation, migration and adhesion of colon cancer cells, which play a significant role in cancer progression and metastasis. On the other hand, LPA_2 and LPA_3 are highly expressed in most ovarian cancer cells.[75] In thyroid cells, expression of LPA_2 was elevated three fold in differentiated thyroid cancer in comparison with normal thyroid or goiter.[76]

In summary, ATX plays significant roles in several human diseases, including cancer. High expression of ATX is found in a number of tumour cell types. Subsequent studies have shown that overexpression of ATX and LPA receptors has a significant function in cancer

progression, invasiveness, and metastasis.

2.11 Drugs Targeting Autotaxin

Because ATX has been linked to a number of human diseases, including cancer, obesity, diabetes, rheumatoid arthritis, multiple sclerosis, neuropathic pain, and Alzheimer's disease,[16] ATX has become an attractive pharmaceutical target for developing new therapies. In particular, substantial progress has been carried out toward recognizing ATX as a clinical objective in the treatment of cancer.[16] Therefore, the potential advantages of inhibiting ATX activity for human health have encouraged efforts by a number of research groups in academic institutions and pharmaceutical companies to determine and distinguish inhibitors of ATX enzyme activity. Different chemical categories of ATX inhibitors have been summarized in several review articles.[3, 4, 32]

The first inhibition of the ATX enzyme was determined by using compounds that are known to chelate metals.[16] L-histidine, the first compound showed to inhibit the lysophospholipase D activity of ATX,[4, 77] inhibited ATX-stimulated migration of both human melanoma cells and ovarian carcinoma cells.

2.11.1 Lipid and Lipid-Based Inhibitors of Autotaxin

Many of the initial ATX inhibitors were lipid-like substrate or product analogues.[4, 78] A number of analogues of LPA and S1P have been evaluated as ATX inhibitors. For example, a cyclic phosphatidic acid (cPA), a naturally occurring lipid bound to human serum albumin,[79] is an analogue of LPA in which the sn-2 hydroxy group forms a 5-membered ring with the sn-3 phosphate[80] (Figure 2-6). An analogue of this compound, carba-cPA (Figure 2-7), was found to inhibit ATX activity without activating LPA receptors. It inhibited A2058 melanoma cell

invasion *in vitro* and B16F10 melanoma metastasis *in vivo*. However, this carba-cPA (ccpA) analogue seems to have further cellular targets, for example ccpA also inhibits LPA production by inhibiting RhoA activation.[81]

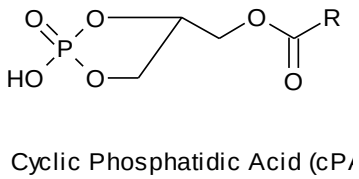

Figure 2-6: Chemical structure of cyclic phosphatidic acid (cPA).

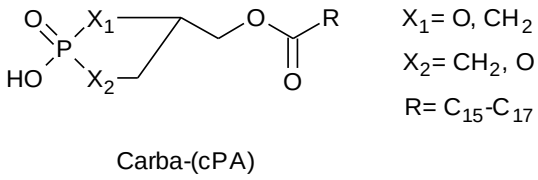

Figure 2-7: Chemical structure of carba analogue of cPA.[80]

Moreover, FTY720, an approved drug for the treatment of relapsing multiple sclerosis,[82] is an analogue of S1P that has been shown to inhibit ATX activity in its phosphorylated form (FTY720-phosphate/FTY-P; Figure 2-8).[4, 32] Van Meeteren et al.[83] have been found that FTY-P is a competitive inhibitor of ATX *in vitro* and did not affect the activity of NPP 1, which is the closest relative of ATX. Once daily oral administration of FTY720 (3 mg/kg) in mice resulted in approximately a 50 % reduction of LPA levels in plasma.[4, 83] These results suggest that FTY720 might exhibit its anticancer effect by targeting ATX-LPA axis.

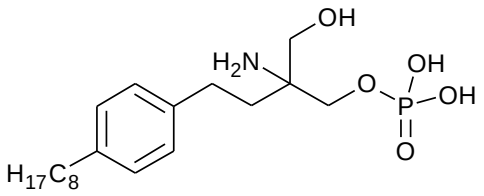

FTY720-P

Figure 2-8: Chemical structure of FTY720-P.[4, 56]

Another example are α-substituted methylene phosphonate analogues of LPA such as the α-bromophosphonate analogue of LPA (BrP-LPA).[4, 16, 32] The *anti*-BrP-LPA (Figure 2-9) and its syn diastereomer exhibited activity at the LPA receptors and inhibited the lysoPLD activity of ATX, with the anti-isomer being more potent.[84] Both isomers significantly reduced tumour volume in breast cancer xenograft models *in vivo*. However, the BrP-LPA displays high hydrophobicity, and it probably exhibits poor distribution across cell membranes.[16]

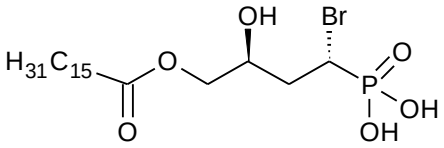

Anti-Bromophosphonate-LPA

Figure 2-9: Chemical structure of Anti-bromophosphonate analogue of LPA.[4, 16]

In fact, many of the early ATX inhibitors were lipid analogues of LPA or other bioactive molecules and were showing potent inhibitory activity of ATX.[4] However, The characteristics of this type of compounds limits their usage as potential lead compounds for drug development.[78] These analogues can act on the ATX enzyme and lead to stimulation of LPA or S1P receptors and initiation of the signalling cascades; therefore, they might have the opposite of their intended outcome.[43] Both LPA and S1P analogues do not display only simple competitive inhibition of

ATX, although they exhibit mixed-type manner of inhibition, they might not interact merely with the active site.[85, 86] Although a number of these analogues show potent inhibitory activity, such derivatives usually suffer from poor solubility and bioavailability due to the presence of a long lipophilic chain, limiting their use for in vivo applications.[4, 32]

2.11.2 Non-Lipid Analogues as Autotaxin Inhibitors

In more recent years, a number of small non-lipid inhibitors have shown more promise. Between these inhibitors, there are great structural differences in both the patent and academic literature, which has been reviewed elsewhere.[3, 4, 32] Among them, a very important class of inhibitors was identified after screening a library of approximately 40,000 drug-like small molecules. A thiazolidinedione-based compound (IC_{50} 2.5 μM) was identified as the most potent ATX inhibitor and was chosen as a lead for further chemical optimization.[4, 87] The potency of the thiazolidinediones is increased dramatically by the introduction of a boronic acid moiety, which was designed to target the oxygen nucleophile of the catalytic Thr residue in ATX. The most potent analogue of these compounds was HA155 (IC_{50} 6 nM; Figure 2-10), which is over 400 times more potent against ATX than the initial screening hit. Also, the crystal structure of rat ATX in complex with the boronic acid inhibitor HA155 indicates that it forms a reversible covalent bond with the Thr209 nucleophile in the hydrophobic pocket of ATX.[4, 35, 88] This compound supports the hypothesis that the boronic acid moiety targets the Thr oxygen nucleophile in the ATX active site (Scheme 2-3), whereas the hydrophobic 4-fluorobenzyl moiety of the inhibitor targets the hydrophobic pocket responsible for lipid binding. Thus, this finding indicates that ATX can be targeted by boronic acids and may also help the development of ATX inhibitors for therapeutic use.

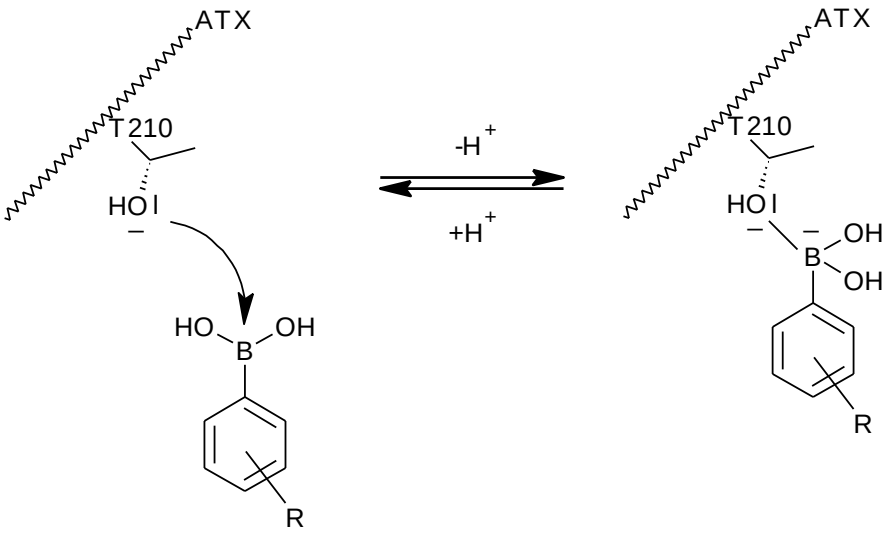

Scheme 2-3: Hypothesized HA155 boronic acid binding to the active site of ATX. (Adapted from[87])

A number of piperidine and piperazine derivatives have also been discovered as ATX inhibitors.[4, 32] The most potent ATX inhibitor among them was PF-8380 (Figure 2-10), which was developed by Pfizer researchers by screening a compound library followed by optimization.[89] PF-8380 has an IC_{50} of 2.8 nM with moderate oral bioavailability ranging from 43 %–83 %. PF-8380 caused more than a 95 % reduction of rat plasma LPA *in vivo* when it was orally administered at a dose of 30 mg/kg within three hours, suggesting that ATX is the main source of LPA during inflammation. Furthermore, at this dose, PF-8380 decreased inflammatory hyperalgesia with a similar efficacy as 30 mg/kg naproxen. Moreover, inhibition of ATX with PF-8380 resulted in reduced invasion and improved response to radiotherapy in glioblastoma cell lines,[90] and pre-treatment of mice with PF-8380 before irradiation significantly delayed the progression of tumour growth *in vivo*.

A virtual screening approach and docking experiments against an ATX catalytic domain homology model identified the pipemidic acid-based inhibitor H2L-7905958.[4, 32] A number of

pipemidic acid derivatives based on this compound were designed, synthesized, and tested against ATX. These studies led to the discovery of an analogue of H2L-7905958 (Figure 2-10) with a meta-trifluoromethyl group that has two-fold greater potency (IC_{50} 0.9 μM) than the lead compound.

Bithionol (Figure 2-10) was determined to be an ATX inhibitor after screening of 960 compounds from the GenPlus library.[4, 32] Bithionol was able to reduce melanoma cell migration and invasion[91] as well as produce a decline in tumour weight in a breast cancer carcinoma model.[16] However, bithionol is highly hydrophobic and probably exhibits poor distribution across cell membranes.

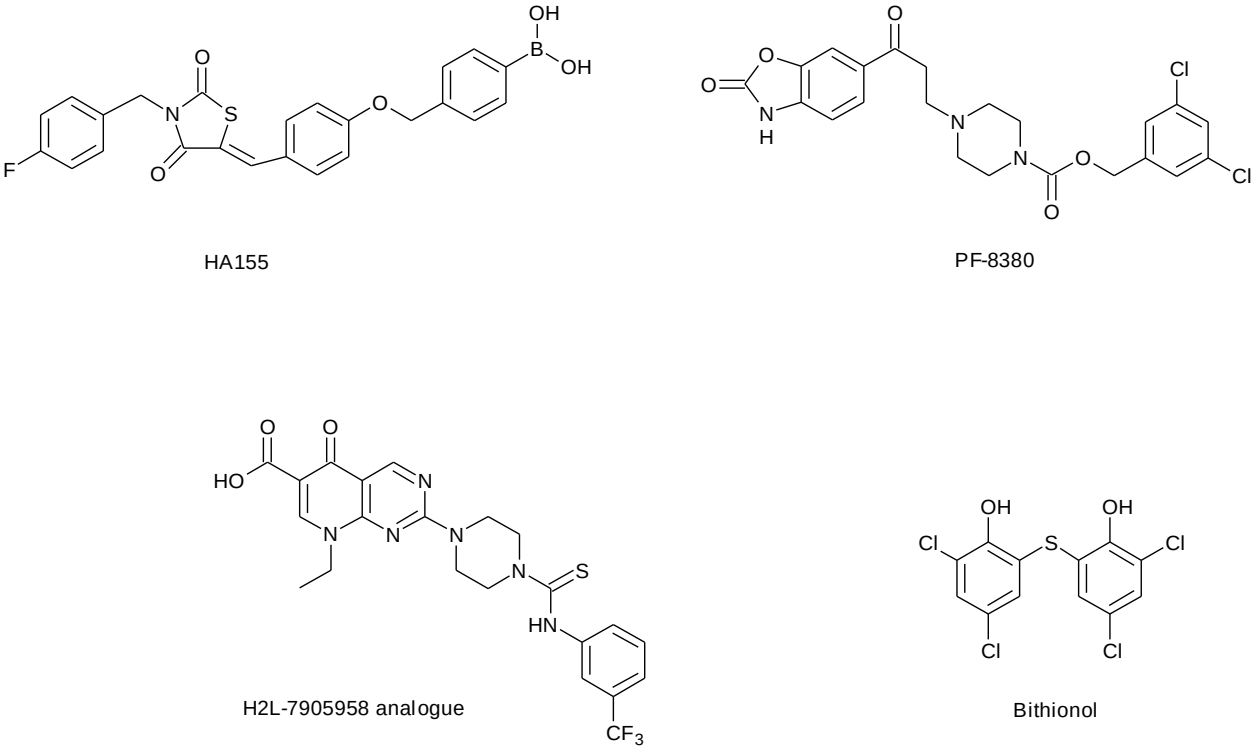

Figure 2-10: Examples of small molecule, non-lipid ATX inhibitors.[4]

To date, GLPG1690, developed by Galapagos, is the only ATX inhibitor that has been reported to proceed into clinical trials (Figure 2-11).[3] GLPG1690 was shown to act as a potent inhibitor for both mouse and human ATX with IC_{50} =224 nM and IC_{50} =131 nM respectively. It has been found to reduce inflammation and displayed high efficacy in a model for chronic obstructive pulmonary disease (COPD).[3] GLPG1690 has successfully completed Phase 1 trial and Galapagos is moving to explore Phase 2 clinical trials for Idiopathic pulmonary fibrosis (IPF).

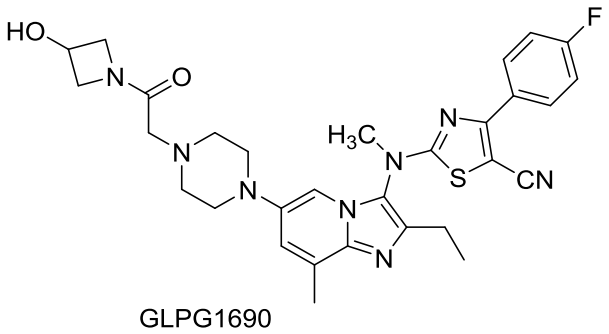

Figure 2-11: Chemical structure of GLPG1690.

2.12 Structure Activity Relationship (Critical Features of Autotaxin Inhibitor)

Initially, numerous LPC analogues were assessed to determine structure activity relationships of ATX substrates[86] because LPC is the main substrate of ATX. Several structural features of LPC (Figure 2-12) were examined to display ATX preference for each modification, thus helping to define ATX substrate recognition. These features involved presence of a choline head group and a polar linker, length and degree of saturation of fatty acid side chain, acyl versus ether linking group of the hydrocarbon chain, and choline oxygen replacement by methylene and nitrogen.

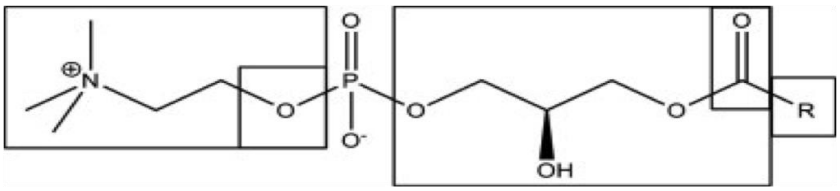

Figure 2-12: Structural features of lysophosphatidylcholine, LPC.

At the beginning, several LPC molecules were examined to investigate which hydrophobic chain length and degree of unsaturation is favorable for ATX. North et al.[86] compared LPC molecules that had 6:0, 8:0, 10:0, 12:0, 14:0, 16:0, 18:0, and 18:1 acyl chains. All of these molecules were evaluated at the same concentrations using the same conditioned media collected from a breast cancer cell culture. North et al.[86] found that 14:0, 16:0, and 18:1 are the optimal substituent chain lengths for LPC compounds as ATX inhibitors. Also, regardless of the length of the hydrophobic chain, ATX shows a preference for an unsaturated tail, yet the location of unsaturation is not important.

In addition, Nishimasu et al.[34] determined the crystal structures of mouse ATX alone and in combination with LPAs that have different acyl-chain lengths and saturations (14:0, 16:0, 18:1, 18:3, and 22:6). The phosphate group, glycerol moiety, and acyl-chain including C1–C12 of LPA are distinguished by the protein in a similar manner in all complexes. One oxygen atom of the phosphate group combines with one Zn^{2+} ion in the protein, whereas the other oxygen atom forms hydrogen bonds with the Asn230 side chain and the OH group and main-chain NH group of the Thr209 residue. The other oxygen atom of the phosphate moiety forms water-mediated hydrogen bonds with Lys208, Asn230, and Asp473. These residues of ATX are highly preserved among the ENPP family enzymes, suggesting that the phosphate group of the substrates is recognized in a similar manner for the ENPP family members. Furthermore, all

ENPP family members, including ATX, revealed maximum activity at pH 8–9, indicating that deprotonation of the Zn^{2+} coordinating residues is essential for the activity. The glycerol moiety of the LPA develops van der Waals interactions with both Thr209 and Leu243 residues, and it forms hydrogen bonds with both Asp311 and Glu308 and its OH group. Similarly, the acyl chain develops van der Waals interactions with Phe210, Leu213, and Tyr306 while it forms a hydrogen bond between its CO group and the OH group of Tyr306.

In combination with ATX-14:0-LPA, the lipid chain is accommodated in the hydrophobic pocket lined by Ile167, Leu216, Ala217, Leu259, Phe273, Trp275, and Met512 residues.[34] The overall structures of the free parts and the complexes are essentially similar, although alteration of a local conformation is detected in the active site. Notably, the side chains of Leu216 and Glu308 twist to accommodate LPA in these complexes. Similarly, in the ATX–16:0-LPA complex, the lipid chain is also accommodated in the hydrophobic pocket. However, when compared to the complex with 14:0-LPA, its electron density is relatively poor. Also, in the complex with 18:0-LPA, the electron density of LPA was not detected, which indicates that it is not bound to the ATX protein in a stable conformation. Therefore, the depth of the hydrophobic pocket is optimum for accommodating the 14:0-LPA lipid tail, and the logical length of the LPC chain of ATX is preferred as 14:0 > 16:0 >18:0. Regardless, in the ATX–18:0-LPA complex, the electron density was observed for LPA in the complexes with 18:1-LPA and 18:3-LPA. The acyl chain of these complexes turns at the unsaturated bonds (C9 = C10 for 18:1-LPA, and C12 = C13 and C15 = C16 for 18:3-LPA) and allows their lipid chain to be accommodated in the hydrophobic pocket. Therefore, these structures revealed that the existence of unsaturated bonds allows the long LPA compounds to be accommodated in the ATX active site consistent with the preference 18:3 > 18:1 > 18:0 for unsaturated bonds of LPC. Finally, in the ATX–22:6-LPA

complex, the longest LPA present in the plasma, the acyl chain turns at an unsaturated bond (C13 = C14) and is lined in a U-shaped conformation in the active site without introducing the lipid tail into the base of the hydrophobic pocket.

After estimating the optimum lengths of LPC chain, the impact of the choline functional group was tested. Both commercially available LPC (with choline head group) and LPA (lacks the choline group; Scheme 2-2) molecules with the same tail lengths, 16:0, 18:0, and 18:1, were identified to inhibit ATX.[86] LPA and its structural analogues can be generalized as having a polar head group, a linkage group, and a hydrophobic chain (Figure 2-13).[92] In all three cases, LPA showed better inhibition than corresponding LPC molecules. This result demonstrated that the presence of the choline head group could damage the recognition of ATX and may lead to destabilizing the substrate complex.

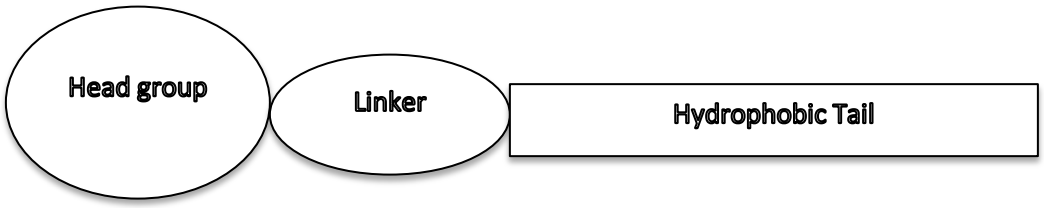

Figure 2-13: Structural regions of LPA and its analogues.

Similarly, the effectiveness of ester versus ether linkages to the hydrocarbon chain was also evaluated by comparing both 16:0 and 18:0 of commercially available lysoPAF (with ether linker) compounds with LPC (with ester linker).[86] As a result, no statistical difference was indicated for ATX inhibition between 16:0 lysoPAF and LPC, and 18:0 lysoPAF and LPC. Thus, the carbonyl functional group is not essential for ATX recognition.

Generally, activation of LPA receptors has been found to be dependent on the fatty acid species. In particular, unsaturated fatty acids of LPAs such as oleic acid (18:1), linoleic acid (18:2), or arachidonic acid (20:4) are more potent in stimulating the LPA receptor and enhancing biological activities than LPA with a saturated fatty acid.[8] Similarly, other studies showed that 1-oleoyl-LPA (18:1), 1-palmitoyl-LPA (16:0), and 1-myristoyl-LPA (14:0) increased the optimal inhibitory effect of LPA for ATX, whereas the LPA with shorter chain (6:0) had no significant effect.[43, 81] This requirement of long acyl chains suggests that LPA and S1P directly interact with a hydrophobic pocket on the ATX enzyme. Therefore, this finding suggests that both LPA and S1P lipids act on the same regulatory site, and ATX is unable to distinguish between LPA and S1P as ligands.

In summary, multiple structural features of LPC and LPA were assessed to determine structure activity relationships of ATX substrates, and the optimal unbranched chain lengths for ATX inhibitors are 14:0, 16:0, and 18:1. Also, ATX shows a preference for the unsaturated tail to allow the lipid chain to be accommodated in the hydrophobic pocket. The choline head group is not required for the recognition of ATX; further, there was no statistical difference between ester and ether linkages to the hydrocarbon chain.

2.13 Enzyme Inhibition

Enzymes have been an important target for therapeutic functions and drug design because of their essential function in biosynthetic pathways; enzyme inhibitors can inactivate a target enzyme or interfere with a specific metabolic pathway.[93] Enzyme inhibitors may reversibly or irreversibly bind to a specific enzyme and inhibit that enzyme in different ways, both *in vivo* and *in vitro*.[94] There have been a number of reversible ATX enzyme inhibitors reported; however,

there are only a limited number of irreversible inhibitors. Irreversible inhibition has an advantage over reversible inhibition; it is comparatively slower because it requires a chemical reaction between the inhibitor and enzyme. Additionally, eliminating or decreasing the concentration of enzyme inhibitors has no significant effect on inhibition activity and synthesis of new enzymes is required. Because we are looking for enzyme inhibitors as an anticancer treatment, irreversible inhibitors are preferred over reversible inhibitors.

There are two main types of irreversible inhibition: nonspecific and specific irreversible inhibition.[94] Nonspecific irreversible inhibition is a simple type of inhibition in which the inhibitor interacts in a direct way with one or more residues on the enzyme, leading to inhibition of the enzyme. This type of inhibitor is not specific to particular types of enzymes, yet it reacts with the side chains of amino acids that have the same reactions in many various enzymes and usually with various residues of the similar enzyme. With specific irreversible inhibition, a non-covalently bound complex between an enzyme and an inhibitor is formed initially, followed by a subsequent reaction to form the irreversibly inhibited enzyme. Typically, the inhibitor binds the enzyme as a substrate, resulting in formation of an enzyme-substrate complex. Then, a reaction takes place within this complex, and finally, an irreversibly inhibited enzyme is produced.

Two forms of specific irreversible inhibitors are known. The first type of inhibitors are usually known as active-site-directed inhibitors (ASDINS).[94] Inhibitors of this type have a chemically reactive group attached to a substrate analogue. Within the enzyme-inhibitor complex, the high concentrations of those groups and residues on the enzyme surface will react together and result in irreversible inhibition. The second type of inhibitors is known as a mechanism-based inhibitor. An inhibitor of this type is not intrinsically reactive; rather, a non-covalent complex is formed between the inhibitor and the enzyme specifically in the active site.

Formation of this bond is followed by a subsequent reaction within that complex that results in formation of a reactive species that reacts with the enzyme to form the irreversibly inhibited species. Furthermore, the inhibitor can exhibit a high extent of specificity to the target enzyme because the formation of the effective inhibitory species formed from the inactive compound includes the catalytic function of the enzyme itself. Also, the absence of the intrinsic reactivity reduces the possibility of undesirable reactions with other tissue constituents.

Additionally, this type of enzyme activity can only be restored by adding more enzymes, but not by adding either products or inhibitors/substrates.[94] This means that recovery from irreversible inhibition requires the synthesis of new enzyme to recover the inhibited enzyme. Generally, the turnover of the enzyme is a dynamic process, and the rate of new enzyme synthesis and removal of the inhibited one is balanced in the cell at any time. The rate of turnover of some enzymes in the liver can have significant implications for scheduling the dosage of irreversible inhibitors for therapeutic usage.[94] Also, the turnover rates of the enzyme can be extremely varied in different tissues from different species.

2.14 Irreversible Inhibitors of Autotaxin

A number of reversible ATX enzyme inhibitors have been reported; however, there are only a limited number of irreversible inhibitors. Specifically, Parrill et al.[95] successfully designed a novel class of compounds to inactivate ATX. Compounds such as mono- and di-fluoromethylphenyl C_{12}-C_{18} phosphodiesters are able to inhibit ATX[95] (Figure 2-14). Inhibition occurs through a mechanism-based process that leads to the development of a reactive species that irreversibly inactivates the ATX enzyme. This reaction has two steps (Scheme 2-4). First, an active group Thr in the catalytic site of ATX attacks the phosphate group of the substrate,

leading to removal of fluoride ion and the formation of a reactive quinone methide (QM). In the second step, the QM reacts with an unknown nucleophilic amino acid side chain (such as lysine, arginine, histidine, aspartate, glutamate, serine, threonine, or cysteine). As a result, the active site is irreversibly modified. Therefore, the production of LPA from LPC, the natural substrate, is prevented.

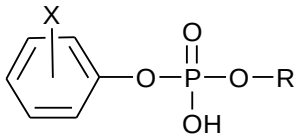

Figure 2-14: Structural formula of inventive compound.
Where R is C_{12-18} alkyl or alkenyl; X is mono- or di fluoromethylphenyl (CH_2F or CHF_2); and it is in either the 2 or 4 position (*ortho*- or *para*-substitution).

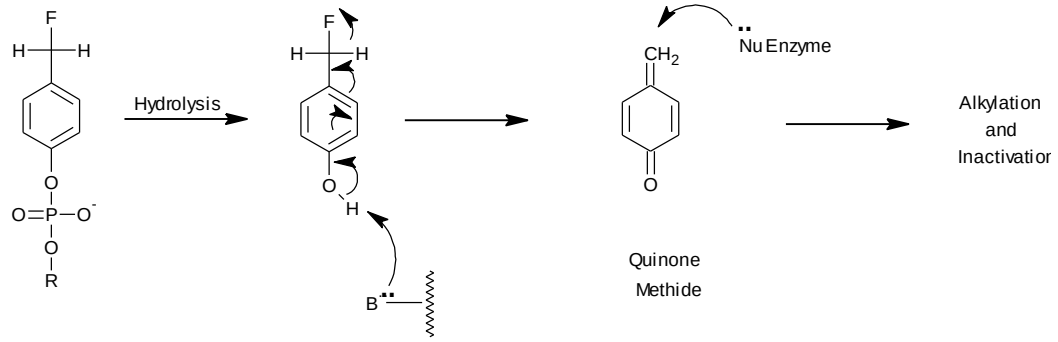

Scheme 2-4: General reaction of inventive compound to inactivate ATX enzyme.[95]

2.15 Autotaxin Degradation/Turnover

Jansen et al.[96] found that ATX is rapidly degraded and cleared from the circulation by the liver through first-pass metabolism. This rapid turnover was unexpected, suggesting that ATX is removed from circulation to a large extent by the liver. This finding is very important and has

significant implications for the development of ATX as an anti-tumour target.

The circulating source and fate of ATX is significant information for examining ATX inhibitors *in vivo* as well as for the rational design of compounds that cause the reduction of ATX circulating levels.[96] The Bollen laboratory has determined the fate of secreted ATX in healthy mice, and it found that the ATX is rapidly cleared from the circulation within minutes by the liver.[96] The experiment showed that about 60 % of injected labeled ATX was maintained in the liver after five minutes, and about 20 % of labeled ATX could still be detected in the blood. Later, the liver-associated radioactivity continued to be reduced, and the amount of labeled ATX decreased after 24 hours. Correspondingly, there was an elevation of radioactivity in the intestine and urine. These results propose that the ATX enzyme is decomposed in the liver because ATX is too large to be filtered by the glomeruli of the kidneys. Indeed, these data strongly propose that the main site of ATX enzyme breakdown is the liver.

In fact, this excessive turnover was surprising and suggests that the ATX enzyme is extensively removed from the circulation through the liver during first-pass metabolism, similar to some hormones such as insulin and glucagon.[96] However, it has been suggested that the ATX enzyme is synthesized regularly at different places that still need to be determined because it can be immediately found in serum. The ATX enzyme is secreted by different cell types such as adipocytes,[10] endothelial cells,[97] and lymphocytes.[98] Therefore, it has been hypothesized that the ATX enzyme is released by different types of cells in serum rather than being produced by one particular kind of tissue. However, the ATX enzyme is also expressed by the liver, indicating that at least part of its synthesis and decomposition is mediated by similar tissue. Additionally, Watanabe et al.[99] have shown that there is an elevation in serum ATX concentration in

hepatectomized rats and rats with liver injury. This finding is consistent with the role of the liver in clearing ATX from the circulation.

CHAPTER 3: PURPOSE OF THE STUDY

3.1 Significance of the Project

ATX-mediated formation of LPA is associated with a number of disease states, including diabetes, obesity, Alzheimer's disease, and various cancers.[16] One particular interest of ours is the relationship between the ATX enzyme and cancer progression. Several studies have implicated the role of ATX–LPA signalling in cancer development and metastasis since the detection of ATX as the autocrine motility factor from melanoma cells. The potential functions of overexpression of ATX in cancer progression, tumour cell invasion, and metastatic processes involving promotion of tumour angiogenesis in several malignant tumour tissues have been frequently identified in subsequent experiments.[8, 19] Because most LPA is produced by ATX activity, an inhibitor of the ATX catalytic site would block subsequent LPA signalling. In fact, inhibition of ATX has been established *in vitro* with numerous compounds that demonstrated promising *in vivo* anticancer properties.[16] Therefore, this would provide an opportunity for introducing new cancer therapies.

There is currently a need to design and synthesize novel, potent, and selective compounds that inhibit ATX. These compounds can provide significant information needed to understand the structural features critical to inhibit ATX for cancer treatment. Previous investigations have determined the importance of ATX-inhibiting compounds having an aryl phosphate or phosphonate moiety, which mimics the phosphate diester of LPC. A cyclic phenol phosphate group structurally mimics the previous aryl phosphate analogues, and it can be hydrolyzed to produce *ortho*-quinone methides ($_O$-QM), which are highly reactive and electrophilic molecules known to modify biological nucleophiles[100] (Scheme 3-1). We propose that inhibition will occur through a mechanism-based process that leads to development of a reactive quinone species that

irreversibly inactivates the ATX enzyme. This pro-drug strategy allows activation to a reactive intermediate that can afford further selectivity for the specific target. In this case, the activating enzyme is also the target for inhibition, potentially providing enhanced target selectivity. Because we are looking for enzyme inhibitors as an anticancer treatment, irreversible inhibitors are preferred over reversible inhibitors.

Our research seeks to prepare and assess a series of cyclic phenol phosphate analogues for their ability to function as irreversible ATX inhibitors. Our research aims to investigate whether pro-drugs that form $_O$-QM can have high selectivity as ATX inhibitors. The proposed cyclic phenol phosphates have not been previously prepared and can thus represent a new orientation for the study of ATX inhibitor analogues and may lead to the development of new treatments for ATX-related human diseases in the future, including cancer.

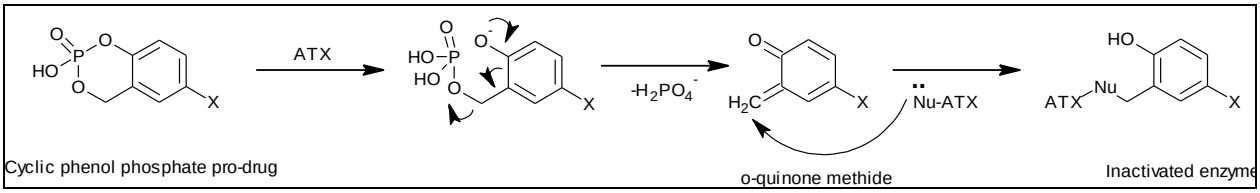

Scheme 3-1: ATX–mediated hydrolysis of cyclic phenol phosphate to $_O$-QM.

3.2 Hypothesis

We hypothesize that cyclic phenol phosphate compounds will inactivate ATX enzyme via covalent modification due to formation of an $_O$-QM mediated by enzyme activation.

3.3 Study objective

The first step toward this goal is synthesizing a series of cyclic phenol phosphate compounds and testing them as irreversible ATX inhibitors.

3.4 Specific Aims for the Objective

To obtain our objective, we outlined the following aims:

1. To synthesize acyl and alkyl ether derivatives of cyclic phenol phosphate compounds.
2. To characterize these compounds by using different techniques such as nuclear magnetic resonance (NMR) and mass spectroscopy (MS).
3. To detect the stability of these compounds.
4. To determine the ability of these compounds to inactivate the ATX enzyme.

CHAPTER 4: METHODOLOGY AND EXPERIMENTS

4.1 Materials/Chemicals

The following chemicals were purchased from Sigma-Aldrich (St. Louis, MO): 4-methoxy-1,3-benzenedimethanol, Boron tribromide (BBr_3) solution (1.0 in methylene chloride), anhydrous Dichloromethane (DCM), Acetic anhydride (Ac_2O), 4-(dimethylamine) pyridine (DMAP), Triethylamine (TEA), Methanol-D4, Deuterium oxide, tert-Butyldimethylsilyl chloride (TBDMSCl), Imidazole, 2-hydroxy-5-methoxybenzaldehyde, Phosphorus (V) oxychloride ($POCl_3$), Dimethyl sulfoxide (DMSO), Salicylaldehyde, 2,5-dihydroxybenzaldehyde, 2,2-dimethoxypropane, *p*-Toluenesulfonic acid (*p*TsOH), Tetraethylammonium fluoride, 1-bromotetradecane, and Hydrogen chloride (HCL) solution 4.0 M in dioxane. Ethyl acetate (EtOAc), Petroleum Ether (PE), DCM, Chloroform, Methanol (MeOH), Ethanol (EtOH), Hexane (Hex), Hydrochloric acid (HCl), Magnesium sulfate ($MgSO_4$), Potassium carbonate (K_2CO_3), Sodium borohydride ($NaBH_4$), Celite™ 545 Filter aid and sea sand used in the flash columns were obtained from Fisher Scientific (Fairlawn, NJ). Chloroform-D and Dimethyl sulfoxide-D6 were obtained from Cambridge Isotope Laboratories Inc. (Andover, MA). Potassium hydroxide (KOH) was obtained from BDH Chemicals (Toronto). Sodium bicarbonate ($NaHCO_3$) and silica gel 60 (0.040-0.063 mm) used in flash columns were obtained from EMD Chemicals Inc. (Gibbstown, NJ). Benzyl bromide and Tetrahydrofuran (THF) extra dry was obtained from ACROS. Formic acid was obtained from EASTMAN KODAK CO. Tris Hydrochloride was obtained from EM science. Perchloric acid was obtained from GFS Chemical CO. HPLC runs were done with HPLC grade water and acetonitrile that were obtained from Fisher Scientific (Fairlawn, NJ).

4.2 Equipments/Instrumentation

TLC aluminium sheets were coated with silica gel 60 F254 purchased from Merck. Rotary evaporator systems consisted of Büchi heating bath B-490, Büchi Rotavapor R-200, and Büchi v700 vacuum pump with attached v850 vacuum controller. Samples in test tubes were concentrated using Eppendorf Concentrator 5301 with Büchi Vac V-700 with attached v850 vacuum controllers. Trace amounts of solvent and moisture were removed using a Trivac High Vacuum Pump. Vortexed reactions utilized a VWR Scientific Products mini vortexer. Water was purified with a Millipore Milli-Q system with a Quantum TEX Cartridge (Mississauga, ON). Incubations took place in a Boekel Grant ORS 200 shaking heating water bath, Freeze drier from Labconco. The pH adjusted by pH meter from VWR Scientific Products. High Performance Liquid Chromatography-Ultraviolet system consisted of an Agilent Series 1200 quaternary pump (G1311A) with online degasser (G1322A), autosampler (G1329A) and photodiode array detector (G1315D) (Agilent Technologies, Mississauga, ON). Analytical column was a 150 × 3 mm Hypersil GOLD phenyl, 5 µ particle size column (Thermo scientific). The HPLC system was controlled by, and data was processed using ChemStation software (Agilent Technologies, Mississauga, ON). NMR experiments were performed on a Bruker AVANCE DPX-500 spectrometer, and data processed by TopSpin 3.2 software. All compounds were drawn and named using ACD/ChemSketch. MS experiments were conducted using AB SCIEX 4000 QTRAP (AB SCIEX instruments) quadrupole linear ion trap mass spectrometer coupled to an Agilent 1100 system consisting of an Agilent 1100 G1311A pump and an Agilent 1100 G1329A autosampler (Agilent Technologies, Mississauga, ON). Data acquisition and analysis was performed using Analyst 1.5.1 software from AB SCIEX. Docking experiments were performed

on Molecular Operating Environment (MOE) software (2014.09) from the Chemical Computing Group.

4.3 Specific Aim 1

4.3.1 Synthesis of Acyl Derivatives of Cyclic Phenol Phosphate Analogues

We have proposed that cyclic phenol phosphate analogues will be prepared by modification of an existing synthetic strategy utilized in the preparation of vitamin B6 analogues.[101] Synthesis of the acyl analogues requires several steps that will provide a general route to this group of analogues (Scheme 4-1). These steps involve deprotection of an alcohol group of a commercially available starting material, followed by protection of the alcohol groups, addition of phosphoryl chloride, cyclization of the phosphate mediated by a base, and esterification using acyl chloride with different side chains (C_{14}, C_{16}, and C_{18}).

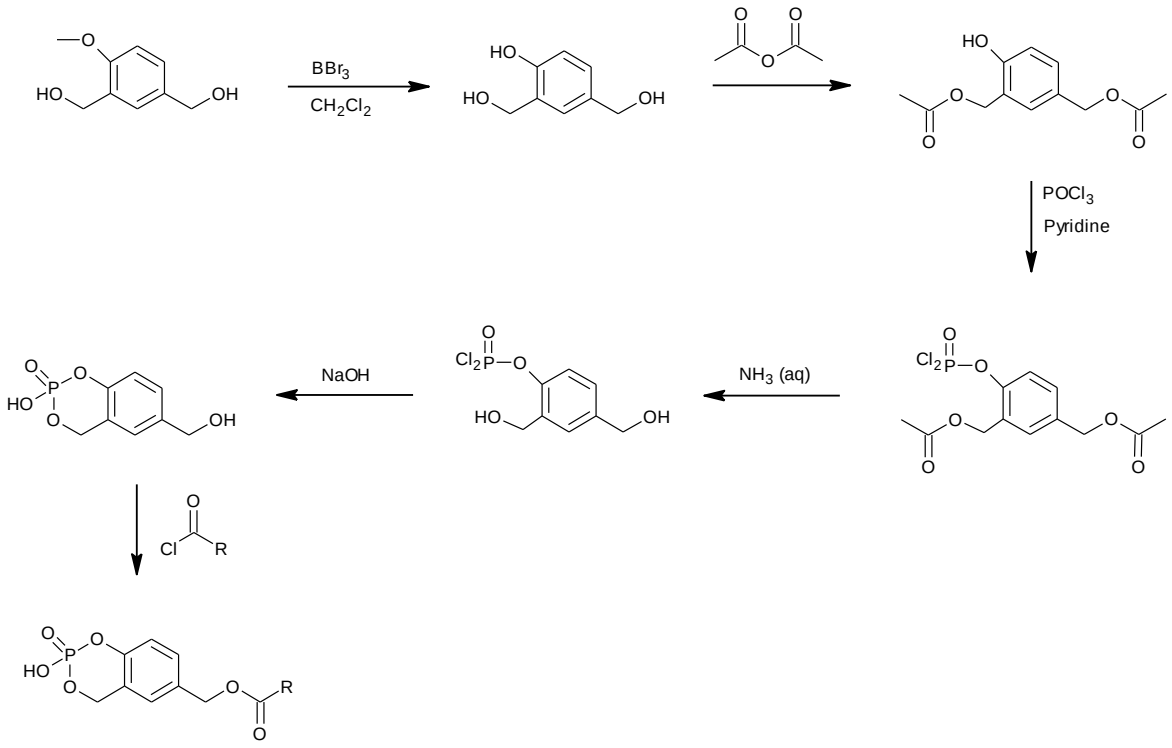

Scheme 4-1: Proposed synthetic scheme for the preparation of acyl derivatives. Where R is ($C_{14, 16,18}$)

4.3.1.1 Demethylation Step[102, 103]

The first step for synthesis of acyl derivatives of cyclic phenol phosphate analogues is the demethylation step. Under a nitrogen atmosphere, compound **1** (4-methoxy-1,3-bezenedimethanol) was dissolved in anhydrous CH_2Cl_2 and the solution was cooled either to -78 °C or 0 °C. BBr_3 (1 M solution in CH_2Cl_2) was added to the cooled solution carefully via a syringe, and the mixture was stirred for two hours. After warming to room temperature (RT), water was added to quench the reaction, and the solution was extracted with DCM. The combined organic layers were washed with 10 % sodium bicarbonate, 1 M HCl, and water. The resulting solution was dried over magnesium sulfate. After filtration, the solvent was removed under vacuum and purified by flash column chromatography over silica (2:1 EtOAc\PE).

4.3.2 Synthesis of Alkyl Ether Derivatives of Cyclic Phenol Phosphate Analogues

We have proposed that a different starting material than the one shown in Scheme 4-1 for the acyl analogues is required to synthesize the alkyl ether analogues (Scheme 4-2). This process involves selective methylation of the hydroxyl group, followed by introduction of the alkyl ether moiety. Next, deprotection of the alcohol group will be carried out before introducing the phosphate group in a similar manner to the acyl derivatives. The length of the carbon side chain (R) will vary from fourteen to eighteen carbons in length (C_{14}, C_{16}, and C_{18}), even though a shorter chain will be prepared to estimate solubility in the determination of aqueous stability. Alkyl bromides will be purchased where available.

All compounds will be analyzed and identified by techniques including, nuclear magnetic resonance (NMR) and mass spectroscopy (MS).

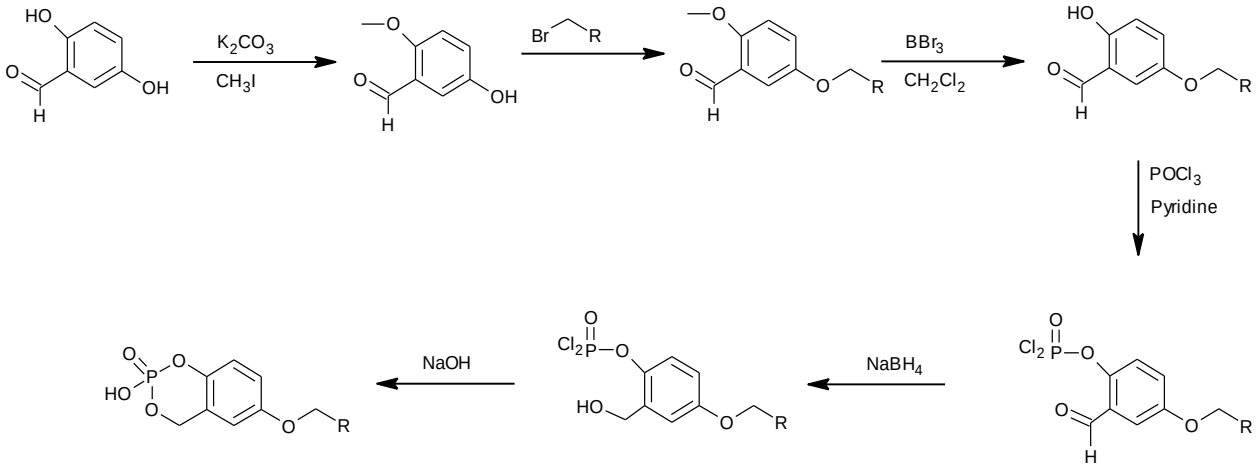

Scheme 4-2: Proposed synthetic scheme for the preparation of alkyl ether derivatives. Where R is ($C_{14, 16,18}$)

4.4 Specific Aim 2

We will verify the stability of the cyclic phenol phosphate compounds in aqueous solution. The synthesized compounds (0.1 mM) will be incubated in 50 mM TRIS buffer pH 8.0 at 37 °C.[104] Reversed-phase high performance liquid chromatography (RP-HPLC) will be used to determine any loss of starting material and forming of decomposition products.[105] The identification of decomposition products will be determined through HPLC and NMR. We will also determine the stability of the shorter chain analogues. If stability is pH dependent, the stability of the longer chain analogues will be determined at the pH where the stability is observed. In addition, solubility of the longer chain analogues will be determined by dilution in 50 mM TRIS buffer (pH 8).

4.4.1 Stability Study Determination

The synthesized compounds in DMSO (50 mM) and internal standard (KA-1-09-2; Figure 4-1) in ACN (50 mM) were added to TRIS buffer (50 mM, pH 8.0) and vortexed for 5 seconds to give final concentrations of 0.1 mM each. The mixture was incubated in sealed containers at 37 °C in the Boekel Grant ORS 200 shaking heating water bath for 5 minute. Aliquots (300 µl) were taken at various time intervals (0 h, 3 h, and 6 h), and samples were analyzed directly by HPLC. Test compounds were verified by the elution time of standards and quantitated by their corresponding standard curves. All eluates were monitored by photodiode array detection, and runs were monitored at 280 nm. Peak areas were calculated and product reported as the ratio of the area of compound/internal standard. The experiment was run in triplicate and the data are reported as the mean ± standard error.

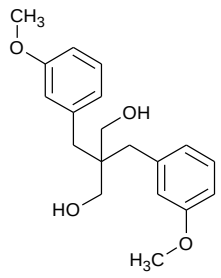

Figure 4-1: Structure of KA-1-09-2 used as the internal standard.

4.4.2 High Performance Liquid Chromatography Analyses

A reverse phase high performance liquid chromatography (RP-HPLC) method was developed to determine purity of the prepared analogues and any loss of starting material and forming of decomposition products. The internal standard was run alongside for comparison (KA-1-09-2; Figure 4-1). The RP-HPLC method employed a 150 × 3 mm Hypersil GOLD phenyl, 5 µ particle size column (Thermo scientific) at a flow rate of 1 ml/min using gradient elution. Solvent A consisted of water with 0.1 % formic acid, and Solvent B was acetonitrile containing 0.1 % formic acid. The HPLC grade acetonitrile and formic acid were filtered through a 0.45 micron filter, whereas Millipore water was used without further purification. Both solvents were sonicated and degassed prior to use. A gradient of 85 % A for 2 min, decreased to 15 % A over 5 min, held isocratic for 1 min, returned to 85 % A in 2 min, and held isocratic for 3 min. The HPLC gradient outlined in Table 4.1 was used to detect and separate compounds. All eluates were monitored by photodiode array detection at 280 nm.

Table 4-1: HPLC gradient program employed for the separation of analogues.

Time (min)	% Solvent A*	% Solvent B**	Flow rate (mL/min)
2.00	85	15	1.00
7.00	15	85	1.00
8.00	15	85	1.00
10.00	85	15	1.00
13.00	85	15	1.00

A* water with 0.1 % formic acid
B** acetonitrile with 0.1 % formic acid

4.5 Specific Aim 3

To determine the ability of the cyclic phenol phosphate compounds to inactivate ATX enzyme, ATX inhibition assays will be carried out as described earlier by our colleagues at the University of Memphis.[54, 78, 86]

4.5.1 Autotaxin Inactivation Analysis

The effectiveness of these analogues will be determined by estimating ATX-mediated hydrolysis of the synthetic LPC analogue FS-3 at certain excitation and emission wavelengths resulting from cleavage of FS-3 by ATX.[95] Briefly, the test protocol will be as follows: ATX inhibition will be determined by using the synthetic substrate FS-3 (Echelon Biosciences, Inc., Salt Lake City, Utah, USA) and concentrated conditioned serum-free medium (CCM) from MDA MB-435 cells as the source of ATX in an assay buffer of (1mM $MgCl_2$, 1mM $CaCl_2$, 5mM KCl, 140mM NaCl, 50mM Tris, pH 8.0). The assay will be performed in 96 well plates in a Synergy-2 plate reader (BioTek, Winooski, Vt.) using LPA as a control. The fluorescence will be measured at excitation and emission wavelengths of 485 and 538 nm, respectively, after

incubation at 37 °C. The data will be normalized to the vehicle control and mean ± standard deviation of triplicated wells will be expressed as a percentage of ATX activity.

4.6 In Silico Docking Studies with Autotaxin

Docking, a computer simulation modeling the interaction between a receptor active site and a ligand, is a significant tool in structure-based drug design.[44] The technique of docking depends on positioning the ligand in various conformations and orientations within the binding site in order to determine optimum binding geometries and energies. Herein, we performed the docking study by using Molecular Operating Environment (MOE) software from the Chemical Computing Group for docking some compounds into ATX. The MOE searches for favorable binding conformations between the ligand and a molecular target, which is usually a protein.[44] Several conformations called "poses" are produced and scored for each ligand. Typically, scoring function indicates favorable hydrophobic, ionic, and hydrogen bond contacts. For good results of docking, low scores must be assigned to good poses.

The crystal structure of mouse ATX with PDB ID: 3NKM and 2.0 Å Resolution was chosen for the docking study. Active site 1 containing the key residue Thr209 was isolated for this docking study (Figure 4-2). A number of ligands were docked to the active site of the ATX enzyme to assess their binding affinity. Ligands consist of (a) LPA with different long side chains (14:0, 16:0, and 18:0) as standard; (b) our synthesized analogues **A1** and **A2**; (c) the proposed alkyl ether derivatives of cyclic phenol phosphate analogues with different long side chains (C_{14}, C_{16}, and C_{18}); (d) the proposed acyl derivatives of cyclic phenol phosphate analogues (C_{14}, C_{16}, and C_{18}); and (e) the mono-fluorophosphodiesters (C_{14}, C_{16}, C_{18}) compounds synthesized by our collaborators as ATX irreversible inhibitors.

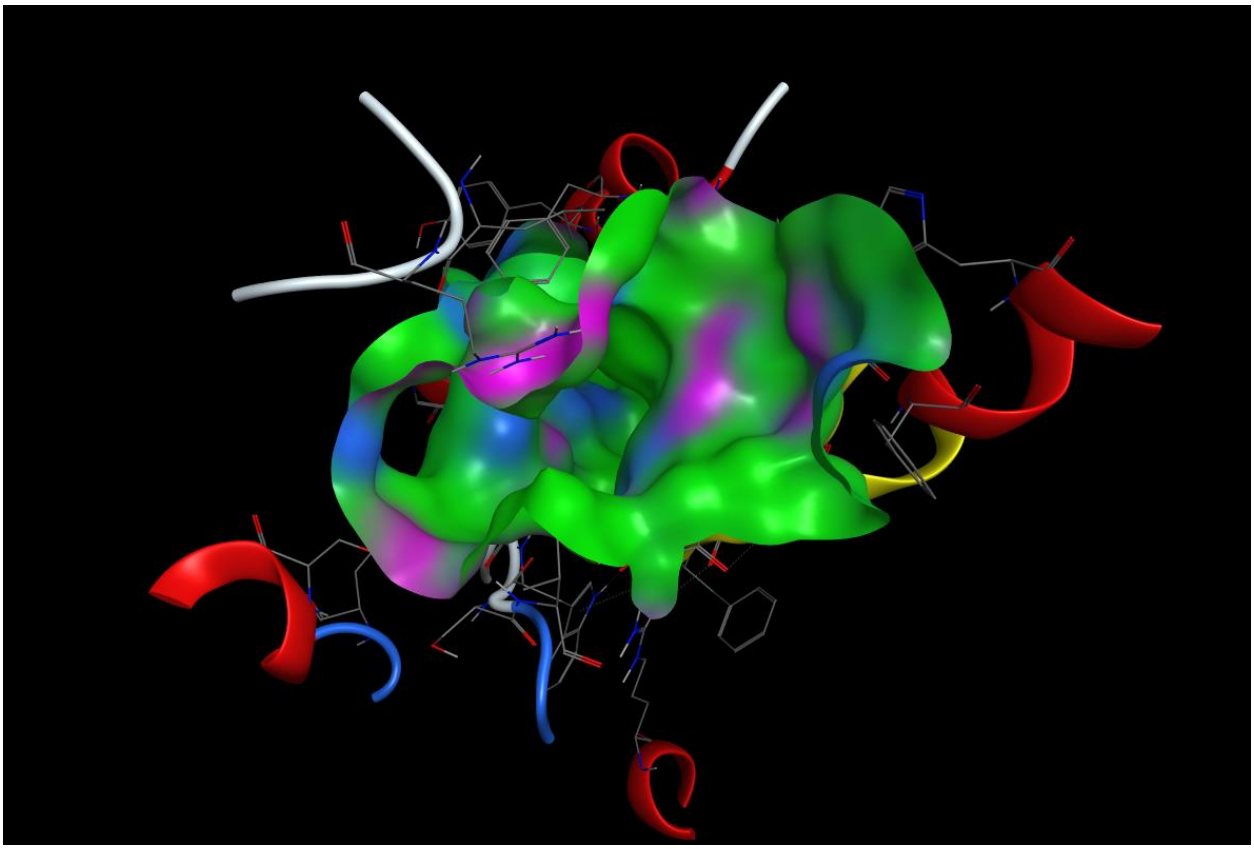

Figure 4-2: The structure of free active site 1 of ATX enzyme (PDB ID: 3NKM at 2.0 Å Resolution).

CHAPTER 5: RESULTS AND DISCUSSION

In order to meet our objective of evaluating cyclic phenol phosphates as ATX inhibitors *in vitro*, we first needed to prepare the novel cyclic compounds. Due to the simple chemical structure of LPA and its effects in cancer, it has attracted the attention of the cancer therapeutics field, and initial studies on the development of therapeutics have typically been based on the LPA scaffold.[71] Therefore, we designed our compounds to mimic LPA-based inhibitors of ATX.[4, 32, 33, 56] Previous studies on ATX inhibitors have suggested that the linker between the aromatic ring and the alkyl chain can be either an acyl or an alkyl ether, and the optimal unbranched chain lengths for ATX inhibitors are 14:0, 16:0, and 18:1.[86] Thus, we proposed two synthetic methodologies that can yield cyclic phenol phosphates with either an acyl (Scheme 4-1) and an alkyl ether linkage (Scheme 4-2). The proposed synthetic analogues of three acyl and three alkyl ether derivatives of cyclic phenol phosphate with side chains of different lengths (C_{14}, C_{16}, and C_{18}) are shown in Figure 5-1 and Figure 5-2, respectively. They have been proposed for the purpose of studying their ability to inhibit ATX.

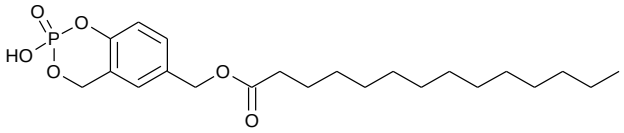

Acyl cyclic phenol phosphate (14:0)

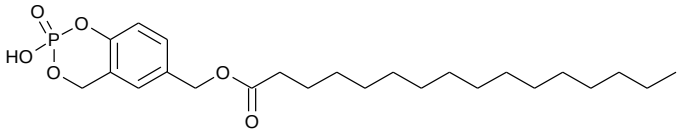

Acyl cyclic phenol phosphate (16:0)

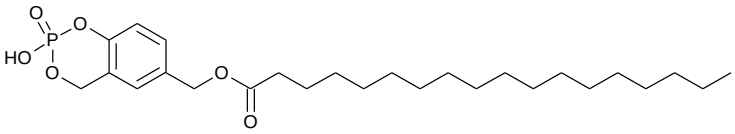

Acyl cyclic phenol phosphate (18:0)

Figure 5-1: Proposed synthetic analogues of acyl cyclic phenol phosphate.

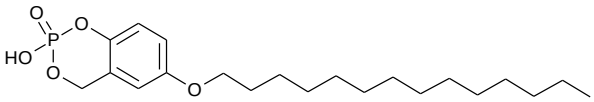

Alkyl ether cyclic phenol phosphate (14:0)

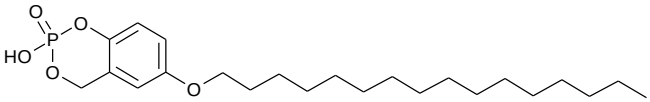

Alkyl ether cyclic phenol phosphate (16:0)

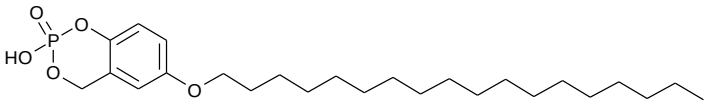

Alkyl ether cyclic phenol phosphate (18:0)

Figure 5-2: Proposed synthetic analogues of alky ether cyclic phenol phosphate.

Different starting materials are required for the two approaches, as outlined in Scheme 4-1 and Scheme 4-2. Our strategy was to develop methods that would allow us to easily incorporate different substituents on our cyclic phosphate scaffold and thereby provide a route to explore structure-activity effects of the side chain. All of the reactions performed in the synthesis of the cyclic phenol phosphates analogues described herein were carried out several times.

5.1 Attempted Synthesis of Acyl Derivatives of Cyclic Phenol Phosphate Analogues

5.1.1 Demethylation Reaction

The commercially available compound **1** (4-methoxy-1,3-bezenedimethanol) was used as the starting material for synthesis of acyl derivatives of cyclic phenol phosphates. The strategy we employed for synthesis of acyl derivatives of cyclic phenol phosphates was to convert the methoxy group into a hydroxyl group by dealkylation, which would then allow for construction of the cyclic phosphate portion of the analogue and provide an easy route to multiple acyl derivatives (Scheme 4-1). The O-dealkylation of ethers remains a basic functional group conversion, mainly as a deprotection method to unmask the hydroxyl group.[106] We utilized BBr_3, a Lewis acid, which is a potent reagent for dealkylation of ethers and is well known for deprotecting methyl aryl ethers.[107, 108] Consequently, we attempted demethylation of the methyl group at position C4 of the aromatic ring of compound **1** using BBr_3. The mechanism of action of BBr_3 for the O-demethylation step is shown in Scheme 5-1. The reaction proceeds via formation of a complex between the boron of the reagent and the ether oxygen atom.[108] The alkyl aryl ether then cleaves at the alkyl oxygen bond, resulting in ArOH and alkyl bromide.

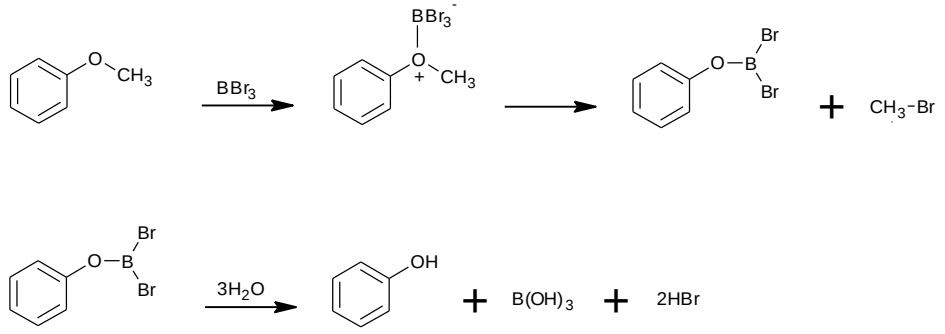

Scheme 5-1: Mechanism of Action of BBr_3 for O-demethylation.[108]

Our initial attempt at demethylation (1:1 BBr_3/**1** (CH_2Cl_2), -78 ^oC) was unsuccessful, resulting in only starting materials (Scheme 5-2). We hypothesized that the alcohol groups interfered with the demethylation, possibly by complexation of the BBr_3, as shown in Figure 5-3. Loman et al.[109] found that problems are encountered and poor yields are obtained with attempts to demethylate nonadjacent methoxy groups or on one aromatic ring, and when a stable chelate is formed. Subsequent attempts with increased ratios of BBr_3 were similarly unsuccessful, although these reactions produced a mixture of unidentified products. To more fully explore this issue, we repeated the demethylation step under increased temperature, different reaction times, and different ratios of starting materials to BBr_3 as shown in Table 5-1. None of these reactions yielded the expected product. In an effort to overcome this issue, we decided that the two hydroxyl groups of **1** should be masked by different protecting groups prior to the dealkylation step.

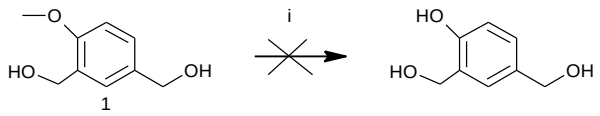

Scheme 5-2: Unsuccessful attempts of demethylation of compound **1**.

Reagents and Conditions: i) BBr_3/DCM, -78 ^{O}C or 0 ^{O}C.

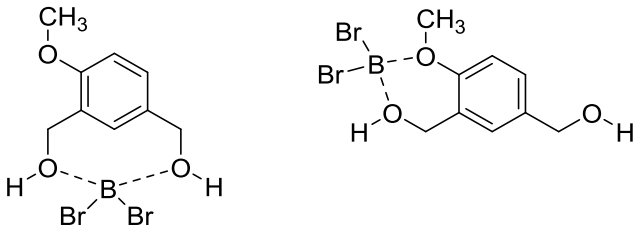

Figure 5-3: Potential BBr_3–starting material interactions.

Table 5-1: Demethylation of different compounds under various conditions.

Compound no.	Mole Comp: BBr_3	Time (h)	Starting Temp (^oC)	Result
1	1:1	2	-78	NMR showed no change in starting material
1	1:1	1	-78	No change in starting material
1	1: 2.5	2	-78	NMR showed unidentified products
1	1: 3.5	2	-78	NMR showed unidentified products
1	1: 3.5	0.5	0	NMR and MS showed unidentified products
1	1:4	2	0	NMR showed unidentified products
1	1:5	1	0	NMR showed unidentified products
2	1: 2.5	2	-78	NMR showed unidentified products
2	1: 2.5	2, 7, 20	-78	NMR showed unidentified products
2	1: 3.5	2	-78	NMR showed unidentified products
2	1: 3.5	2	0	NMR showed unidentified products
3	1: 3.5	2, 4	0	NMR showed unidentified products
4	1:5	4	0	NMR showed unidentified products
4	1:5	1.5	0	NMR showed unidentified products
4	1:10	2	0	NMR showed unidentified products

5.1.2 Acetyl Protection[110]

Protection of the two hydroxyl groups of compound **1** via acetylation was performed. Acetylation with Ac_2O, DMAP, and TEA at RT afforded an acetylated compound **2** as yellow oil (83.74 %) (Scheme 5-3). The product was analyzed using NMR techniques, and the NMR

spectrum of protected compound **2** is shown in Figure 5-4. However, the demethylation of the compound **2** with different ratios of BBr_3 at low temperature (Table 5-1) gave unidentified products, as shown in Figure 5-5.

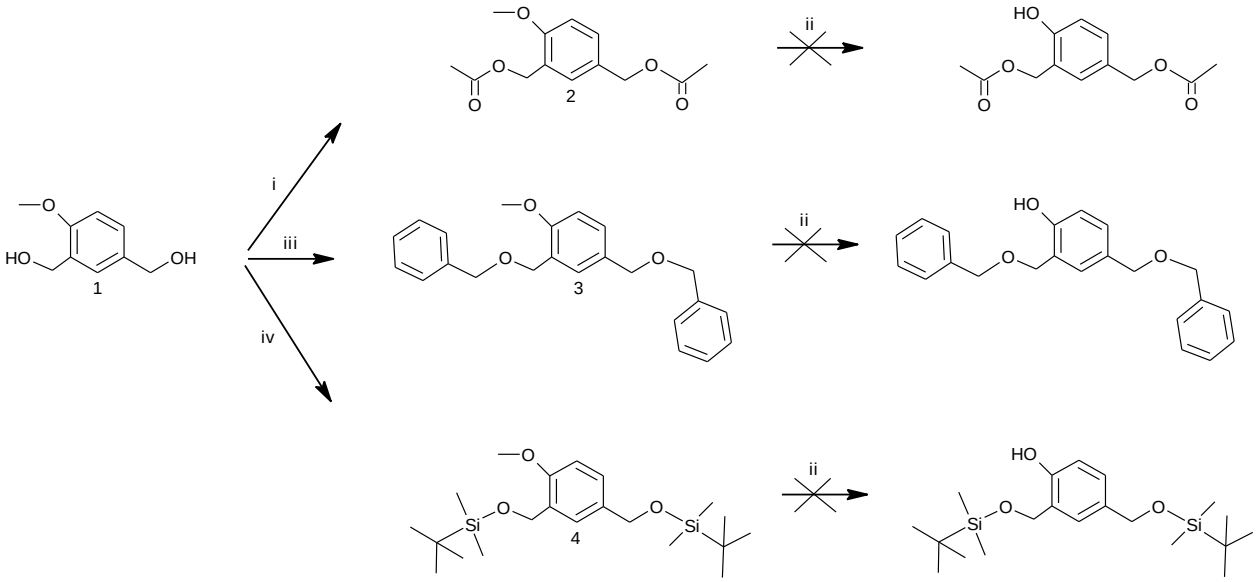

Scheme 5-3: Demethylation of compound **1** after protection with different groups.

Reagents and Conditions: i) Ac_2O, DMAP, TEA, RT, 83 %; ii) BBr_3/DCM, -78 ^{O}C or 0 ^{O}C; iii) benzyl bromide, KOH, THF, RT, 53 %; iv) TBDMSCl, imidazole, DCM, RT, 53 %.
2: ^{1}H NMR (500 MHz, D_2O): δ (ppm) 2.07 (3H, s); 2.11 (3H, s); 3.84 (3H, s); 5.04 (2H, s); 5.15 (2H, s); 6.87 (1H, d, J = 8.2 Hz); 7.33 (2H, m).
3: ^{1}H NMR (500 MHz, D_2O): δ (ppm) 3.87 (3H, s); 4.56 (1H, s); 4.58 (1H, s); 4.66 (4H, d, J = 4.4); 6.90 (1H, d, J = 8.4); 7.33 (3H, m); 7.40 (8H, m); 7.48 (1H, d, J = 2.1 Hz).
4: ^{1}H NMR (500 MHz, D_2O): δ (ppm) 0.13 (6H, s); 0.15 (6H, s); 0.97 (9H, s); 0.99 (9H, s); 3.84 (3H, s); 7.73 (2H, s); 4.79 (2H, s); 6.81 (1H, d, J = 8.5 Hz); 7.19, 7.21 (1H, dd, J = 2.1 Hz); 7.48 (1H, s).

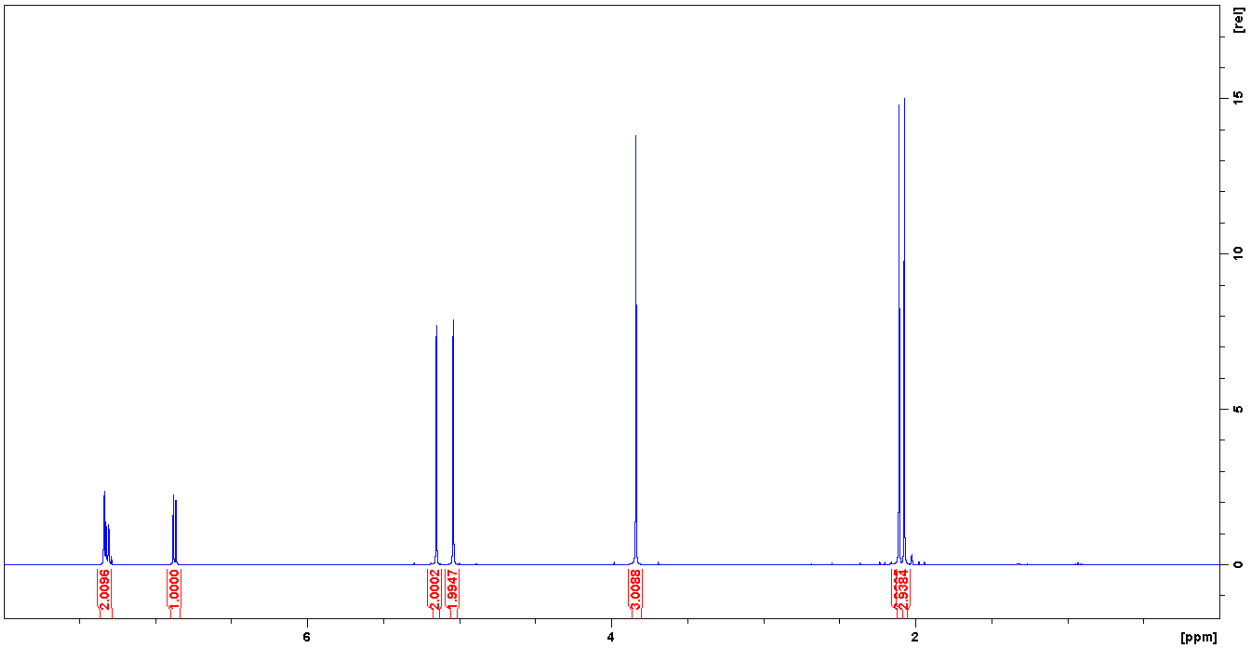

Figure 5-4: ^{1}H NMR data of compound **2** in $CDCl_3$.

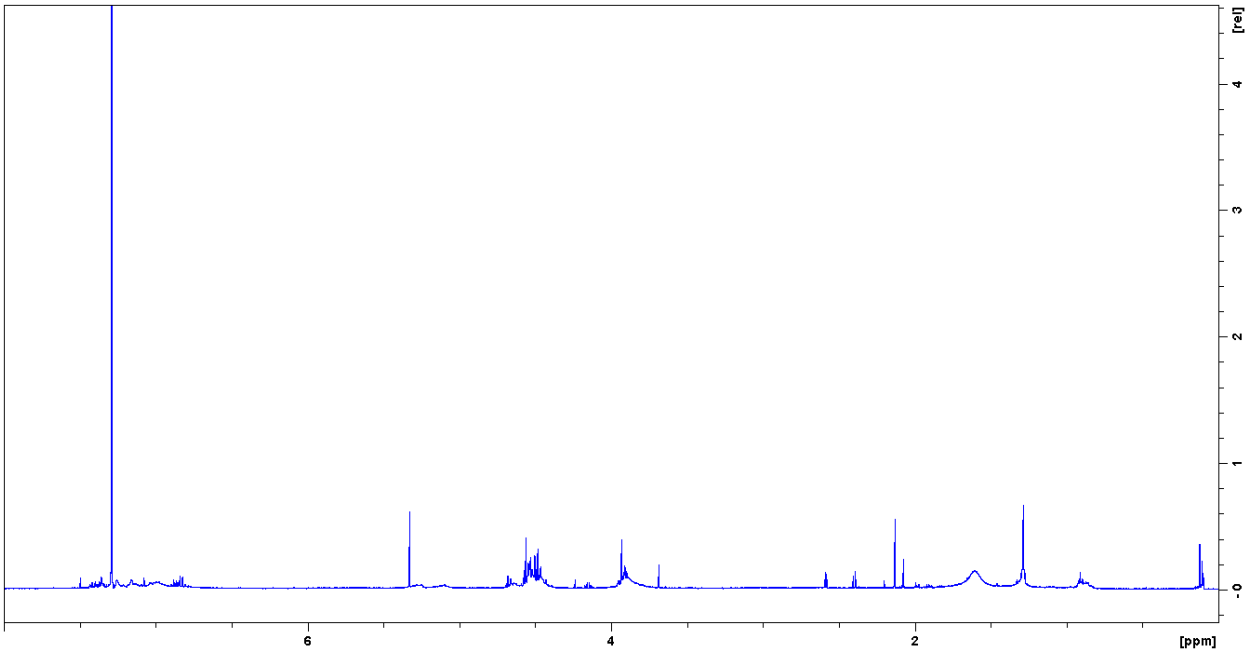

Figure 5-5: Sample of ^{1}H NMR data for attempted demethylation of compound **2**.

Although protection of the starting material, compound **1**, with an acetyl group was successful, the demethylation reaction after the acetylation was unsuccessful. It is possible that the reaction did not occur at the required position. This failure of the reaction could be due to

several reasons. One possibility may be that the BBr_3 reacted with other oxygen atoms (*) instead of the ether oxygen, which may lead to the loss of the acetate group during hydrolysis (Scheme 5-4). Alternatively the boron complex is formed and the bromide ion attacks one of the benzyl carbons with loss of acetate, and we think this mechanism is more likely in this case.

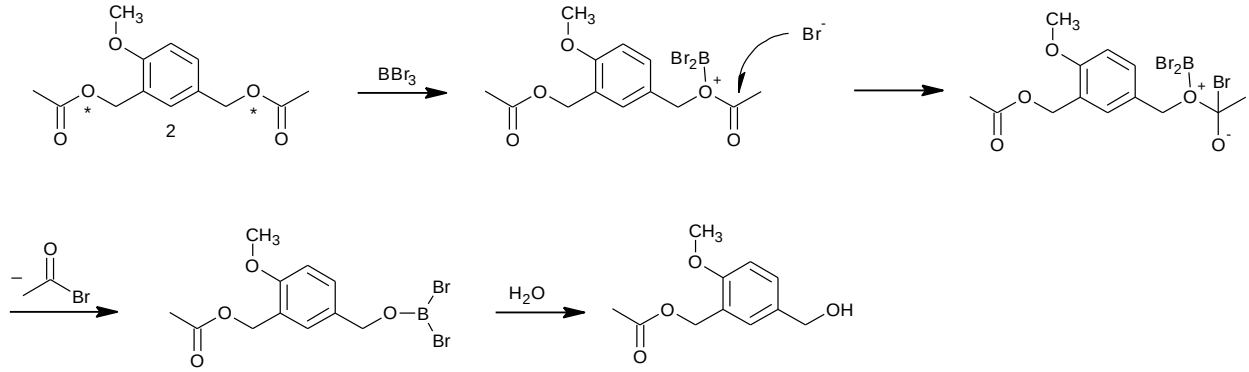

Scheme 5-4: Potential interaction of BBr_3 with compound **2**.

Another reason may be due to the electron-withdrawing effect of the acetate group. Therefore, both acetate groups may pull electron density toward them, which may have an effect on the whole reaction because they decrease the nucleophilicity of the methoxy O-atom. We believe that the electron-withdrawing effect of the acetates is likely responsible as they would be too electrophilic to react with BBr_3.

5.1.3 Benzyl Protection[111]

A second protecting group was chosen to avoid the potential Lewis acid catalyzed protecting group hydrolysis. The two hydroxyl groups of **1** were protected via benzylation. Compound **1** was benzylated using benzyl bromide and KOH in THF at RT to give compound **3** as a yellowish oil (53.05 %), and Figure 5-6 shows the NMR spectrum of **3**. Attempts at

demethylation of compound **3** also did not result in the anticipated product, (Scheme 5-3) despite altering the temperature and ratio of BBr_3 to **3** (Table 5-1), as shown in NMR (Figure 5-7).

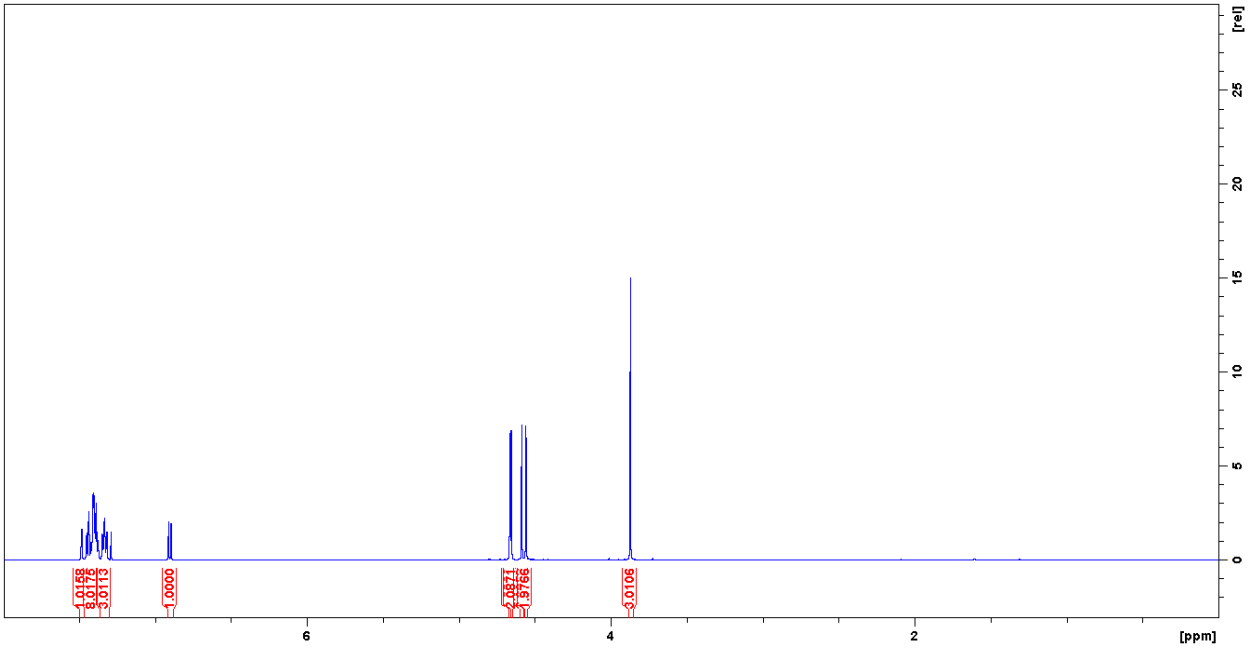

Figure 5-6: ^{1}H NMR data of compound **3** in $CDCl_3$.

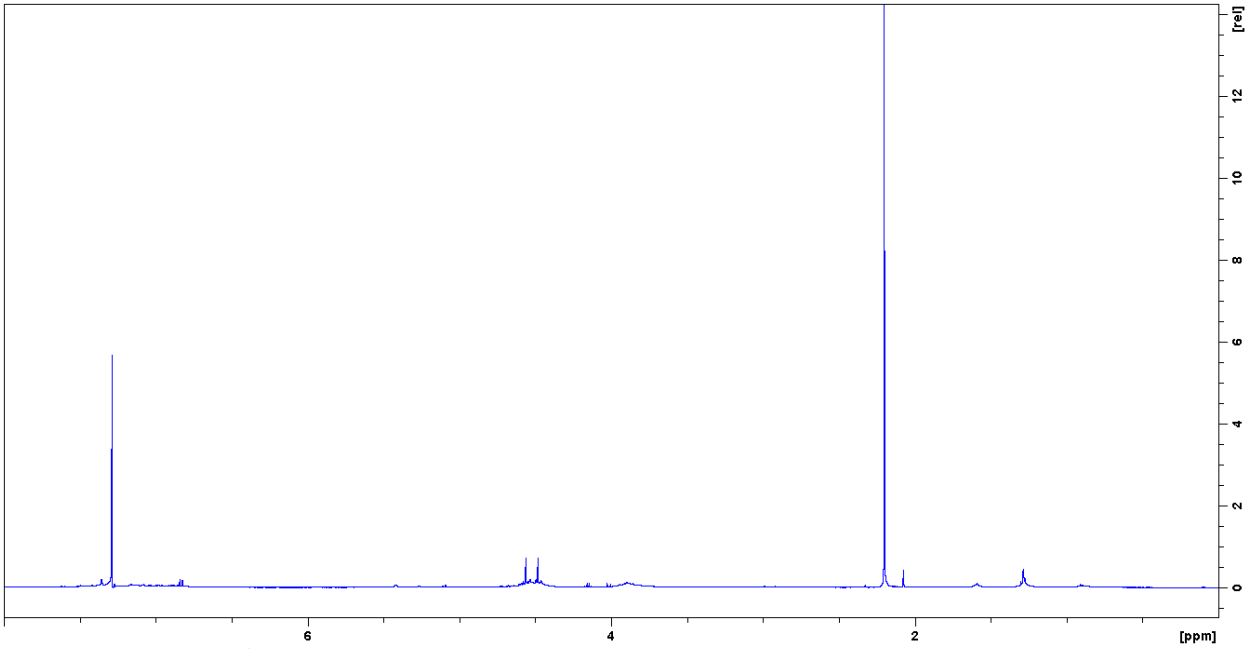

Figure 5-7: Sample ^{1}H NMR data for attempted demethylation of compound 3.

Although benzyl protection of the starting material, compound **1**, was successful, the dealkylation reaction after the benzylation was again unsuccessful. This failure of the reaction could be due to several possibilities. First, it could be due to the BBr_3 interacting with other oxygen atoms (*) instead of the ether oxygen (Scheme 5-5). Multiple ether oxygen atoms are present as well as multiple benzyl CH_2 positions, any of which may undergo dealkylation, leading to a mixture of products, as outlined in Scheme 5-5. It may simply be that under our conditions there was insufficient selectivity for reaction of BBr_3 with the desired site.

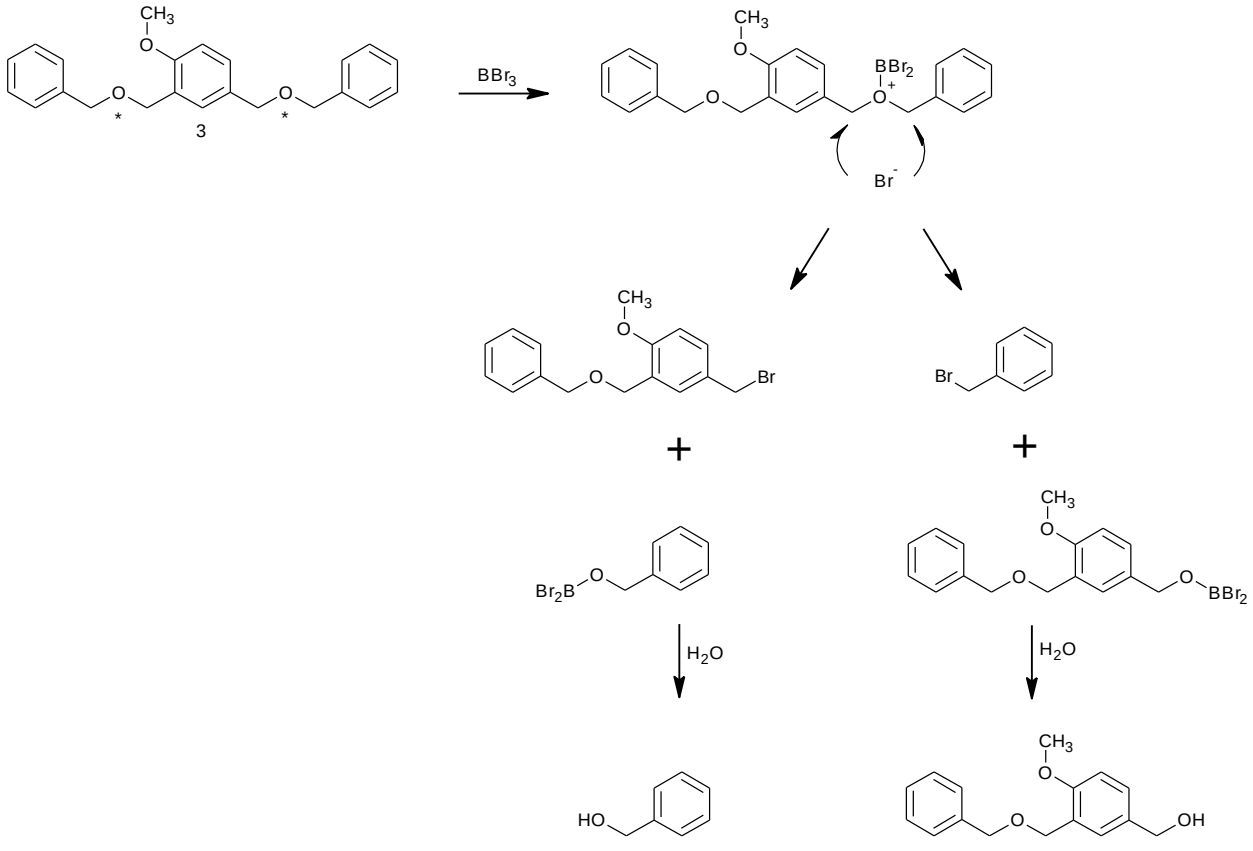

Scheme 5-5: Potential interaction of BBr_3 with compound **3**.

5.1.4 Silyl Protection[112]

It is possible that the electron-withdrawing effect of the benzyl or the acetyl groups in our previous attempts at demethylation might have contributed to the poor outcome, we decided to try using an electron-donating protecting group. Compound **1** was treated with tert-butyldimethylsilyl chloride (TBDMSCl) and imidazole in DCM at RT, which gave compound **4** as a colorless oil (53.85 %). The product was analyzed using NMR techniques, and the ^{1}H NMR spectrum of protected compound **4** is shown in Figure 5-8. Again the demethylation of compound **4** with different BBr_3 ratios at different times (Table 5-1), after protection of the two hydroxyl groups with the tert-butyldimethylsilyl (TBDMS) group, did not afford the expected product (Scheme 5-3), as shown in NMR (Figure 5-9).

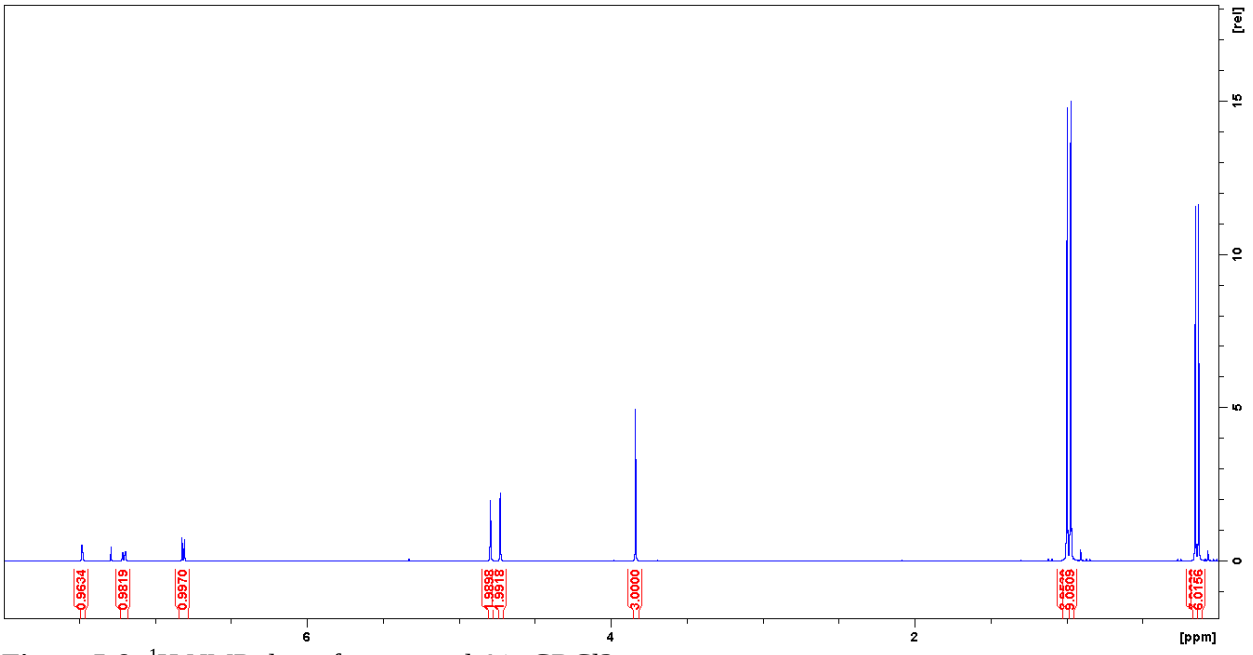

Figure 5-8: ^{1}H NMR data of compound **4** in CDCl3.

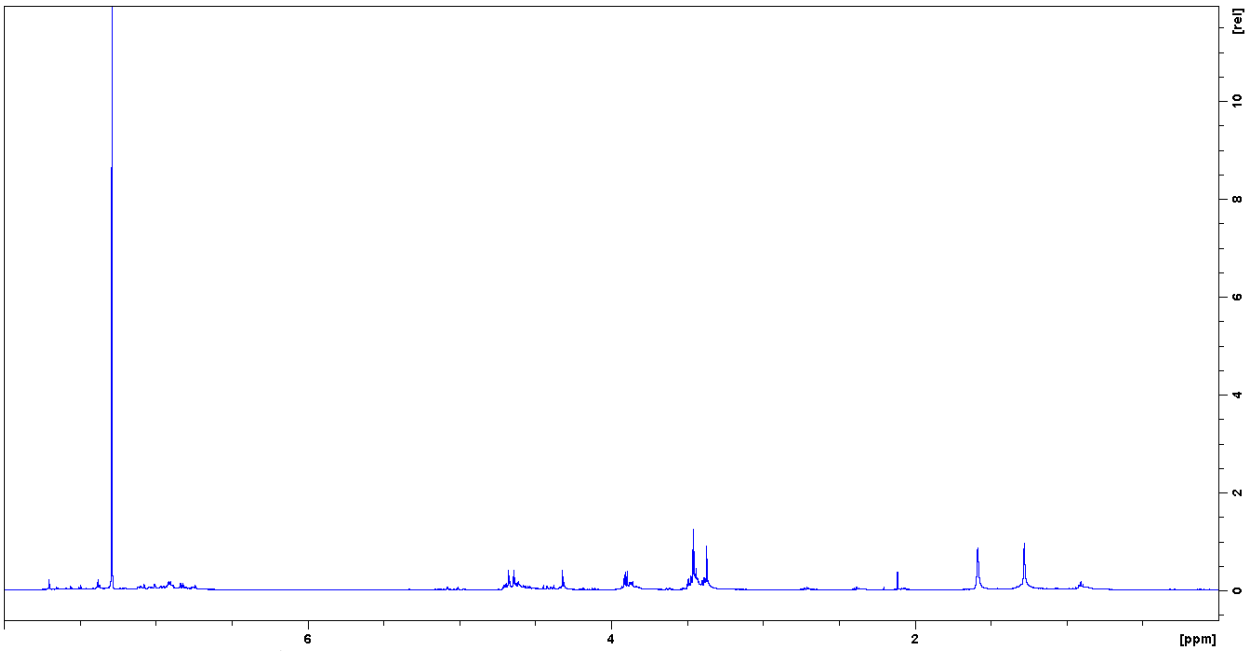

Figure 5-9: Sample of ^{1}H NMR data for attempted demethylation of compound **4** in $CDCl_3$.

Our last attempt at this strategy was the incorporation of an electron-donating TBDMS protecting group. As in the previous approaches, we were able to successfully protect the alcohol groups, but the demethylation reaction was once again unsuccessful. This failure might be due to the BBr_3 reacting with other oxygen atoms (*) instead of the ether oxygen (Scheme 5-6). Since the TBDMS is an electron-donating group, the increased electron density at the benzyl oxygens may increase their reactivity with BBr_3.

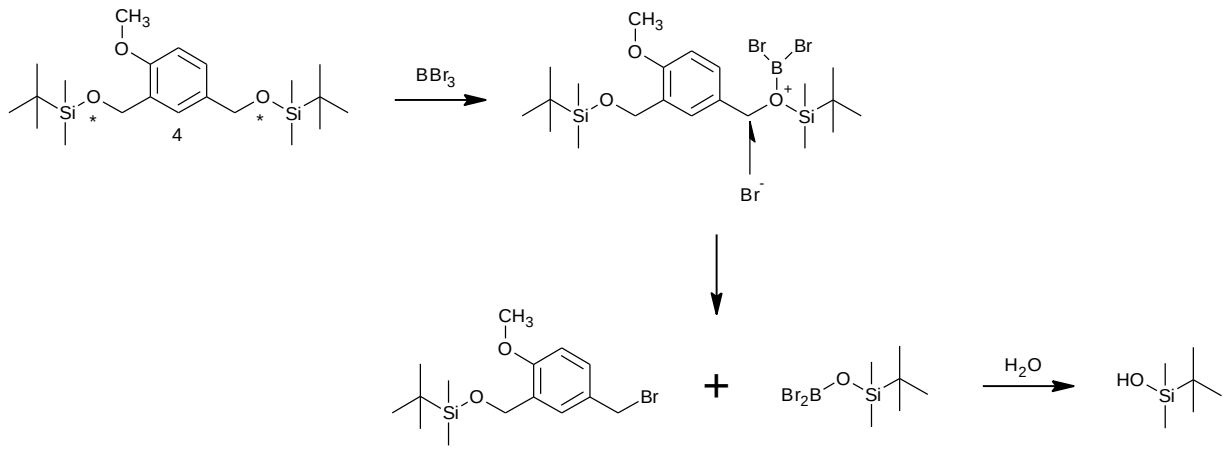

Scheme 5-6: Potential interaction of BBr_3 with compound **4**.

5.1.5 Attempted Demethylation Reaction Under Various Conditions

Because protecting groups having an effect on demethylation reactions, we also decided to investigate other features of the demethylation reaction, such as solvent, reactant ratios, and temperature that will be discussed in more detail further on.

5.1.5.1 Solvent

DCM is frequently used as a solvent for the demethylation reaction. As Sharghi et al.[113] have shown using BBr_3 for demethylation at low temperature in DCM produced a high-percentage yield. By protecting compound **1** with different protecting groups (acetyl, benzyl, and silyl), all of the protected compounds **2**, **3**, and **4** become more lipid soluble. Therefore, solubility in the DCM should not be an issue, and we observed no solubility problems.

5.1.5.2 Ratio

It is recommended to utilize one equivalent of BBr_3 for each ether group to be dealkylated; however, low yields have been reported in some cases.[108] Thus, we tried different

ratios of the dealkylating reagent, starting with one equivalent of BBr_3 and then gradually increasing the amount of the reagent to make sure that we had a sufficient excess of BBr_3. As Table 5-1 shows, the 1:1 ratio resulted in no change, so clearly an excess of BBr_3 was necessary. However, using more BBr_3 resulted in multiple reactions occurring. Thus, it solves the problem of no reaction occurring, but it creates a different problem: multiple reaction products.

5.1.5.3 Temperature

McOmie et al.[108] showed that BBr_3 is a potent and selective reagent for demethylation of aryl methyl ethers, and aromatic ethers can be cleaved by BBr_3 at low temperature. Because the BBr_3 dealkylation reactions are highly exothermic, low temperatures are typically used.[107] Therefore, we performed the dealkylation reactions using BBr_3 under different low temperatures, as shown in Table 5-1, to try to make the reaction selective and to obtain a good yield.

Overall, for the synthesis of acyl derivatives of cyclic phenol phosphate analogues, the dealkylation reactions were unsuccessful either directly or after protection with different groups, although we used a variety of dealkylating reagent amounts and temperatures. We are uncertain why this reaction did not work, but it is probably because there are many competing reaction sites, so we either obtained too little or no desired product. Therefore, we conclude that one or more structural feature(s) of compound **1** prevent the demethylation reaction from occurring. Obviously, the proposed synthetic demethylation step proved practically challenging, as the expected products were not obtained.

5.2 Attempted Synthesis of Alkyl Ether Derivatives of Cyclic Phenol Phosphate Analogues

Because attempts at demethylation of **1** were unsuccessful, we turned our attention to the second approach, which is to synthesize alkyl ether derivatives of cyclic phenol phosphate analogues. We proposed a synthetic pathway that involves selective methylation of the hydroxyl group, followed by introduction of the alkyl ether moiety (Scheme 4-2). Next, deprotection of the alcohol group will be carried out before introducing the phosphate group in a similar manner to the acyl derivatives. The length of the carbon side chain (R) will vary from fourteen to eighteen carbons in length, even though a shorter chain will be prepared as a model reaction for the determination of aqueous stability.

However, the proposed synthetic pathway (Scheme 4-2) of preparation of alkyl ether derivatives was modified to avoid the demethylation step in this pathway (due to our previous experience) and to determine that a cyclization with $POCl_3$ could be carried out to obtain our proposed analogues (Figure 5-2). Therefore, we proposed a modified synthetic pathway that focused on constructing the active portion of our analogues, the cyclic phenol phosphate group, without the long side chains that will be shown in more detail further on (Section 5.2.1).

5.2.1 Pathway 1: Cyclic Phenol Phosphate Analogues without Long Side Chain

The starting materials for our second approach were commercially available: compound **5** (Salicylaldehyde) and compound **6** (2-hydroxy-5-methoxybenzaldehyde). Notably, these compounds provide the advantage of shortening the proposed synthetic step by three reactions (Scheme 5-7). A reduction of both compound **5** and **6** separately with $NaBH_4$ in MeOH at RT produced compound **7** (the alcohol) as white crystals (56.09 %) and **8** as yellowish white crystals

(53.19 %) respectively (Scheme 5-7). The addition and intramolecular cyclization of the phosphate group was carried out through treatment of the alcohol with a base (TEA) in THF at -70 ^{O}C, followed by the addition of $POCl_3$.[114] The reaction mixture was brought to room temperature in stages: to -40 ^{O}C for one hour, and then to RT overnight. Then, the crude mixture was filtered, concentrated under vacuum, and purified by flash column chromatography over silica (1:1 Hex/EtOAc). The product was shaken with water and dried to yield analogue 1 (**A1**) as white crystals (52.06 %) and analogue 2 (**A2**) as beige crystals (67.51 %), respectively (Scheme 5-7). This pathway successfully produced **A1**, unsubstituted cyclic phenol phosphate (Figure 5-10), and **A2,** methoxy-substituted cyclic phenol phosphate (Figure 5-11).

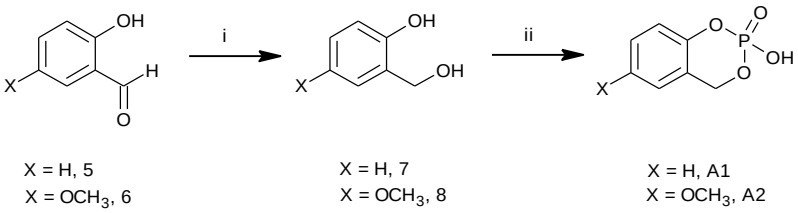

Scheme 5-7: Synthetic pathway for preparation of cyclic phenol phosphate with no chain (**A1**) or with short side chain (**A2**).
Reagents and Conditions: i) $NaBH_4$, MeOH, RT; ii) $POCl_3$, THF, TEA, −70 °C, 1 h, −40 °C, 1 h, RT, overnight.
A1: ^{1}H NMR (500 MHz, D_2O): δ (ppm) 5.14, 5.16 (1H, s); 6.89 (1H, d, J = 8.4 Hz); 7.00 (1H, m); 7.06 (1H, d, J = 6.3 Hz); 7.21 (1H, m). ^{31}P-NMR (202 MHz, D_2O): δ (ppm) -5.97. ^{13}C NMR (125 MHz, D_2O): δ (ppm) 67.00, 118.30, 121.60, 123.07, 125.49, 129.09, 150.62. ESI-MS (m/z) = 187.1 $[M+H]^+$
A2: ^{1}H NMR (500 MHz, D_2O): δ (ppm) 3.67 (3H, s); 5.10, 512 (1H, s); 6.66 (1H, d, J = 2.8 Hz); 6.79 (1H, dd, J = 2.8 Hz, J = 9.0 Hz); 6.85 (1H, d, J = 9.0 Hz). ^{31}P-NMR: (202 MHz, D_2O): δ (ppm) -5.82. ^{13}C NMR (125 MHz, D_2O): δ (ppm) 55.73, 66.93, 110.27, 114.78, 119.22, 122.37, 144.75, 154.25. ESI-MS (m/z) = 217.2 $[M+H]^+$

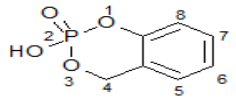

2-hydroxy-4H-1,3,2-benzodioxaphosphorin-2-oxide
(A1)

Figure 5-10: Molecular structure of unsubstituted alkyl ether of cyclic phenol phosphate analogue 1 (**A1**) with Molecular Formula ($C_7H_7O_4P$) and Molecular Weight (186.101842).

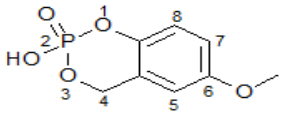

2-hydroxy-6-methoxy-4H-1,3,2-benzodioxaphosphorin-2-oxide

(A2)

Figure 5-11: Molecular structure of methoxy substituted alkyl ether of cyclic phenol phosphate analogue 2 (**A2**) with Molecular Formula ($C_8H_9O_5P$) and Molecular Weight (216.127822).

5.2.2 Pathway 2: Cyclic Phenol Phosphate Analogues with Long Side Chains

The previous pathway successfully provided us with two analogues: **A1** (without a side chain) and **A2** (with only a methoxy group side chain). This method served as a model reaction to confirm that we could install the cyclic phosphate moiety in the presence of an alkyl ether functional group. We then set our sights on preparing the phenol/alcohol starting material with long chain alkyl ether. Thus, for preparation of alkyl ether derivatives of the cyclic phenol phosphate with long side chains (C_{14}, C_{16}, and C_{18}), a different synthetic pathway was proposed and adapted from the literature[112] in order to introduce the long side chain first, and then carry out the cyclization to obtain the corresponding analogues (Scheme 5-8). Most of this pathway was done in cooperation with a summer student (Sarah Petriew).

A benefit to the proposed procedure for preparing the phenol/alcohol derivatives is that the starting material (**9**) is commercially available (2,5-dihydroxybenzaldehyde). As outlined in Scheme 5-8, the 5-OH group can be selectively protected and then followed by reduction of the benzyl alcohol and protection of the phenol/alcohol. Deprotection of the 5-OH, then addition of the corresponding alkyl chain at the 5-position, and finally deprotection of the phenol/alcohol would yield the necessary precursor for phosphate cyclization.

Compound **9** was treated with TBDMSCl and imidazole in DCM at RT, which gave compound **10** exclusively as a yellow oil (82.5 %); this selectivity is likely due to a meta-directing effect of the aldehyde. A reduction of compound **10** with $NaBH_4$ in EtOH at 0 °C afforded compound **11** as a white solid. In order to protect the two hydroxyl groups, compound **11** was treated with 2,2-dimethoxypropane and *p*TsOH in acetone at RT to give compound **12** as a yellow oil. The silyl ether of compound **12** was deprotected by treatment with tetraethylammonium fluoride in THF at RT to produce compound **13**. Functionalization of the 5-OH with alkyl ether was carried out via a nucleophilic displacement of the appropriate alkyl bromide under basic conditions. Thus, 1-bromotetradecane and K_2CO_3 were directly added to compound **13** in THF at 70 °C and afforded compound **14** as a yellow oil. Finally, the two hydroxyl groups of compound **14** were deprotected using 4.0 M HCl in dioxane/THF at RT to yield compound **15** as a white solid. All of the compounds prepared were in agreement with literature outcomes.[112]

The final step of this process was to incorporate the cyclized phosphate group. We used the procedure developed and shown previously on a small scale (Section 4.2.1). Compound **15** (30-50 mg) was treated with $POCl_3$ and TEA in THF at -70 °C for one hour, -40 °C for one hour, and then warmed to RT overnight. However, the desired product (**A3**) was not observed, even after several attempts (Scheme 5-8). We did not observe any solubility issues with the C_{14} substituted precursor. The polar head groups and alkyl chains may form micellar-like complexes, which could internalize the reactive groups. This seems unlikely, however, given that THF possesses both polar and non-polar solvation characteristics. Due to a lack of compound **15**, we were unable to carry out this reaction under different conditions. Additionally, trying this reaction on a larger scale may also be helpful.

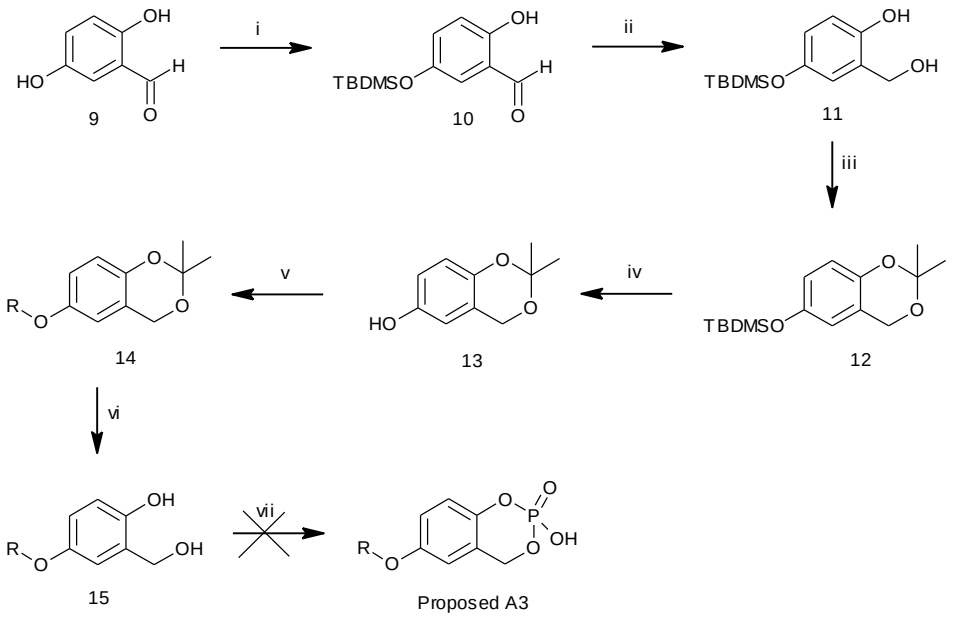

Scheme 5-8: Synthetic pathway to alkyl ether derivatives of cyclic phenol phosphate with 14:0 long side chain analogue **3** (**A3**).
Reagents and Conditions: i) tBDMS-Cl, imidazole, CH_2Cl_2, RT, overnight; ii) $NaBH_4$, EtOH, 0 °C to RT, 2 h; iii) 2,2-dimethoxypropane, *p*TsOH(cat), acetone, RT, 48 h; iv) tetraethylammonium fluoride, THF, RT, 2 h; v) Bromoalkyl (1-bromotetradecane), THF, K_2CO_3, 70 °C, 24 h; vi) HCl 4.0 M in dioxane, THF, RT, 24 h; vii) $POCl_3$, THF, TEA, −70 °C, 1 h, −40 °C, 1 h, RT, overnight.
15: ^{1}H NMR (500 MHz, D_2O): δ (ppm) 0.91 (3H, t); 1.28 (20H, m); 1.45 (2H, quin); 1.76 (2H, quin); 3.90 (2H, t); 4.85 (2H, s); 6.64 (1H, d, J = 2.6 Hz); 6.77, 6.79 (1H, dd, J = 2.6 Hz); 6.83 (1H, d, J = 8.5 Hz).

5.3 Stability Study

One concern when assessing mechanism-based enzyme inactivators is the possibility that the substrate may spontaneously decompose under the conditions used for the enzyme assay. Spontaneous formation of an $_O$-QM outside of the enzyme active site could result in an enzyme inactivation that is not the result of the enzyme's catalytic mechanism. This type of reactive intermediate formation would result in diminished target selectivity and is generally undesirable. We therefore decided to examine the stability of our compounds in the ATX assay system in the absence of the enzyme to confirm that any ATX inhibitory activity that was measured was a likely reflection of catalytic activity. We examined the hydrolytic stability of our synthesized

cyclic phenol phosphate analogues **A1** (unsubstituted cyclic phenol phosphate) and **A2** (methoxy-substituted cyclic phenol phosphate) in TRIS buffer (50 mM) at pH 8.0 and 37 °C. We reasoned that these analogues should be acceptable as model compounds for this family as they retain the cyclic phosphate group, and any differences in substituent effects from the alkoxy groups should be evident in our methoxy derivative (**A2**). Our stability experiments revealed that both analogues were stable under these conditions as no change in substrate peak areas was observed over six hours, indicating that **A1** and **A2** showed stability against non-enzymatic decomposition (Figure 5-12 and 5-13 respectively).

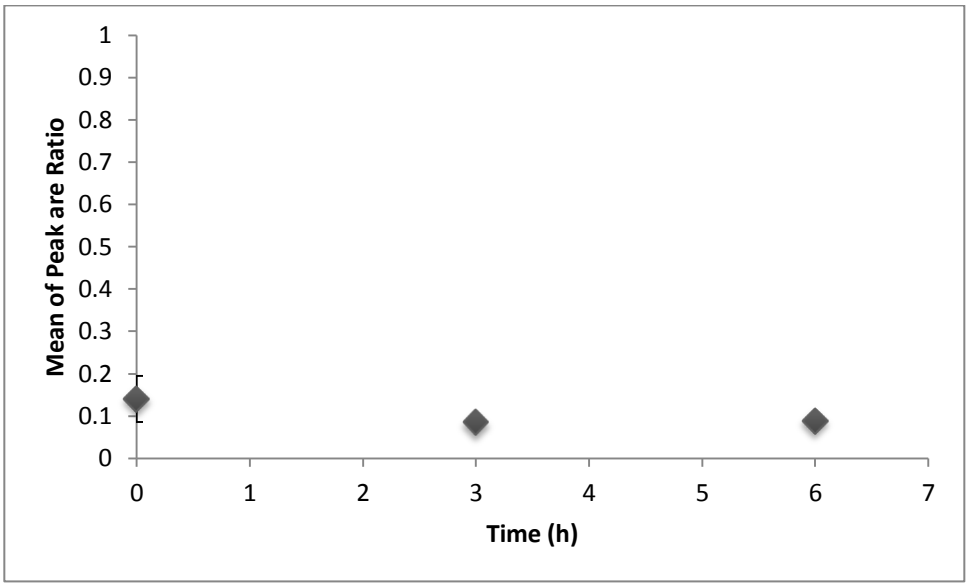

Figure 5-12: Stability study results of A1.
0.1 mM **A1** analogue in TRIS buffer (50 mM; pH 8) over time (h) at 37 □C. Absorbance at λ = 280 nm. The experiment was run in triplicate using HPLC to measure change in starting material. The peak area under the curve was normalized to the 0.1 mM internal standard (KA-1-09-2).

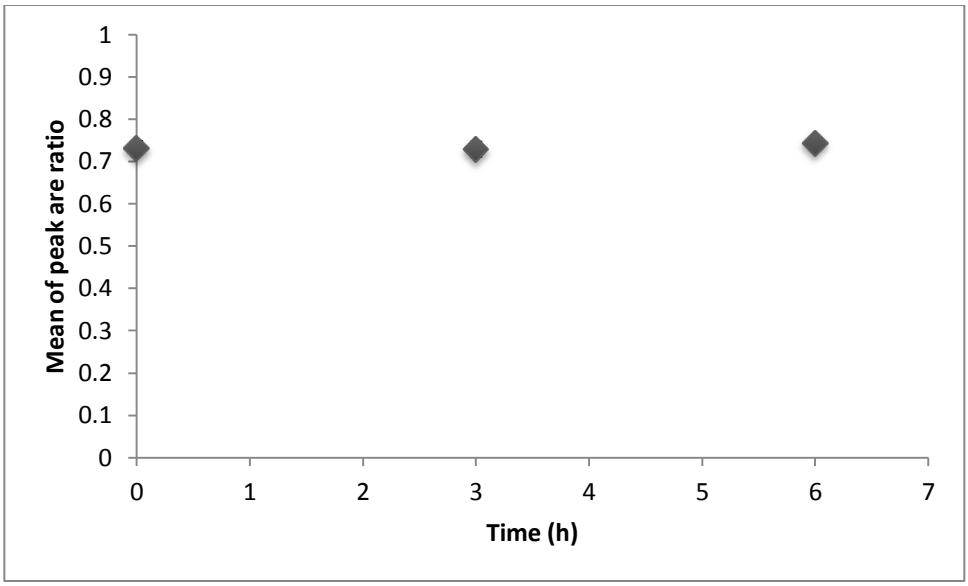

Figure 5-13: Stability study results of A2.
0.1 mM **A2** analogue in TRIS buffer (50 mM; pH 8) over time (h) at 37 □C. Absorbance at λ = 280 nm. The experiment was run in triplicate using HPLC to measure change in starting material. The peak area under the curve was normalized to the 0.1 mM internal standard (KA-1-09-2).

5.4 ATX Inhibition Assay

At this time, we have two cyclic phenol phosphate analogues, **A1** and **A2**, and these compounds have been submitted to our colleagues at the University of Memphis for assessment of their ability to inactivate ATX *in vitro*. However, they have not yet been able to carry out the ATX inhibition assay.

5.5 Preliminary in Silico Docking Studies of Cyclic Phenol Phosphate Analogues with Autotaxin

After submitting **A1** and **A2** for ATX inhibition assay, and because we think without the long chains they may not be great inhibitors, we are using the docking studies to draw comparisons between these analogues and the proposed one (with long side chain C_{14}, C_{16}, and C_{18}), to see if our hypothesis agrees with what we expect: that the hydrophobic chain will

influence enzyme binding. Therefore, several ligands were docked to the free active site of the ATX enzyme (PDB ID: 3NKM) to compare them. The list of ligands consist of (a) LPA with different long side chains (14:0, 16:0, and 18:0) as standard; (b) our synthesized analogues **A1** and **A2**; (c) the proposed alkyl ether derivatives of cyclic phenol phosphate analogues with different long side chains (C_{14}, C_{16}, and C_{18}); (d) the proposed acyl derivatives of cyclic phenol phosphate analogues (C_{14}, C_{16}, and C_{18}); and (e) the mono-fluorophosphodiesters (C_{14}, C_{16}, C_{18}) compounds synthesized by our collaborators as ATX irreversible inhibitors. For good docking results, low scores must be assigned to good poses for more favorable binding conformations between the ligand and ATX. Table 5-2 shows the results of docking these ligands. We compared the scores of ligands with different long side chains and found no major difference between them. However, **A1** (the unsubstituted cyclic phenol phosphate) and **A2** (the methoxy-substituted cyclic phenol phosphate) show the highest values: -5.0872 and -4.6969, respectively. This result indicates that the long side chains of the other ligands play a role in binding to ATX. Also, the effect of ester versus ether linkage to the hydrocarbon chain was also evaluated by comparing both proposed acyl and alkyl ether derivatives of cyclic phenol phosphate analogues with long side chains (C_{14}, C_{16}, and C_{18}), and no major differences were observed between them. This indicates that the carbonyl functional group is not required for ATX binding.

Table 5-2: Scores of docking different ligands with ATX.

No.	Ligand Name	Ligand Structure	S*	ATX-ligand complex**	ATX-ligand interaction**
1	14:0-LPA	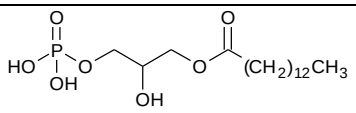	-7.8227	Figure 5-14	Figure 5-15
2	16:0-LPA	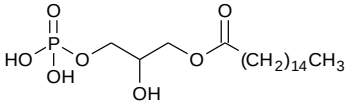	-8.8659	Figure 5-16	Figure 5-17
3	18:0-LPA	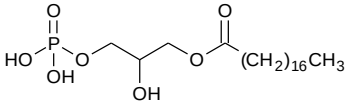	-8.5223	Figure 5-18	Figure 5-19
4	A1	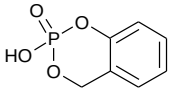	-5.0872	Figure 5-20	Figure 5-21
5	A2	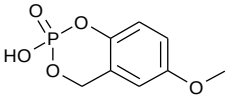	-4.6969	Figure 5-22	Figure 5-23
6	Proposed alkyl ether cyclic phenol phosphate (14:0)	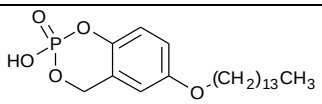	-8.5971	Figure 5-24	Figure 5-25
7	Proposed alkyl ether cyclic phenol phosphate (16:0)	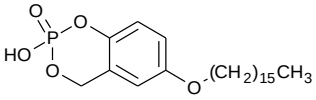	-8.4368	Figure 5-26	Figure 5-27
8	Proposed alkyl ether cyclic phenol phosphate (18:0)	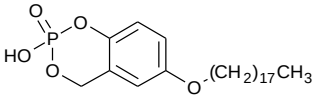	-8.9798	Figure 5-28	Figure 5-29
9	Proposed acyl cyclic phenol phosphate (14:0)	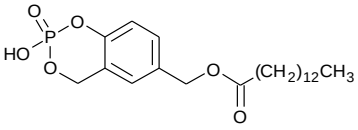	-8.9927	Figure 5-30	Figure 5-31
10	Proposed acyl cyclic phenol phosphate (16:0)	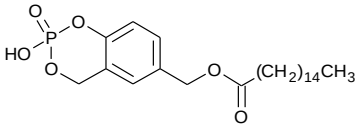	-8.2032	Figure 5-32	Figure 5-33
11	Proposed acyl cyclic phenol phosphate (18:0)	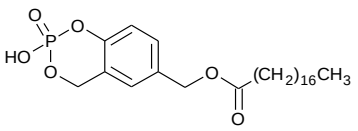	-9.2624	Figure 5-34	Figure 5-35

No.	Ligand Name	Ligand Structure	S*	ATX-ligand complex**	ATX-ligand interaction**
12	(14:0)-p-monofluorophosphodiester	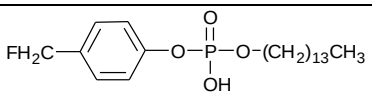	-8.8739	Figure 5-36	Figure 5-37
13	(16:0)-p-monofluorophosphodiester	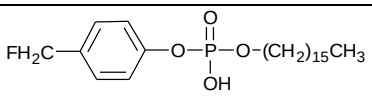	-8.7912	Figure 5-38	Figure 5-39
14	(18:0)-p-monofluorophosphodiester	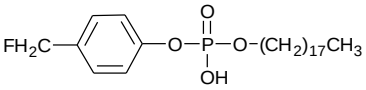	-8.2561	Figure 5-40	Figure 5-41

*For scoring function, lower scores indicate more favorable poses. The unit for scoring function is kcal/mol

**All figures can be found in Table 5-3

Table 5-3: List of all figures of ATX-ligand complex and ATX-ligand interaction for each ligand.

No.	ATX-ligand complex figure	ATX-ligand interaction figure***
1	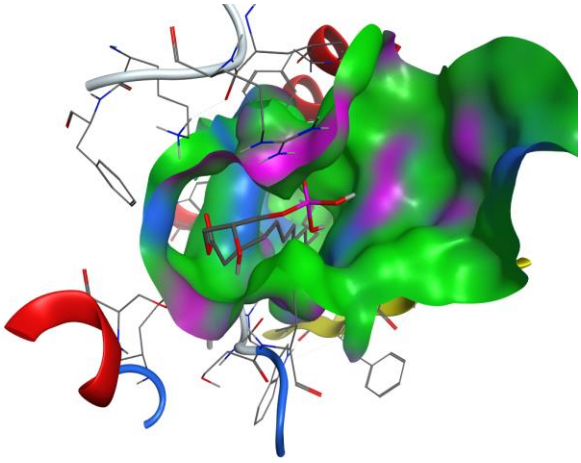 **Figure 5-14:** ATX-ligand (no.1) complex	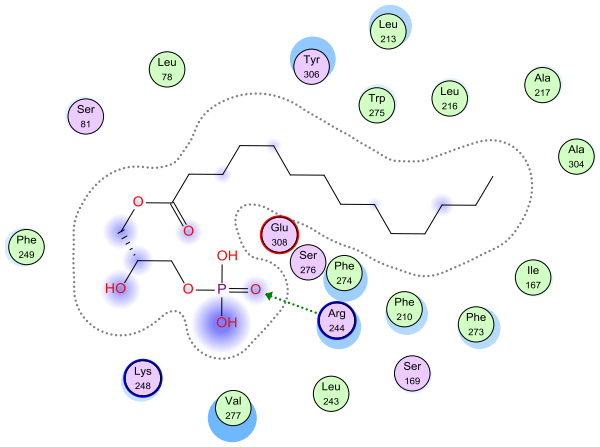 **Figure 5-15:** ATX-ligand (no.1) interaction

No.	ATX-ligand complex figure	ATX-ligand interaction figure***
2	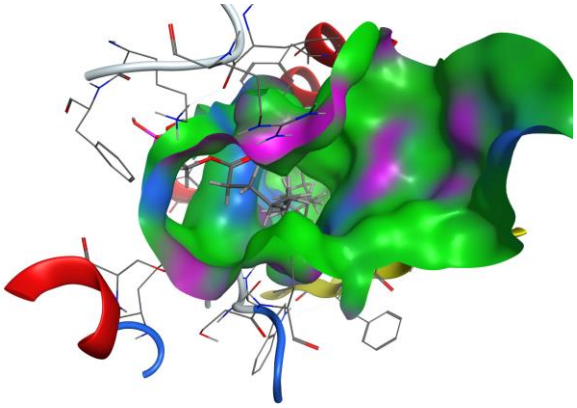 **Figure 5-16:** ATX-ligand (no.2) complex	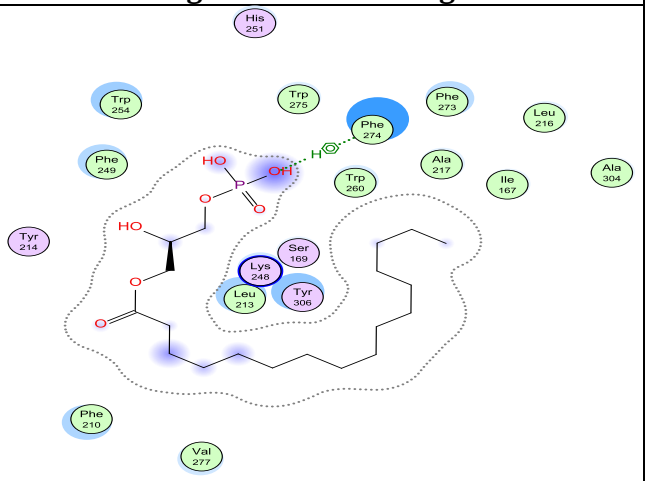 **Figure 5-17:** ATX-ligand (no.2) interaction
3	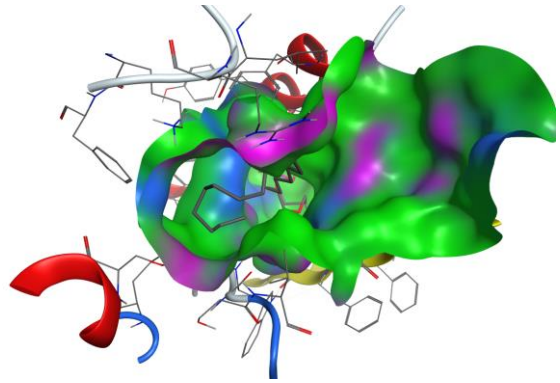 **Figure 5-18:** ATX-ligand (no.3) complex	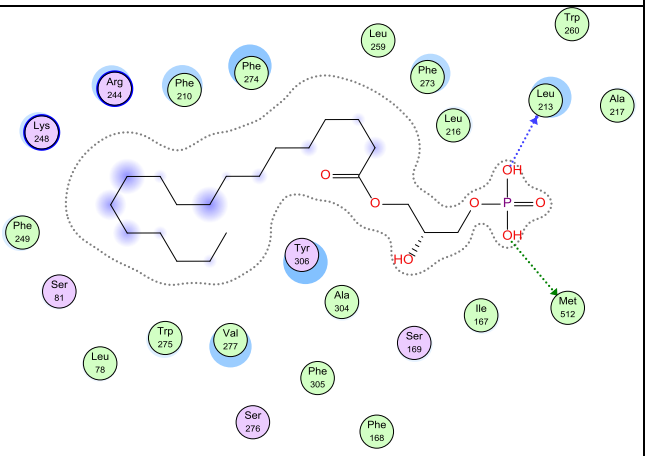 **Figure 5-19:** ATX-ligand (no.3) interaction
4	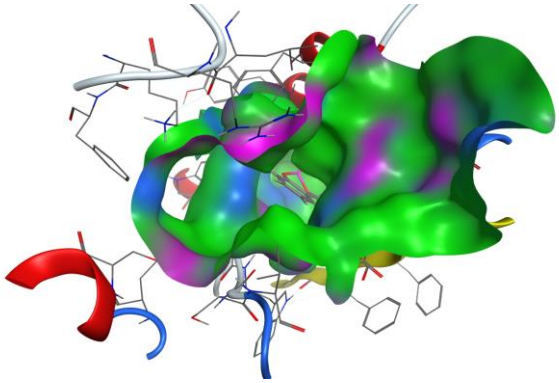 **Figure 5-20:** ATX-ligand (no.4) complex	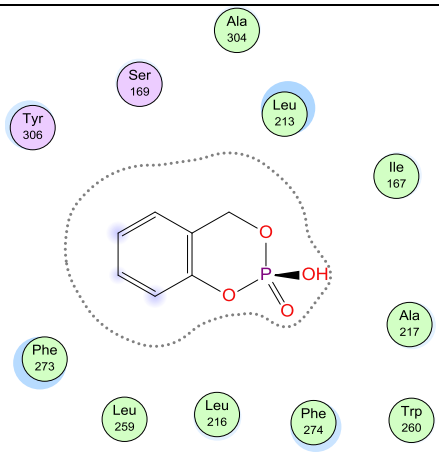 **Figure 5-21:** ATX-ligand (no.4) interaction

No.	ATX-ligand complex figure	ATX-ligand interaction figure***
5	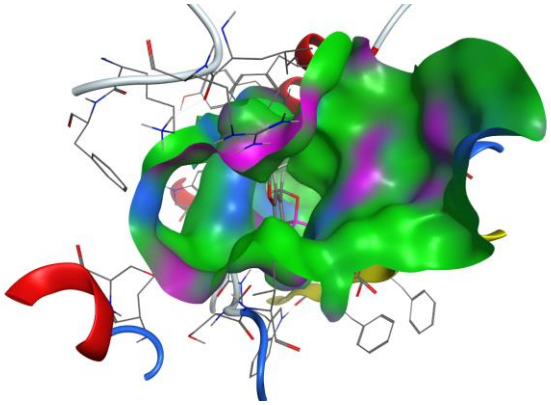 **Figure 5-22:** ATX-ligand (no.5) complex	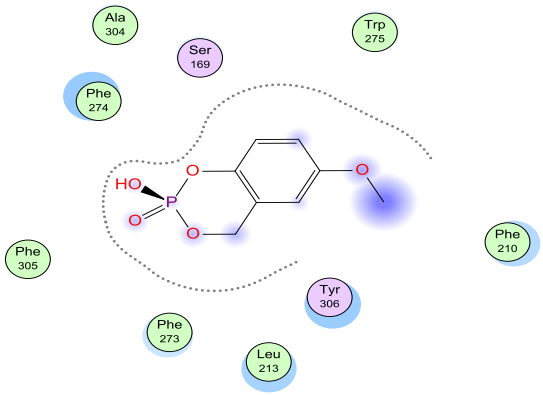 **Figure 5-23:** ATX-ligand (no.5) interaction
6	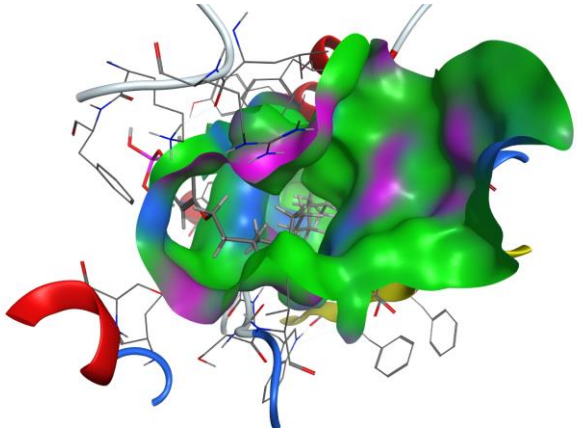 **Figure 5-24:** ATX-ligand (no.6) complex	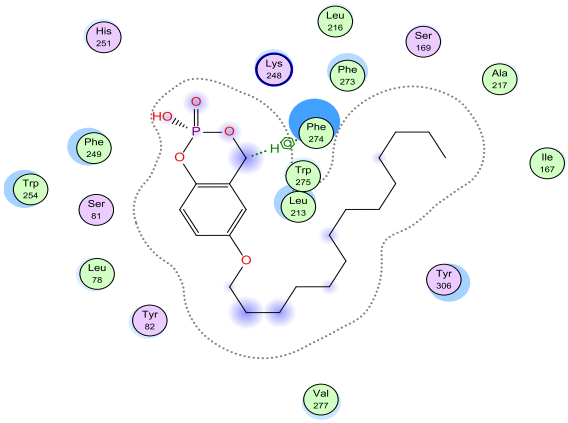 **Figure 5-25:** ATX-ligand (no.6) interaction
7	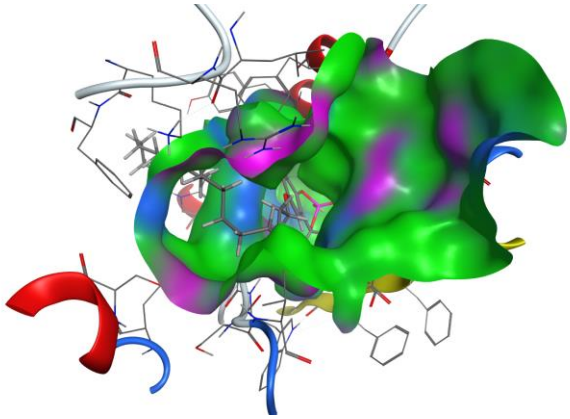 **Figure 5-26:** ATX-ligand (no.7) complex	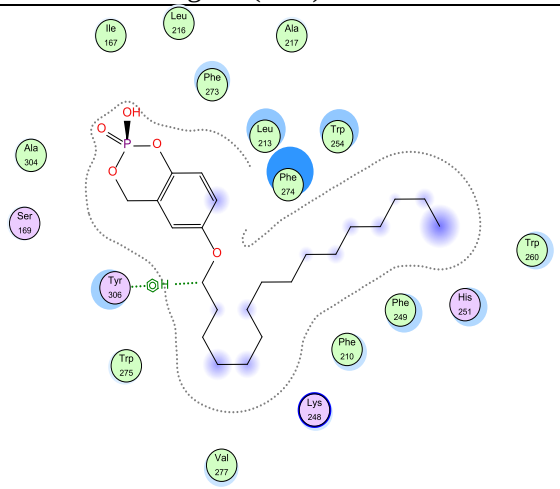 **Figure 5-27:** ATX-ligand (no.7) interaction

No.	ATX-ligand complex figure	ATX-ligand interaction figure***
8	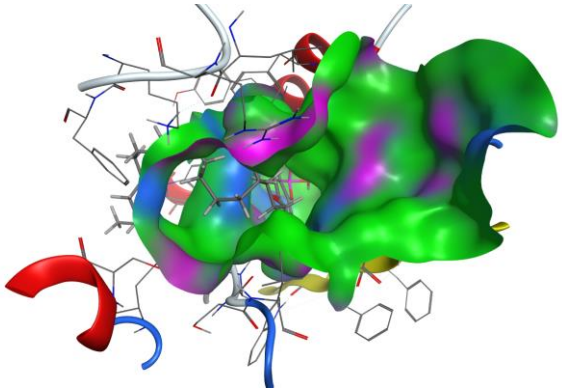 **Figure 5-28:** ATX-ligand (no.8) complex	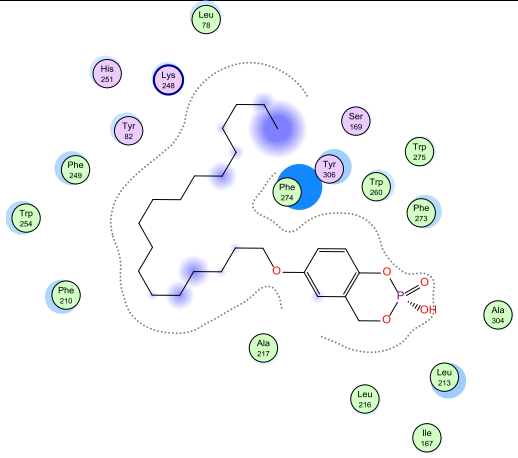 **Figure 5-29:** ATX-ligand (no.8) interaction
9	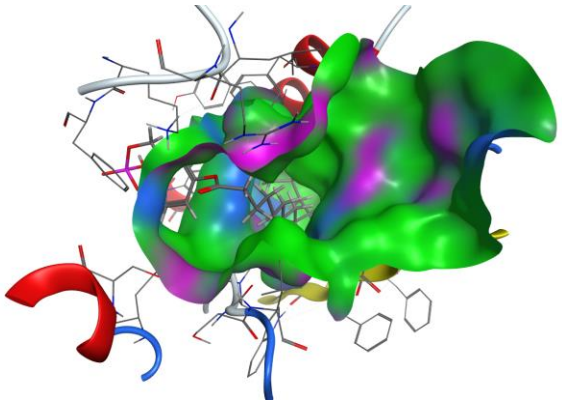 **Figure 5-30:** ATX-ligand (no.9) complex	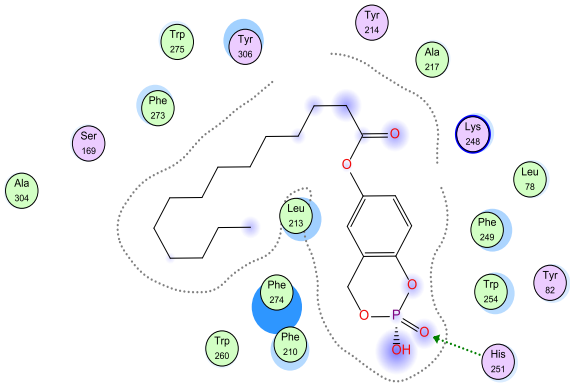 **Figure 5-31:** ATX-ligand (no.9) interaction
10	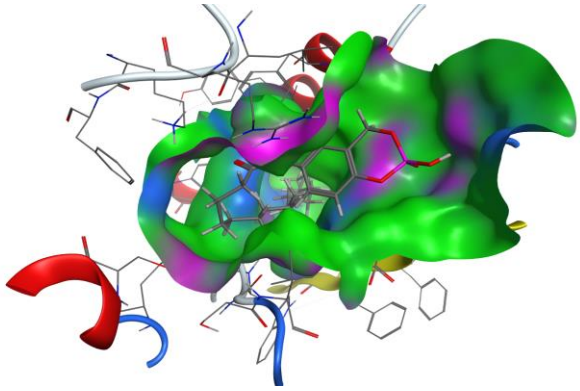 **Figure 5-32:** ATX-ligand (no.10) complex	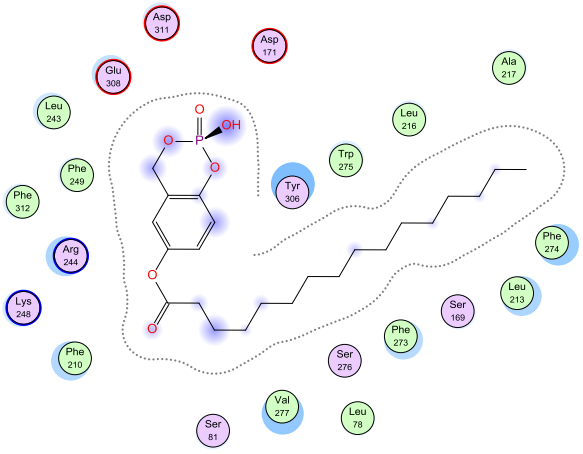 **Figure 5-33:** ATX-ligand (no.10) interaction

No.	ATX-ligand complex figure	ATX-ligand interaction figure***
11	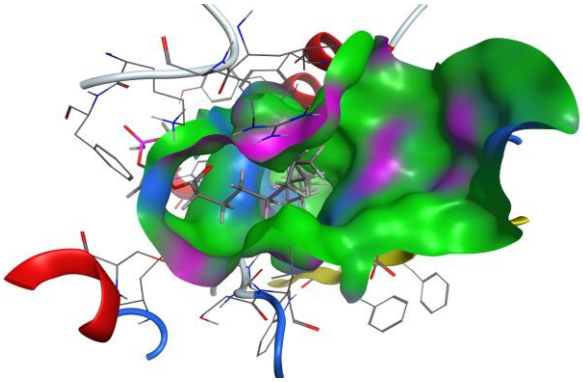 **Figure 5-34:** ATX-ligand (no.11) complex	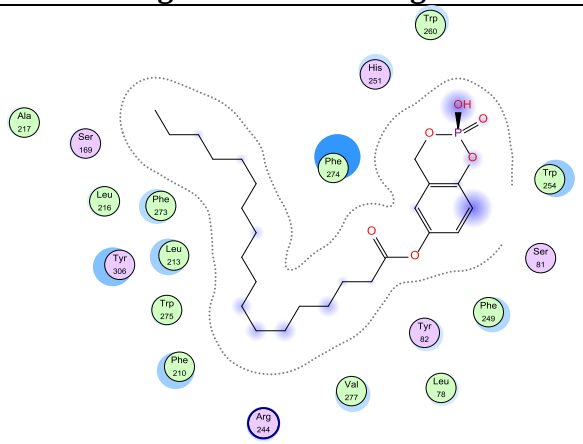 **Figure 5-35:** ATX-ligand (no.11) interaction
12	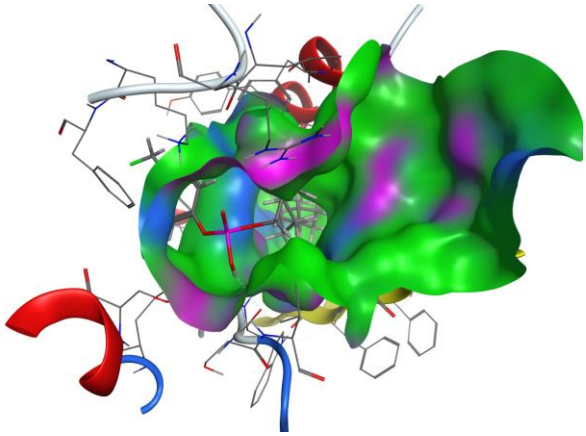 **Figure 5-36:** ATX-ligand (no.12) complex	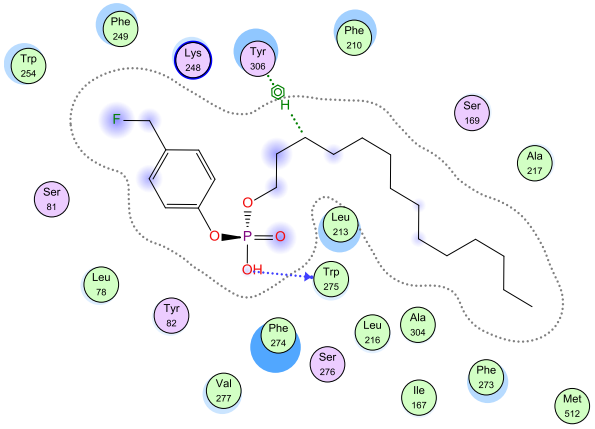 **Figure 5-37:** ATX-ligand (no.12) interaction
13	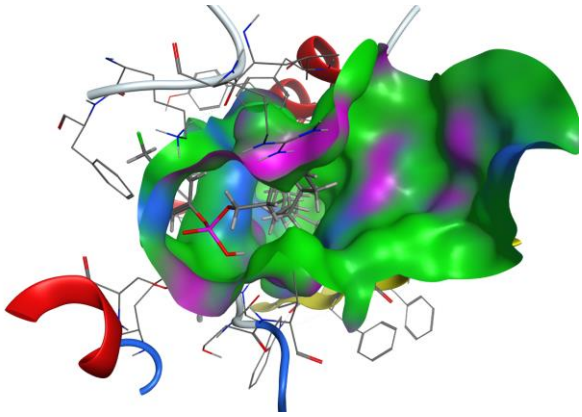 **Figure 5-38:** ATX-ligand (no.13) complex	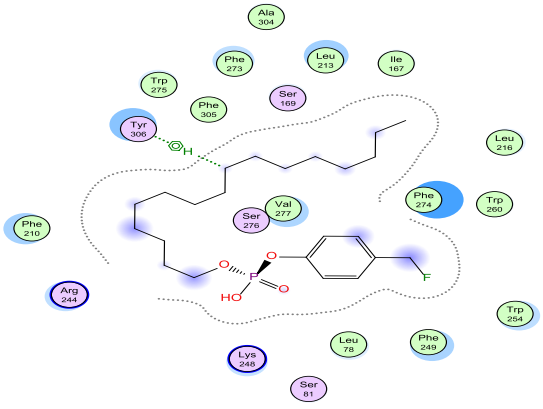 **Figure 5-39:** ATX-ligand (no.13) interaction

No.	ATX-ligand complex figure	ATX-ligand interaction figure***
14	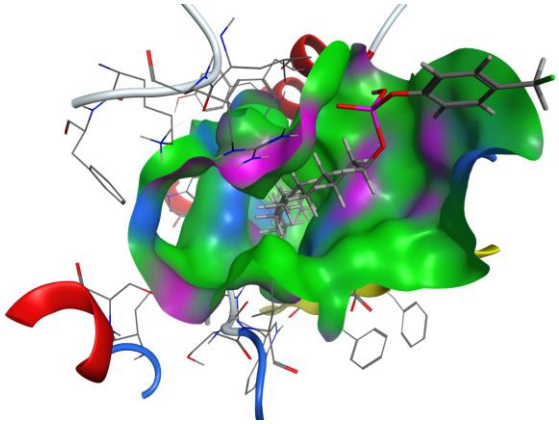 **Figure 5-40:** ATX-ligand (no.14) complex	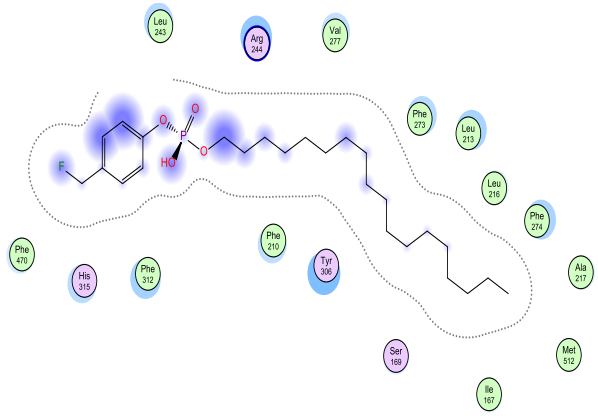 **Figure 5-41:** ATX-ligand (no.14) interaction

***

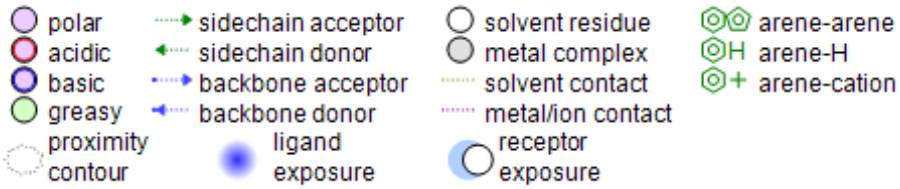

CHAPTER 6: CONCLUSIONS

6.1 Summary and Conclusion

In summary, our research seeks to prepare and assess a series of acyl and alkyl ether derivatives of cyclic phenol phosphate analogues for their ability to function as irreversible ATX inhibitors *in vitro*. Our results demonstrate that the demethylation step for synthesis of acyl derivatives of cyclic phenol phosphate analogues did not afford the expected product, either directly or after protection of the hydroxyl groups by different groups such as acetyl, benzyl, or TBDMS. It is unclear why the methyl group at position C4 of the aromatic ring of compound **1** cannot be removed under these conditions (Table 5-1). Thus, we conclude that one or more structural features of compound **1** prevent the demethylation reaction from occurring. Obviously, the proposed synthetic demethylation step proved practically challenging as the expected products were not obtained. Therefore, because attempts at demethylation of **1** were unsuccessful, our attention turned to the second approach, which was the synthesis of alkyl ether derivatives of cyclic phenol phosphate analogues. We attempted a different procedure and successfully synthesized **A1** (unsubstituted cyclic phenol phosphate) and **A2** (the methoxy-substituted cyclic phenol phosphate). Also, we proposed a different pathway for synthesis of alkyl ether derivatives of cyclic phenol phosphate analogues with long side chains (C_{14}, C_{16}, and C_{18}), and although we were able to prepare a precursor with C_{14} side chain, our attempts at incorporation of the cyclic phosphate moiety were unsuccessful.

We also evaluated the stability of the synthesized analogues **A1** and **A2** under certain conditions, and both **A1** and **A2** were stable. Both analogues have been submitted to our colleagues at the University of Memphis for assessment of their ability to inactivate ATX *in vitro*, and we are awaiting these results.

Molecular modeling was done by docking a number of potential ATX ligands to the active site of crystal structure of mouse ATX. These preliminary results revealed no great differences between these ligands. However, both **A1** (with no chain) and **A2** (with short chain) show the highest values (i.e. lowest affinity), which indicate that the long side chains of the other ligands play a role in binding to ATX.

In conclusion, the proposed cyclic phenol phosphates have not been previously prepared, and thus they represent a new orientation for the study of ATX inhibitor compounds and may lead to the development of new treatments for ATX-related human diseases in the future, including cancer.

CHAPTER 7: FUTURE RESEARCH DIRECTIONS

At this time, we have synthesized two cyclic phenol phosphate analogues of alkyl ether derivatives (**A1** and **A2)**. These analogues have been submitted to the Parrill-Baker laboratory at the University of Memphis in the United States to determine the ability of these compounds to inactivate ATX enzyme *in vitro*. Completion of the synthesis of alkyl ether derivatives of cyclic phenol phosphate analogues with long side chains (C_{14}, C_{16}, and C_{18}) analogues will be needed to obtain a complete set for ATX inhibition assay. The synthetic challenge that remained was incorporation of the cyclized phosphate group. More of the phenol/alcohol starting material (compound **15**) possessing long C_{14} chain alkyl ether could be made and scaled up, as outlined in Scheme 5-8, so the phosphate cyclization step could be reperformed. The lipophilicity of **15**, due to the long side chain, could interfere with the phosphate cyclization reaction. Different conditions could be used, such as changing the solvent and temperature. Also, starting materials with long side chains (C_{16} and C_{18}) alkyl ether could be made by using the same synthetic pathway for preparing **15** (Scheme 5-8), but using 1-bromohexadecane and 1-bromooctadecane, respectively, instead of 1-bromotetradecane. One potential approach to forming the required analogues is trying a shorter chain length to see if this works and optimize reaction conditions based on this.

If these compounds show promise, then synthesizing non-LPA analogues of cyclic phenol phosphate should be considered and could be other potential directions for this project. Because our analogues carry a long aliphatic chain, such long chain based compounds are not predicted to afford favorable pharmacokinetics properties. Nevertheless, they are promising leads compounds that are able to develop more drug-like inhibitors by structural variations. For

instance, the long aliphatic chain can be replaced by more drug-like chains. In our case, a great place to start would be HA155 (calculated log *P* 5.41, MOE) (Figure 2-9). The boronic acid moiety in HA155 inhibitor targets the Thr oxygen nucleophile in the ATX active site, whereas the hydrophobic 4-fluorobenzyl moiety of the inhibitor targets the hydrophobic pocket responsible for lipid binding.[4, 35, 88] Therefore, replacing the boronic acid with our cyclic phenol phosphate group may help the development of new ATX inhibitors for therapeutic use (Figure 7-1).

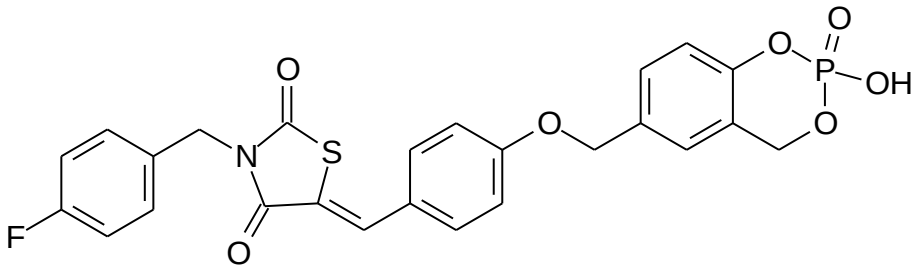

Figure 7-1: New developed ATX inhibitor.

Finally, it would be instructive to confirm that the cyclic phenol phosphate pro-drug is indeed converted to an *o*-QM by ATX *in* vitro. A common method for determining quinone methide formation is via trapping with glutathione and formation of stable adducts which can be identified using mass spectrometric techniques.[104]

REFERENCES

1. Liang, X.-J.; Chen, C.; Zhao, Y.; Wang, P. C. Circumventing Tumor Resistance to Chemotherapy by Nanotechnology. *Methods Mol Biol* **2010,** 596, 467-488.

2. Stefan, C.; Jansen, S.; Bollen, M. NPP-type ectophosphodiesterases: unity in diversity. *Trends Biochem Sci* **2005,** 30, 542-50.

3. Castagna, D.; Budd, D. C.; Macdonald, S. J.; Jamieson, C.; Watson, A. J. Development of Autotaxin Inhibitors: An Overview of the Patent and Primary Literature. *J Med Chem* **2016,** 59, 5604-21.

4. Barbayianni, E.; Kaffe, E.; Aidinis, V.; Kokotos, G. Autotaxin, a secreted lysophospholipase D, as a promising therapeutic target in chronic inflammation and cancer. *Prog Lipid Res* **2015,** 58, 76-96.

5. Stracke, M. L.; Krutzsch, H. C.; Unsworth, E. J.; Arestad, A.; Cioce, V.; Schiffmann, E.; Liotta, L. A. Identification, purification, and partial sequence analysis of autotaxin, a novel motility-stimulating protein. *J Biol Chem* **1992,** 267, 2524-9.

6. Umezu-Goto, M.; Kishi, Y.; Taira, A.; Hama, K.; Dohmae, N.; Takio, K.; Yamori, T.; Mills, G. B.; Inoue, K.; Aoki, J.; Arai, H. Autotaxin has lysophospholipase D activity leading to tumor cell growth and motility by lysophosphatidic acid production. *J Cell Biol* **2002,** 158, 227-233.

7. Tokumura, A.; Majima, E.; Kariya, Y.; Tominaga, K.; Kogure, K.; Yasuda, K.; Fukuzawa, K. Identification of human plasma lysophospholipase D, a lysophosphatidic acid-producing enzyme, as autotaxin, a multifunctional phosphodiesterase. *J Biol Chem* **2002,** 277, 39436-42.

8. Okudaira, S.; Yukiura, H.; Aoki, J. Biological roles of lysophosphatidic acid signaling through its production by autotaxin. *Biochimie* **2010,** 92, 698-706.

9. Moolenaar, W. H. Bioactive lysophospholipids and their G protein-coupled receptors. *Exp Cell Res***1999,** 253, 230-238.

10. Ferry, G.; Tellier, E.; Try, A.; Gres, S.; Naime, I.; Simon, M. F.; Rodriguez, M.; Boucher, J.; Tack, I.; Gesta, S.; Chomarat, P.; Dieu, M.; Raes, M.; Galizzi, J. P.; Valet, P.; Boutin, J. A.; Saulnier-Blache, J. S. Autotaxin is released from adipocytes, catalyzes lysophosphatidic acid synthesis, and activates preadipocyte proliferation - Up-regulated expression with adipocyte differentiation and obesity. *J Biol Chem* **2003,** 278, 18162-18169.

11. Rancoule, C.; Attane, C.; Gres, S.; Fournel, A.; Dusaulcy, R.; Bertrand, C.; Vinel, C.; Treguer, K.; Prentki, M.; Valet, P.; Saulnier-Blache, J. S. Lysophosphatidic acid impairs glucose homeostasis and inhibits insulin secretion in high-fat diet obese mice. *Diabetologia* **2013,** 56, 1394-402.

12. Bourgoin, S. G.; Zhao, C. Autotaxin and lysophospholipids in rheumatoid arthritis. *Curr Opin Investig Drugs* **2010,** 11, 515-26.

13. Inoue, M.; Xie, W.; Matsushita, Y.; Chun, J.; Aoki, J.; Ueda, H. Lysophosphatidylcholine induces neuropathic pain through an action of autotaxin to generate lysophosphatidic acid. *Neuroscience* **2008,** 152, 296-8.

14. Inoue, M.; Ma, L.; Aoki, J.; Chun, J.; Ueda, H. Autotaxin, a synthetic enzyme of lysophosphatidic acid (LPA), mediates the induction of nerve-injured neuropathic pain. *Mol Pain* **2008,** 4, 6.

15. Samadi, N.; Bekele, R.; Capatos, D.; Venkatraman, G.; Sariahmetoglu, M.; Brindley, D. N. Regulation of lysophosphatidate signaling by autotaxin and lipid phosphate phosphatases with respect to tumor progression, angiogenesis, metastasis and chemo-resistance. *Biochimie* **2011,** 93, 61-70.

16. Parrill, A. L.; Baker, D. L. Autotaxin inhibitors: a perspective on initial medicinal chemistry efforts. *Expert Opinion on Therapeutic Patents* **2010,** 20, 1619-1625.

17. Houben, A. J.; Moolenaar, W. H. Autotaxin and LPA receptor signaling in cancer. *Cancer Metastasis Rev* **2011,** 30, 557-65.

18. Nam, S. W.; Clair, T.; Campo, C. K.; Lee, H. Y.; Liotta, L. A.; Stracke, M. L. Autotaxin (ATX), a potent tumor motogen, augments invasive and metastatic potential of ras-transformed cells. *Oncogene* **2000,** 19, 241-7.

19. Federico, L.; Pamuklar, Z.; Smyth, S. S.; Morris, A. J. Therapeutic potential of autotaxin/lysophospholipase d inhibitors. *Curr Drug Targets* **2008,** 9, 698-708.

20. Leblanc, R.; Peyruchaud, O. New insights into the autotaxin/LPA axis in cancer development and metastasis. *Exp Cell Res* **2015,** 333, 183-189.

21. Willier, S.; Butt, E.; Grunewald, T. G. Lysophosphatidic acid (LPA) signalling in cell migration and cancer invasion: a focussed review and analysis of LPA receptor gene expression on the basis of more than 1700 cancer microarrays. *Biol Cell* **2013,** 105, 317-33.

22. Boutin, J. A.; Ferry, G. Autotaxin. *Cell Mol Life Sci* **2009,** 66, 3009-21.

23. Kawagoe, H.; Stracke, M. L.; Nakamura, H.; Sano, K. Expression and transcriptional regulation of the PD-Ialpha/autotaxin gene in neuroblastoma. *Cancer Res* **1997,** 57, 2516-21.

24. Hoelzinger, D. B.; Mariani, L.; Weis, J.; Woyke, T.; Berens, T. J.; McDonough, W. S.; Sloan, A.; Coons, S. W.; Berens, M. E. Gene expression profile of glioblastoma multiforme invasive phenotype points to new therapeutic targets. *Neoplasia* **2005,** 7, 7-16.

25. Kishi, Y.; Okudaira, S.; Tanaka, M.; Hama, K.; Shida, D.; Kitayama, J.; Yamori, T.; Aoki, J.; Fujimaki, T.; Arai, H. Autotaxin is overexpressed in glioblastoma multiforme and contributes to cell motility of glioblastoma by converting lysophosphatidylcholine to lysophosphatidic acid. *J Biol Chem* **2006,** 281, 17492-500.

26. Zhang, G.; Zhao, Z.; Xu, S.; Ni, L.; Wang, X. Expression of autotaxin mRNA in human hepatocellular carcinoma. *Chin Med J (Engl)* **1999,** 112, 330-2.

27. Masuda, A.; Nakamura, K.; Izutsu, K.; Igarashi, K.; Ohkawa, R.; Jona, M.; Higashi, K.; Yokota, H.; Okudaira, S.; Kishimoto, T.; Watanabe, T.; Koike, Y.; Ikeda, H.; Kozai, Y.; Kurokawa, M.; Aoki, J.; Yatomi, Y. Serum autotaxin measurement in haematological malignancies: a promising marker for follicular lymphoma. *Br J Haematol* **2008,** 143, 60-70.

28. Yang, S. Y.; Lee, J.; Park, C. G.; Kim, S.; Hong, S.; Chung, H. C.; Min, S. K.; Han, J. W.; Lee, H. W.; Lee, H. Y. Expression of autotaxin (NPP-2) is closely linked to invasiveness of breast cancer cells. *Clin Exp Metastasis* **2002,** 19, 603-8.

29. Stassar, M. J.; Devitt, G.; Brosius, M.; Rinnab, L.; Prang, J.; Schradin, T.; Simon, J.; Petersen, S.; Kopp-Schneider, A.; Zoller, M. Identification of human renal cell carcinoma associated genes by suppression subtractive hybridization. *Br J Cancer* **2001,** 85, 1372-82.

30. Kehlen, A.; Englert, N.; Seifert, A.; Klonisch, T.; Dralle, H.; Langner, J.; Hoang-Vu, C. Expression, regulation and function of autotaxin in thyroid carcinomas. *Int J Cancer* **2004,** 109, 833-8.

31. Yang, Y.; Mou, L.; Liu, N.; Tsao, M. S. Autotaxin expression in non-small-cell lung cancer. *Am J Respir Cell Mol Biol* **1999,** 21, 216-22.

32. Barbayianni, E.; Magrioti, V.; Moutevelis-Minakakis, P.; Kokotos, G. Autotaxin inhibitors: a patent review. *Expert Opin Ther Pat* **2013,** 23, 1123-32.

33. Parrill, A. L.; Baker, D. L. Autotaxin inhibition: challenges and progress toward novel anti-cancer agents. *Anticancer Agents Med Chem* **2008,** 8, 917-23.

34. Nishimasu, H.; Okudaira, S.; Hama, K.; Mihara, E.; Dohmae, N.; Inoue, A.; Ishitani, R.; Takagi, J.; Aoki, J.; Nureki, O. Crystal structure of autotaxin and insight into GPCR activation by lipid mediators. *Nat Struct Mol Biol* **2011,** 18, 205-12.

35. Hausmann, J.; Kamtekar, S.; Christodoulou, E.; Day, J. E.; Wu, T.; Fulkerson, Z.; Albers, H. M.; van Meeteren, L. A.; Houben, A. J.; van Zeijl, L.; Jansen, S.; Andries, M.; Hall, T.; Pegg, L. E.; Benson, T. E.; Kasiem, M.; Harlos, K.; Kooi, C. W.; Smyth, S. S.; Ovaa, H.; Bollen, M.; Morris, A. J.; Moolenaar, W. H.; Perrakis, A. Structural basis of substrate discrimination and integrin binding by autotaxin. *Nat Struct Mol Biol* **2011,** 18, 198-204.

36. Hausmann, J.; Perrakis, A.; Moolenaar, W. H. Structure-function relationships of autotaxin, a secreted lysophospholipase D. *Adv Biol Regul* **2013,** 53, 112-7.

37. Moolenaar, W. H.; Perrakis, A. Insights into autotaxin: how to produce and present a lipid mediator. *Nat Rev Mol Cell Biol* **2011,** 12, 674-679.

38. Perrakis, A.; Moolenaar, W. H. Autotaxin: structure-function and signaling. *J Lipid Res* **2014,** 55, 1010-1018.

39. Nishimasu, H.; Ishitani, R.; Aoki, J.; Nureki, O. A 3D view of autotaxin. *Trends Pharmacol Sci* **2012,** 33, 138-45.

40. Murata, J.; Lee, H. Y.; Clair, T.; Krutzsch, H. C.; Arestad, A. A.; Sobel, M. E.; Liotta, L. A.; Stracke, M. L. cDNA cloning of the human tumor motility-stimulating protein, autotaxin, reveals a homology with phosphodiesterases. *J Biol Chem* **1994,** 269, 30479-84.

41. Moolenaar, W. H. Lysophospholipids in the limelight: autotaxin takes center stage. *J Cell Biol* **2002,** 158, 197-9.

42. Yung, Y. C.; Stoddard, N. C.; Chun, J. LPA receptor signaling: pharmacology, physiology, and pathophysiology. *J Lipid Res* **2014,** 55, 1192-1214.

43. van Meeteren, L. A.; Moolenaar, W. H. Regulation and biological activities of the autotaxin-LPA axis. *Prog Lipid Res* **2007,** 46, 145-60.

44. *Molecular Operating Environment (MOE), 2014.09; Chemical Computing Group Inc., 1010 Sherbooke St. West, Suite #910, Montreal, QC, Canada, H3A 2R7, 2014.*

45. Zhou, A.; Huntington, J. A.; Pannu, N. S.; Carrell, R. W.; Read, R. J. How vitronectin binds PAI-1 to modulate fibrinolysis and cell migration. *Nat Struct Biol* **2003,** 10, 541-4.

46. Lee, H. Y.; Clair, T.; Mulvaney, P. T.; Woodhouse, E. C.; Aznavoorian, S.; Liotta, L. A.; Stracke, M. L. Stimulation of tumor cell motility linked to phosphodiesterase catalytic site of autotaxin. *J Biol Chem* **1996,** 271, 24408-12.

47. Zalatan, J. G.; Fenn, T. D.; Brunger, A. T.; Herschlag, D. Structural and functional comparisons of nucleotide pyrophosphatase/phosphodiesterase and alkaline phosphatase: implications for mechanism and evolution. *Biochemistry* **2006,** 45, 9788-803.

48. Jansen, S.; Perrakis, A.; Ulens, C.; Winkler, C.; Andries, M.; Joosten, R. P.; Van Acker, M.; Luyten, F. P.; Moolenaar, W. H.; Bollen, M. Structure of NPP1, an ectonucleotide pyrophosphatase/phosphodiesterase involved in tissue calcification. *Structure* **2012,** 20, 1948-59.

49. Clair, T.; Aoki, J.; Koh, E.; Bandle, R. W.; Nam, S. W.; Ptaszynska, M. M.; Mills, G. B.; Schiffmann, E.; Liotta, L. A.; Stracke, M. L. Autotaxin hydrolyzes sphingosylphosphorylcholine to produce the regulator of migration, sphingosine-1-phosphate. *Cancer Res* **2003,** 63, 5446-53.

50. Su, S. C.; Hu, X.; Kenney, P. A.; Merrill, M. M.; Babaian, K. N.; Zhang, X. Y.; Maity, T.; Yang, S. F.; Lin, X.; Wood, C. G. Autotaxin-lysophosphatidic acid signaling axis mediates

tumorigenesis and development of acquired resistance to sunitinib in renal cell carcinoma. *Clin Cancer Res* **2013,** 19, 6461-72.

51. Aoki, J.; Inoue, A.; Okudaira, S. Two pathways for lysophosphatidic acid production. *Biochim Biophys Acta* **2008,** 1781, 513-8.

52. Brindley, D. N. Hepatic secretion of lysophosphatidylcholine: A novel transport system for polyunsaturated fatty acids and choline. *J Nutr Biochem* **1993,** 4, 442-449.

53. Brindley, D. N.; Lin, F. T.; Tigyi, G. J. Role of the autotaxin-lysophosphatidate axis in cancer resistance to chemotherapy and radiotherapy. *Biochim Biophys Acta* **2013,** 1831, 74-85.

54. Gupte, R.; Siddam, A.; Lu, Y.; Li, W.; Fujiwara, Y.; Panupinthu, N.; Pham, T. C.; Baker, D. L.; Parrill, A. L.; Gotoh, M.; Murakami-Murofushi, K.; Kobayashi, S.; Mills, G. B.; Tigyi, G.; Miller, D. D. Synthesis and pharmacological evaluation of the stereoisomers of 3-carba cyclic-phosphatidic acid. *Bioorg Med Chem Lett* **2010,** 20, 7525-7528.

55. Tanaka, M.; Okudaira, S.; Kishi, Y.; Ohkawa, R.; Iseki, S.; Ota, M.; Noji, S.; Yatomi, Y.; Aoki, J.; Arai, H. Autotaxin stabilizes blood vessels and is required for embryonic vasculature by producing lysophosphatidic acid. *J BiolChem* **2006,** 281, 25822-25830.

56. Albers, H. M. H. G.; Ovaa, H. Chemical Evolution of Autotaxin Inhibitors. *Chem Rev* **2012,** 112, 2593-2603.

57. Giganti, A.; Rodriguez, M.; Fould, B.; Moulharat, N.; Coge, F.; Chomarat, P.; Galizzi, J. P.; Valet, P.; Saulnier-Blache, J. S.; Boutin, J. A.; Ferry, G. Murine and human autotaxin alpha, beta, and gamma isoforms: gene organization, tissue distribution, and biochemical characterization. *J Biol Chem* **2008,** 283, 7776-89.

58. Hashimoto, T.; Okudaira, S.; Igarashi, K.; Hama, K.; Yatomi, Y.; Aoki, J. Identification and biochemical characterization of a novel autotaxin isoform, ATXdelta, with a four-amino acid deletion. *J Biochem* **2012,** 151, 89-97.

59. Bollen, M.; Gijsbers, R.; Ceulemans, H.; Stalmans, W.; Stefan, C. Nucleotide pyrophosphatases/phosphodiesterases on the move. *Crit Rev Biochem Mol Biol* **2000,** 35, 393-432.

60. Gijsbers, R.; Ceulemans, H.; Stalmans, W.; Bollen, M. Structural and catalytic similarities between nucleotide pyrophosphatases/phosphodiesterases and alkaline phosphatases. *J Biol Chem* **2001,** 276, 1361-8.

61. Aoki, J.; Taira, A.; Takanezawa, Y.; Kishi, Y.; Hama, K.; Kishimoto, T.; Mizuno, K.; Saku, K.; Taguchi, R.; Arai, H. Serum lysophosphatidic acid is produced through diverse phospholipase pathways. *J Biol Chem* **2002,** 277, 48737-44.

62. Ishii, S.; Noguchi, K.; Yanagida, K. Non-Edg family lysophosphatidic acid (LPA) receptors. *Prostaglandins Other Lipid Mediat* **2009,** 89, 57-65.

63. Aoki, J. Mechanisms of lysophosphatidic acid production. *Semin Cell Dev Biol* **2004,** 15, 477-89.

64. Choi, J. W.; Herr, D. R.; Noguchi, K.; Yung, Y. C.; Lee, C. W.; Mutoh, T.; Lin, M. E.; Teo, S. T.; Park, K. E.; Mosley, A. N.; Chun, J. LPA receptors: subtypes and biological actions. *Annu Rev Pharmacol Toxicol* **2010,** 50, 157-86.

65. Goding, J. W.; Grobben, B.; Slegers, H. Physiological and pathophysiological functions of the ecto-nucleotide pyrophosphatase/phosphodiesterase family. *Biochim Biophys Acta* **2003,** 1638, 1-19.

66. Tokumura, A.; Kanaya, Y.; Miyake, M.; Yamano, S.; Irahara, M.; Fukuzawa, K. Increased production of bioactive lysophosphatidic acid by serum lysophospholipase D in human pregnancy. *Biol Reprod* **2002,** 67, 1386-92.

67. Tokumura, A.; Kume, T.; Fukuzawa, K.; Tahara, M.; Tasaka, K.; Aoki, J.; Arai, H.; Yasuda, K.; Kanzaki, H. Peritoneal fluids from patients with certain gynecologic tumor contain elevated levels of bioactive lysophospholipase D activity. *Life Sci* **2007,** 80, 1641-9.

68. Nakamura, K.; Nangaku, M.; Ohkawa, R.; Okubo, S.; Yokota, H.; Ikeda, H.; Aoki, J.; Yatomi, Y. Analysis of serum and urinary lysophospholipase D/autotaxin in nephrotic syndrome. *Clin Chem Lab Med* **2008,** 46, 150-1.

69. Sutphen, R.; Xu, Y.; Wilbanks, G. D.; Fiorica, J.; Grendys, E. C., Jr.; LaPolla, J. P.; Arango, H.; Hoffman, M. S.; Martino, M.; Wakeley, K.; Griffin, D.; Blanco, R. W.; Cantor, A. B.; Xiao, Y. J.; Krischer, J. P. Lysophospholipids are potential biomarkers of ovarian cancer. *Cancer Epidemiol Biomarkers Prev* **2004,** 13, 1185-91.

70. Baumforth, K. R.; Flavell, J. R.; Reynolds, G. M.; Davies, G.; Pettit, T. R.; Wei, W.; Morgan, S.; Stankovic, T.; Kishi, Y.; Arai, H.; Nowakova, M.; Pratt, G.; Aoki, J.; Wakelam, M. J.; Young, L. S.; Murray, P. G. Induction of autotaxin by the Epstein-Barr virus promotes the growth and survival of Hodgkin lymphoma cells. *Blood* **2005,** 106, 2138-46.

71. Gotoh, M.; Fujiwara, Y.; Yue, J.; Liu, J.; Lee, S.; Fells, J.; Uchiyama, A.; Murakami-Murofushi, K.; Kennel, S.; Wall, J.; Patil, R.; Gupte, R.; Balazs, L.; Miller, D. D.; Tigyi, G. J. Controlling cancer through the autotaxin-lysophosphatidic acid receptor axis. *Biochem Soc Trans* **2012,** 40, 31-6.

72. Hama, K.; Aoki, J.; Fukaya, M.; Kishi, Y.; Sakai, T.; Suzuki, R.; Ohta, H.; Yamori, T.; Watanabe, M.; Chun, J.; Arai, H. Lysophosphatidic acid and autotaxin stimulate cell motility of neoplastic and non-neoplastic cells through LPA1. *J Biol Chem* **2004,** 279, 17634-9.

73. David, M.; Wannecq, E.; Descotes, F.; Jansen, S.; Deux, B.; Ribeiro, J.; Serre, C. M.; Gres, S.; Bendriss-Vermare, N.; Bollen, M.; Saez, S.; Aoki, J.; Saulnier-Blache, J. S.; Clezardin, P.; Peyruchaud, O. Cancer Cell Expression of Autotaxin Controls Bone Metastasis Formation in Mouse through Lysophosphatidic Acid-Dependent Activation of Osteoclasts. *PLOS One* **2010,** 5.

74. Shida, D.; Kitayama, J.; Yamaguchi, H.; Okaji, Y.; Tsuno, N. H.; Watanabe, T.; Takuwa, Y.; Nagawa, H. Lysophosphatidic acid (LPA) enhances the metastatic potential of human colon carcinoma DLD1 cells through LPA1. *Cancer Res* **2003,** 63, 1706-11.

75. Erickson, J. R.; Hasegawa, Y.; Fang, X.; Eder, A.; Mao, M.; Furui, T.; Aoki, J.; Morris, A.; Mills, G. B. Lysophosphatidic acid and ovarian cancer: a paradigm for tumorogenesis and patient management. *Prostaglandins Other Lipid Mediat* **2001,** 64, 63-81.

76. Schulte, K. M.; Beyer, A.; Kohrer, K.; Oberhauser, S.; Roher, H. D. Lysophosphatidic acid, a novel lipid growth factor for human thyroid cells: over-expression of the high-affinity receptor edg4 in differentiated thyroid cancer. *Int J Cancer* **2001,** 92, 249-56.

77. Clair, T.; Koh, E.; Ptaszynska, M.; Bandle, R. W.; Liotta, L. A.; Schiffmann, E.; Stracke, M. L. L-histidine inhibits production of lysophosphatidic acid by the tumor-associated cytokine, autotaxin. *Lipids Health Dis* **2005,** 4, 5.

78. Gupte, R.; Patil, R.; Liu, J. X.; Wang, Y. H.; Lee, S. C.; Fujiwara, Y.; Fells, J.; Bolen, A. L.; Emmons-Thompson, K.; Yates, C. R.; Siddam, A.; Panupinthu, N.; Pham, T. C. T.; Baker, D. L.; Parrill, A. L.; Mills, G. B.; Tigyi, G.; Miller, D. D. Benzyl and Naphthalene Methylphosphonic Acid Inhibitors of Autotaxin with Anti-invasive and Anti-metastatic Activity. *Chem Medchem* **2011,** 6, 922-935.

79. Kobayashi, T.; Tanaka-Ishii, R.; Taguchi, R.; Ikezawa, H.; Murakami-Murofushi, K. Existence of a bioactive lipid, cyclic phosphatidic acid, bound to human serum albumin. *Life Sci* **1999,** 65, 2185-2191.

80. Baker, D. L.; Fujiwara, Y.; Pigg, K. R.; Tsukahara, R.; Kobayashi, S.; Murofushi, H.; Uchiyama, A.; Murakami-Murofushi, K.; Koh, E.; Bandle, R. W.; Byun, H. S.; Bittman, R.; Fan, D.; Murph, M.; Mills, G. B.; Tigyi, G. Carba analogs of cyclic phosphatidic acid are selective inhibitors of autotaxin and cancer cell invasion and metastasis. *J Biol Chem* **2006,** 281, 22786-93.

81. Uchiyama, A.; Mukai, M.; Fujiwara, Y.; Kobayashi, S.; Kawai, N.; Murofushi, H.; Inoue, M.; Enoki, S.; Tanaka, Y.; Niki, T.; Kobayashi, T.; Tigyi, G.; Murakami-Murofushi, K. Inhibition of transcellular tumor cell migration and metastasis by novel carba-derivatives of cyclic phosphatidic acid. *Biochim Biophys Acta* **2007,** 1771, 103-12.

82. Scott, L. J. Fingolimod: a review of its use in the management of relapsing-remitting multiple sclerosis. *CNS Drugs* **2011,** 25, 673-98.

83. van Meeteren, L. A.; Brinkmann, V.; Saulnier-Blache, J. S.; Lynch, K. R.; Moolenaar, W. H. Anticancer activity of FTY720: phosphorylated FTY720 inhibits autotaxin, a metastasis-enhancing and angiogenic lysophospholipase D. *Cancer Lett* **2008,** 266, 203-8.

84. Zhang, H.; Xu, X.; Gajewiak, J.; Tsukahara, R.; Fujiwara, Y.; Liu, J.; Fells, J. I.; Perygin, D.; Parrill, A. L.; Tigyi, G.; Prestwich, G. D. Dual activity lysophosphatidic acid receptor pan-antagonist/autotaxin inhibitor reduces breast cancer cell migration in vitro and causes tumor regression in vivo. *Cancer Res* **2009,** 69, 5441-9.

85. van Meeteren, L. A.; Ruurs, P.; Christodoulou, E.; Goding, J. W.; Takakusa, H.; Kikuchi, K.; Perrakis, A.; Nagano, T.; Moolenaar, W. H. Inhibition of autotaxin by lysophosphatidic acid and sphingosine 1-phosphate. *J Biol Chem* **2005,** 280, 21155-61.

86. North, E. J.; Osborne, D. A.; Bridson, P. K.; Baker, D. L.; Parrill, A. L. Autotaxin structure-activity relationships revealed through lysophosphatidylcholine analogs. *Bioorg Med Chem* **2009,** 17, 3433-3442.

87. Albers, H. M.; van Meeteren, L. A.; Egan, D. A.; van Tilburg, E. W.; Moolenaar, W. H.; Ovaa, H. Discovery and optimization of boronic acid based inhibitors of autotaxin. *J Med Chem* **2010,** 53, 4958-67.

88. Albers, H. M.; Hendrickx, L. J.; van Tol, R. J.; Hausmann, J.; Perrakis, A.; Ovaa, H. Structure-based design of novel boronic acid-based inhibitors of autotaxin. *J Med Chem* **2011,** 54, 4619-26.

89. Gierse, J.; Thorarensen, A.; Beltey, K.; Bradshaw-Pierce, E.; Cortes-Burgos, L.; Hall, T.; Johnston, A.; Murphy, M.; Nemirovskiy, O.; Ogawa, S.; Pegg, L.; Pelc, M.; Prinsen, M.; Schnute, M.; Wendling, J.; Wene, S.; Weinberg, R.; Wittwer, A.; Zweifel, B.; Masferrer, J. A novel autotaxin inhibitor reduces lysophosphatidic acid levels in plasma and the site of inflammation. *J Pharmacol Exp Ther* **2010,** 334, 310-7.

90. Bhave, S. R.; Dadey, D. Y.; Karvas, R. M.; Ferraro, D. J.; Kotipatruni, R. P.; Jaboin, J. J.; Hallahan, A. N.; Dewees, T. A.; Linkous, A. G.; Hallahan, D. E.; Thotala, D. Autotaxin Inhibition with PF-8380 Enhances the Radiosensitivity of Human and Murine Glioblastoma Cell Lines. *Front Oncol* **2013,** 3, 236.

91. Saunders, L. P.; Ouellette, A.; Bandle, R.; Chang, W. C.; Zhou, H.; Misra, R. N.; De La Cruz, E. M.; Braddock, D. T. Identification of small-molecule inhibitors of autotaxin that inhibit melanoma cell migration and invasion. *Mol Cancer Ther* **2008,** 7, 3352-62.

92. Tigyi, G.; Parrill, A. L. Molecular mechanisms of lysophosphatidic acid action. *Prog Lipid Res* **2003,** 42, 498-526.

93. Ghanem, E.; Raushel, F. M. Enzymes: The Active Site. *ENCYCLOPEDIA OF LIFE SCIENCES* **2007**.

94. McDonald, A. G.; Tipton, K. F. Enzymes: Irreversible Inhibition. *ENCYCLOPEDIA OF LIFE SCIENCES* **2012**.

95. Parrill, A. L.; Baker, D. L.; Montedonico, L. D. Mechanism Inactivators of Autotaxin. *J Biol Chem* **2011,** 270, 25651-25655.

96. Jansen, S.; Andries, M.; Vekemans, K.; Vanbilloen, H.; Verbruggen, A.; Bollen, M. Rapid clearance of the circulating metastatic factor autotaxin by the scavenger receptors of liver sinusoidal endothelial cells. *Cancer Lett* **2009,** 284, 216-21.

97. Ptaszynska, M. M.; Pendrak, M. L.; Bandle, R. W.; Stracke, M. L.; Roberts, D. D. Positive feedback between vascular endothelial growth factor-A and autotaxin in ovarian cancer cells. *Mol Cancer Res* **2008,** 6, 352-363.

98. Kanda, H.; Newton, R.; Klein, R.; Morita, Y.; Gunn, M. D.; Rosen, S. D. Autotaxin, an ectoenzyme that produces lysophosphatidic acid, promotes the entry of lymphocytes into secondary lymphoid organs. *Nat Immunol* **2008,** 9, 415-423.

99. Watanabe, N.; Ikeda, H.; Nakamura, K.; Ohkawa, R.; Kume, Y.; Tomiya, T.; Tejima, K.; Nishikawa, T.; Arai, M.; Yanase, M.; Aoki, J.; Arai, H.; Omata, M.; Fujiwara, K.; Yatomi, Y. Plasma lysophosphatidic acid level and serum autotaxin activity are increased in liver injury in rats in relation to its severity. *Life Sci* **2007,** 81, 1009-1015.

100. Pande, P.; Shearer, J.; Yang, J. H.; Greenberg, W. A.; Rokita, S. E. Alkylation of nucleic acids by a model quinone methide. *J Am Chem Soc* **1999,** 121, 6773-6779.

101. Sakamoto, K.; Wada, K.; Ito, H.; Hongo, K. Novel Vitamin B6 Derrivative. U.S. Patent WO2008139965 A1, Nov 20, 2008.

102. Zhang, F.; Bolton, J. L. Synthesis of the equine estrogen metabolites 2-hydroxyequilin and 2-hydroxyequilenin. *Chem Res Toxicol* **1999,** 12, 200-3.

103. Keun Son, J.; Ho Lee, S.; Nagarapu, L.; Jahng, Y. A Simple Synthesis of Nordihydroguaiaretic Acid and Its Analogues. *Bull. Korean Chem. Soc* **2005,** 26, 1117-1120.

104. Billinsky, J. L.; Marcoux, M. R.; Krol, E. S. Oxidation of the lignan nordihydroguaiaretic acid. *Chem Res Toxicol* **2007,** 20, 1352-1358.

105. Maini, S.; Hodgson, H. L.; Krol, E. S. The UVA and Aqueous Stability of Flavonoids Is Dependent on B-Ring Substitution. *J Agric Food Chem* **2012,** 60, 6966-6976.

106. Weissman, S. A.; Zewge, D. Recent advances in ether dealkylation. *Tetrahedron* **2005,** 61, 7833-7863.

107. Ryu, I.; Matsubara, H.; Yasuda, S.; Nakamura, H.; Curran, D. P. Phase-vanishing reactions that use fluorous media as a phase screen. Facile, controlled bromination of alkenes by

dibromine and dealkylation of aromatic ethers by boron tribromide. *J Am Chem Soc* **2002,** 124, 12946-12947.

108. McOmie, J. F. W.; Watts, M. L.; West, D. E. Demethylation of Aryl Methyl Ethers by Boron Tribromide. *Tetrahedron* **1968,** 24, 2289-2292.

109. Bachelor, F. W.; Loman, A. A.; Snowdon, L. R. Synthesis of pinosylvin and related heartwood stilbenes. *Can J Chem* **1970,** 48, 1554-1557.

110. Berry, D. J.; DiGiovanna, C. V.; Metrick, S. S.; Murugan, R. Catalysis by 4-dialkylaminopyridines. *ARKIVOC* **2001,** i, 201-226.

111. Rao, H.; Senthilkumar, S. A convenient procedure for the synthesis of allyl and benzyl ethers from alcohols and phenols. *Proc. Indian Acad. Sci.* **2001,** 113, 191-196.

112. Tasler, S.; Baumgartner, R.; Ammendola, A.; Schachtner, J.; Wieber, T.; Blisse, M.; Rath, S.; Zaja, M.; Klahn, P.; Quotschalla, U.; Ney, P. Thienopyrimidines as beta3-adrenoceptor agonists: hit-to-lead optimization. *Bioorg Med Chem Lett* **2010,** 20, 6108-15.

113. Sharghi, H.; Tamaddon, F. BeCl2 as a new highly selective reagent for dealkylation of aryl-methyl ethers. *Tetrahedron* **1996,** 52, 13623-13640.

114. Rios Morales, E. H.; Balzarini, J.; Meier, C. Stereoselective synthesis and antiviral activity of methyl-substituted cycloSal-pronucleotides. *J Med Chem* **2012,** 55, 7245-52.